Mussel-inspired Multifunctional Polymeric Materials
with Bioengineering Applications

by

Lin Li

A thesis submitted in partial fulfillment of the requirements for the degree of

Doctor of Philosophy

in
Chemical Engineering

Department of Chemical and Materials Engineering
University of Alberta

Abstract

Mussels can obtain strong underwater attachment to virtually all kinds of surfaces including rocks, metals, wood structures, polymers and concretes by secreting mussel foot proteins to form byssus. Great efforts have been dedicated to understanding this behavior and it is found that an catecholic amino acid 3,4-dihydroxyphenyl-*L*-alanine (DOPA) plays a crucial role in achieving this remarkable adhesion performance by actively involved in various catechol-mediated interactions such as covalent bonding, hydrogen bonding, metal coordination, cation-π interaction and aromatic interaction. Recently the self-healing capability of myssel byssal threads has attracted great attention and it is found that catechol-mediated reversible interactions such as catechol-metal coordination, catechol-boronate dynamic covalent interaction and hydrogen bonding also contribute to the recovery of material structure after damage. Inspired by all these interactions actively functioned in aqueous environment, numerous polymeric materials with various bioengineering applications can be designed and developed.

In this thesis, a detailed review on mussel adhesion behaviors and various mussel-inspired polymeric materials based on different DOPA chemistry was presented first followed by three original research projects on developing novel mussel-inspired functional polymers for bioengineering applications, using reversible addition-fragmentation chain transfer (RAFT) polymerization. In the first project, a versatile approach to prepare antifouling coatings bearing polymer loops

was demonstrated. An ABA triblock copolymer employing catechol-functionalized poly(*N,N*-dimethylacrylamide) (PDMA) as the adhesive A block and poly(ethylene glycol) (PEG) as the antifouling B block was prepared. By simple drop coating, this triblock copolymer can form a layer of loops onto substrate surface with the assistance of two adhesive anchoring blocks, which is compared with a layer of brushes prepared by drop-coating an AB diblock copolymer with the same anchoring block and half of the middle PEG chain length. The protein adsorption tests using quartz crystals microbalance with dissipation (QCM-D) demonstrate that the loops-coated surfaces show enhanced antifouling performance over the brushes-coated surfaces with similar end graft density.

In the second project, a novel injectable self-healing hydrogel with anti-biofouling property was preapred and new mussel-inspired self-healing mechanisms, catechol-mediated hydrogen bonding and aromatic interactions, were unveiled. An ABA triblock copolymer using catechol-functionalized poly(*N*-isopropylacrylamide) (PNIPAM) as the thermo-sensitive A block and poly(ethylene oxide) (PEO) as the hydrophilic and antifouling B block was synthesized. The hydrogel prepared through self-assembly of this triblock copolymer exhibits excellent thermo-sensitivity and antifouling performance. Surprisingly this hydrogel can withstand repeated deformation and recover its mechanical properties and structure within seconds in metal-free aqueous environment. By characterizing hydrogels prepared by different triblock copolymers, it is concluded that catechol-mediated hydrogen bonding and aromatic interactions are responsble for achieving this remarkable self-healing performance.

In the third project, an injetable self-healing hydrogel with antimicrobial and antifouling properties was prepared. An ABA tri-block copolymer employing catechol functionalized PEG as the thermo-sensitive A block and poly{[2-(methacryloyloxy)-ethyl] trimethyl ammonium iodide}(PMETA) as the hydrophilic and antimicrobial B block was synthesized. The hydrogel prepared through self-assembly of this triblock copolymer shows excellent sol-gel thermo-reversibility, can effectively inhibit the growth of *E. coli* (>99.8% reduction in bacterial counts) and prevent nonspecific cell attachment. What's more, it can heal autonomously from repeated damage, through mussel-inspired catechol-mediated hydrogen bonding and aromatic interactions, exhibiting great potential in various bioengineering applications.

Preface

This thesis is an original work by Lin Li (L. Li) under the supervision from Prof. Hongbo Zeng (H. Zeng).

Chapter 2 of this thesis has been published as L. Li, B. Yan, L. Zhang, Y. Tian and H. Zeng, Mussel-inspired antifouling coatings bearing polymer loops, *Chem Commun* 2015, 51, 15780-15783. I was primarily responsible for the data collection and analysis as well as the manuscript composition. B. Yan instructed the polymer synthesis and L. Zhang assisted with the AFM imaging. Y. Tian joined in the research design. H. Zeng was the supervisory author and was involved in the experimental design and manuscript composition.

Chapter 3 of this thesis has been published as L. Li, B. Yan, J. Yang, L. Chen, H. Zeng, Novel mussel-inspired injectable self-healing hydrogel with anti-biofouling property, *Adv Mater* 2015, 27, 1294-1299. I was primarily responsible for the data collection and analysis as well as the manuscript composition. B. Yan instructed the polymer synthesis. J. Yang conducted the experiments for the antifouling assay and cytotoxicity assay. L. Chen joined in the research design. H. Zeng was the supervisory author and was involved in the experimental design and manuscript composition.

Chapter 4 of this thesis has been submitted to *ACS Appl Mater Interfaces* as L. Li, B. Yan, W. Huang, J. Yang, L. Chen, H. Zeng, Injectable self-healing hydrogel with antimicrobial and antifouling properties. I was primarily responsible for the data collection and analysis as well as the manuscript composition. B. Yan

instructed the polymer synthesis. W. Huang conducted the experiments for the antimicrobial assay. J. Yang conducted the experiments for the antifouling assay. L. Chen joined in the research design. H. Zeng was the supervisory author and was involved in the experimental design and manuscript composition.

Acknowledgements

Table of Contents

List of Tables

List of Figures

List of Abbreviations

AFM	Atomic force microscopy
AIBN	Azobisisobutyronitrile
APBA	2-acrylamidophenylboronic acid
ATRP	Atom transfer radical polymerization
BDBA	1,3-benzenediboronic acid
BSA	Bovine serum albumin
DAPI	4,6-diamidino-2-phenylindole
DCM	Dichloromethane
DI	Deionized
DMA	N,N-Dimethylacrylamide
DMAEMA	2-(dimethylamino)ethyl methacrylate
DMSO	Dimethyl sulfoxide
DOPA	3,4-dihydroxyphenyl-L-alanie
E. Coli	*Escherichia coli*
EDTA	Ethylenediaminetetraacetic acid
FECO	Fringes of equal chromatic order
GNPs	Gold nanoparticles
GPC	Gel permeation chromatography
GQDs	Graphene quantum dots
IEP	Isoelectric points
LB	Luria-Bertani

LCST	Lower critical solution temperature
Mc	*Mytilus Californianus*
Me	*Mytilus edulis*
MEO$_2$MA	2-(2-methoxyethoxy)ethyl methacrylate
mfp	mussel foot protein
MTT	3-(4,5-dimethylthiazol-2-yl)-2,5-diphenyltetrazolium bromide
NMR	Nuclear Magnetic Resonance
OEGMA	Oligo(ethylene glycol) methacrylate
PAA	Polyallylamine
PBS	Phosphate buffer saline
PDA	Polydopamine
PDAA	Polydodecylacrylamide
PEG	Poly(ethylene glycol)
PEO	Poly(ethylene oxide)
PFPA	Perfluorophenyl acrylate
PMETA	Poly{[2-(methacryloyloxy)-ethyl] trimethyl ammonium iodide}
PNIPAM	Poly(*N*-isopropylacrylamide)
preCOLs	Pre-polymerized collagens
PS	Polystyrene
PVP	Polyvinylpyrrolidone
QAS	Quaternary ammonium salts
QCM-D	Quartz crystals microbalance with dissipation
R_F	Flory radius

rms	root-mean-square
SCPs	Soft colloidal probes
SDS	Sodium dodecyl sulphate
SFA	Surface forces apparatus
TA	Tannic acid
THF	Tetrahydrofuran
tmp	thread matrix proteins
UV	Ultraviolet

List of Publications

Peer Reviewed Journals:

1. <u>L. Li</u>, W. Smitthipong, H. Zeng, Mussel-inspired hydrogels for biomedical and environmental applications, *Polym Chem*, 2015, 6, 353-358.

2. <u>L. Li</u>, B. Yan, J. Yang, L. Chen, H. Zeng, Novel mussel-inspired injectable self-healing hydrogel with anti-biofouling property, *Adv Mater*, 2015, 27, 1294-1299.

3. <u>L. Li</u>, B. Yan, L. Zhang, Y. Tian, H. Zeng, Mussel-inspired antifouling coatings bearing polymer loops, *Chem Commun*, 2015, 51, 15780-15783.

4. <u>L. Li</u>, H. Zeng, Marine mussel adhesion and bio-inspired wet adhesives, *Biotribology*, 2016, 5, 44-51.

5. <u>L. Li</u>, B. Yan, W. Huang, J. Yang, L. Chen, H. Zeng, Injectable self-healing hydrogel with antimicrobial and antifouling properties, *ACS Appl Mater Interfaces*, submitted.

6. Y. Wang, <u>L. Li</u>, Y. Kotsuchibashi, S. Vshyvenko, Y. Liu, D. Hall, H. Zeng, R. Narain, Self-healing and injectable shear thinning hydrogels based on dynamic oxaborole-diol covalent crosslinking, *ACS Biomater Sci Eng*, 2016, DOI: 10.1021/ acsbiomaterials.6b00527.

7. H. Lu, Y. Wang, <u>L. Li</u>, Y. Kotsuchibashi, R. Narain, H. Zeng, Temperature- and pH-responsive benzoboroxole-based polymers for flocculation and enhanced dewatering of fine particle suspensions, *ACS Appl Mater Interfaces*, 2015, 7, 27176-27187.

8. H. Y. Yoo, J. Huang, L. Li, M. Foo, H. Zeng, D. S. Hwang, Nanomechanical contribution of collagen and von Willebrand factor A in marine underwater adhesion and its implication for collagen manipulation, *Biomacromolecules*, 2016, 17, 946-953.

9. Q. Liu, X. Lu, L. Li, H. Zhang, G. Liu, H. Zhong, H. Zeng, Probing the reversible Fe^{3+}-DOPA mediated bridging interaction in mussel foot protein-1, *J Phys Chem C*, 2016, 120, 21670-21677.

10. H. Zeng, C. Shi, J. Huang, L. Li, G. Liu, H. Zhong, Recent experimental advances on hydrophobic interactions at solid/water and fluid/water interfaces, *Biointerphases*, 2016, 11, 018903.

11. H. Zeng, J. Huang, Y. Tian, L. Li, M. V. Tirrell, J. N. Israelachvili, Adhesion and detachment mechanisms between polymer and solid substrate surfaces: using polystyrene-mica as a model system, *Macromolecules*, 2016, 49, 5223-5231.

Book Chapters:

1. H. Zeng, Q. Lu, B. Yan, J. Huang, L. Li, Z. Liao, Mussel Adhesives, Bioadhesion and Biomimetics: From Nature to Applications, Pan Stanford Publishing Pte. Ltd, 2015, 49-84.

2. L. Li, J. Chen, B. Yan, H. Zeng, Intrinsic Self-healing Polymeric Materials for Engineering and Environmental Applications, Smart Materials for Advanced Environmental Applications, The Royal Society of Chemistry, 2016, 139-164.

1 General Introduction[1]

1.1 Mussel adhesion behaviors and mussel foot proteins

Dwelling in rocky seaside, marine mussels not only benefit from the respiratory gas and rich nutrients brought by moving aerated seawater, but also evolve adaptability to the lift and drag of turbulent waves. Mussels can obtain secure underwater attachment to various surfaces including rocks, metals, wood structures, polymers and concretes through the formation of tenacious byssus.[1, 2] The internal mussel structure is illustrated in Figure 1.1a. The open and close of the mussel shells is controlled by two adductors located at the anterior and posterior sides of mussel body. During a typical attachment process, the mussel foot first stretches out of the shells to conduct a "tiptoeing" exploration on the substratum to locate a suitable spot (mussel prefers high energy and rough surfaces to low energy and smooth surfaces).[3, 4] Then liquid proteins are secreted from the ventral groove in mussel foot and cure immediately when exposure to seawater to form byssus consisting of adhesive plaque, thread, stem and root (at the base of mussel foot). Byssal threads are joined at the stem, connecting 12 retractor muscles which are responsible for the byssal tension. Finally, mussel foot can either initiate a new round of exploration and attachment or retract back to the shells, leaving the tensile

---

[1] Parts of this chapter were published in:
i) L. Li, H. Zeng, *Biotribology*, 2016, 5, 44-51.
ii) L. Li, W. Smitthipong, H. Zeng, *Polym Chem*, 2015, 6, 353-358.
iii) L. Li, J. Chen, B. Yan, H. Zeng, Intrinsic Self-healing Polymeric Materials for Engineering and Environmental Applications, Smart Materials for Advanced Environmental Applications, The Royal Society of Chemistry, 2016, 139-164.

byssal threads connecting the mussel shells and the adhesive byssal plaques holding fast to the foreign surfaces. [5-8]
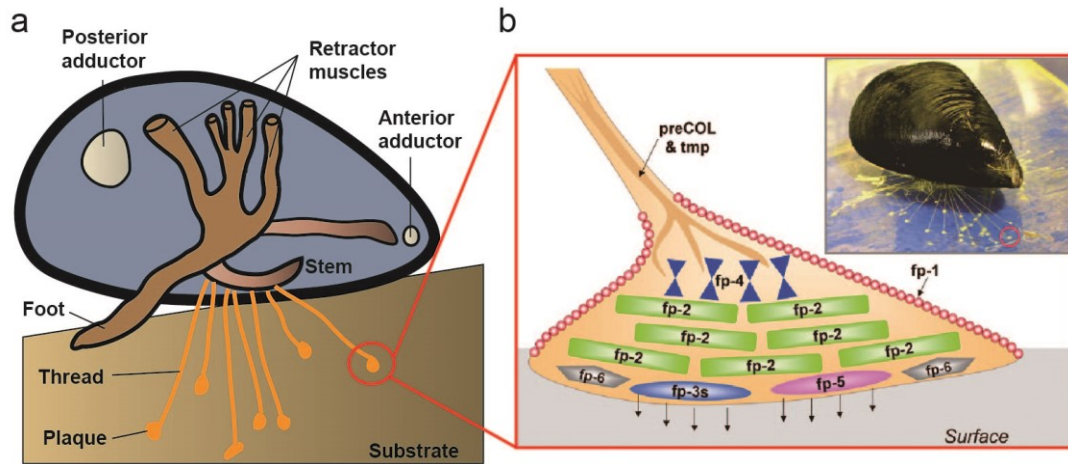
Figure 1.1 (a) Schematic of a mussel on a half shell and byssus structure. One of the byssal plaques (red circle) is enlarged as a schematic (b) to illustrate the approximate distribution of known proteins, with the inset showing the attachment of a mussel to a sheet of mica (reproduced from reference 9).

To understand the tenacity of byssal threads and the adhesion of byssal plaques, biochemistry of mussel byssus has been extensively explored. The byssal thread owns a flexible inner core made of pre-polymerized collagens (preCOLs) and thread matrix proteins (tmp) and is coated by a hardened thin layer of cuticle.[7, 9-11] The proteins confined to the byssal thread and plaque include mussel foot protein (mfp)-1, mfp-2, mfp-3, mfp-4, mfp-5 and mfp-6 (Figure 1.1b and Table 1.1). All these proteins contain an amino acid 3,4-dihydroxyphenyl-L-alanie (DOPA) formed by post-translational modification of tyrosine and have high isoelectric points (IEP) while differ vastly in sequences. Mfp-1 is the first identified phenolic protein with a molecular weight of 108 KDa and a DOPA content of 10-15 mol%. It would

undergo an oxidase or metal ions-mediated crosslinking to form protective cuticles covering the byssal threads and plaques[12-14]. Exclusively presented in the inner part of the plaque, mfp-2 is the most abundant structural component contributing to 25%-40 % of the plaque proteins. Its knot-like secondary structure provides mfp-2 a protease resistance [15, 16]. With a mass of ~6KDa, mfp-3 is the smallest foot protein identified in the byssal plaque. Located at the interface between the plaque and the substrate, mfp-3 is considered to play a critical role in mussel adhesion, especially with its structural flexibility due to small size and considerably high DOPA content (~25 mol%) compared with other foot proteins [17-19]. Mfp-4 has a relatively large mass and low DOPA level. Located between mfp-2 and the distal part of the preCOLs, mfp-4 is proposed to act as a coupling agent to connect the byssal thread and plaque [20, 21]. Similar to mfp-3, mfp-5 is located at the plaque-substrate interface with a high DOPA content approaching 30 mol% [22], indicating the relation between DOPA and the remarkable mussel wet adhesion capability. As the last identified plaque protein, mfp-6 is located close to both the surface of the adhesive plaque and the bulk plaque proteins. It is anticipated to provide a link between DOPA-rich surfaces and the bulk foot proteins [23]. The most important function of mfp-6 is the capability to reduce oxidized DOPA-quinone to DOPA to maintain proper redox balance for efficient adhesion of mfp-3 and mfp-5 [24].

Table 1.1 Comparison of mfps found in or near the mussel byssal plaque

Protein	Species	Mass (KDa)	IEP	Dopa (mol%)	Location	Features	Ref
Mfp-1	Me	108	10.5	10-15	Exclusively in the cuticle	Protective coating	[14]
Mfp-2	Me	42-47	9-10	2-3	Inside the plaque	Structural component	[15]

Mfp-3	Me	6	>10.5	25	Plaque-substrate interface	Key role in mussel adhesion	[17]
Mfp-4	Mc	93	10.5	2	Inside the plaque	Mediate links between thread and plaque	[21]
Mfp-5	Me	9.5	9	28	Plaque-substrate interface	Key role in mussel adhesion	[22]
Mfp-6	Mc	11.6	9.5	<5	Plaque-substrate interface	Special role in maintaining redox balance	[23]

Note: Me and Mc denote *Mytilus edulis* and *Mytilus Californianus,* respectively.

1.2 Interactions in mussel foot proteins

The interactions involved in mussel foot proteins (mfps) are generally classified into two types: the interactions between mfps to foreign surfaces (adhesion) and the interactions within mfps (cohesion or cross-linking). The amino acid DOPA which exists pervasively in mfps is believed to be pivotal to both the underwater adhesion and cohesion, credited to its versatile reaction chemistry. As illustrated in Figure 1.2, DOPA has two chemical forms, the unoxidized catechol forms and oxidized quinone forms, both of which exist in the seawater environment and contribute to the universal adhesion and protein cross-linking.[25]

As for the adhesion, catechols can form coordination bonds with inorganic surfaces such as metal ions or metal oxides while quinones can form covalent bonds with organic surfaces such as those bearing amines or thiols.[26] Acting respectively as hydrogen donors and acceptors, both catechols and quinones can form hydrogen bonding with polar surfaces such as mica.[27] While in possession of benzene ring, both forms can have π-π interactions with aromatic compound surfaces and cation-π

interactions with positively charged surfaces.[28] As for the cohesion, catechols can complex ferric ions to form pH-dependent reversible cross-linking, which are further extensively implied in achieving materials' self-healing.[29, 30] Through enzymes or oxidants, catehols are oxidized to quinones which either react actively with nucleophiles such as thiols and amines through Michael addition and Schiff base reaction to from cross-linkings, or with other catechols to form di-DOPA crosslinkings via radical coupling.[25, 31, 32]
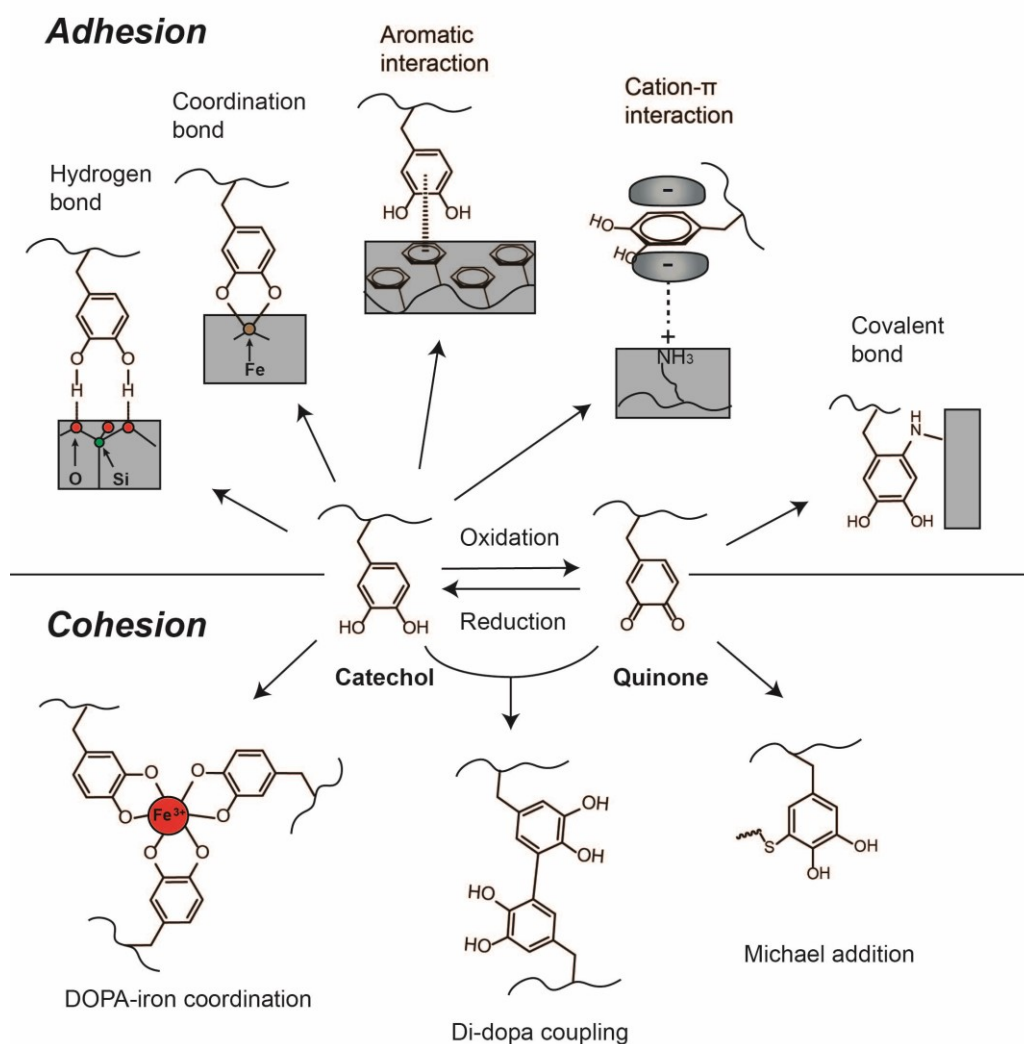
Figure 1.2 DOPA-mediated reaction chemistry in mussel foot proteins.

1.3   Mussel-inspired polymeric materials

Inspired by the miraculous DOPA chemistry adopted by mussel, various functional materials such as wet adhesives, functional coatings[33-41] and self-healing materials [42-44] have been devised and developed.

1.3.1   Mussel-inspired adhesives

Most conventional engineered polymer-based adhesives cannot be applied onto tissues or scaffold surfaces due to a loss of their surface activities in wet environments and the side effects of toxic chemicals currently used in most commercial adhesives. The remarkable wet adhesion and cohesion capability and biocompatible nature thus make mussel foot proteins promising candidates as tissue adhesives.[45, 46] However, the extensive use of mussel foot proteins in biomedical applications has been restrained by their limited quantities and tedious extraction and purification work [47-49]. Therefore, alternative approaches based on recombinant technologies and bio-mimetics have been developed. During the past decade, various recombinant mfps have been mass-produced in host organism *Escherichia coli* (*E. Coli*)[50-55], and multiple challenges including low yield, low DOPA content and insufficient adhesion strength have been conquered in some recent studies [56, 57]. As for the biomimetic approaches, peptides resembling the amino acid sequence and DOPA content of mfps were synthesized through peptide polymerization methods[58-61], however, the troublesome and labouring peptide synthesis process still spurred the development of simplified polymer mimics.

To this end, catechol groups have been incorporated into the polymeric backbones such as polystyrene (PS),[62] polydodecylacrylamide (PDAA),[63]

polyvinylpyrrolidone (PVP),[65] poly(methyl methacrylate)-poly(methacrylic acid)-poly(methyl methacrylate) block copolymer [64] and poly(propylene oxide)-poly(ethylene oxide) block copolymer,[65] through means of copolymerization or pendant modification[66]. Using oxidants such as O_2, Fe^{3+}, sodium periodate, hydrogen peroxide, or enzymes such as horseradish peroxide, simplified catechol-containing polymer mimics of mussel foot proteins could cross-link via di-DOPA coupling, or through reaction with thiol- and amine-functionalized materials via Michael addition and Schiff base reaction. [67, 68]

1.3.2   Mussel-inspired functional coatings

The preparation of mussel-inspired functional coatings is generally achieved either by "grafting to" method using the mussel-mimetic adhesive anchors or "grafting from" method employing mussel-mimetic surface initiators [69], or by the utilization of versatile platform of polydopamine[70] (Figure 1.3). Various properties such as antifouling [71-75], antimicrobial [76-78], anticorrosion [79-81], biological lubrication[82] and superhydrophobicity [83, 84] could be introduced to target surfaces through the immobilization of different functional coating materials via DOPA chemistry.

1.3.2.1   Surface anchors

Unlike surface anchors such as thiols[85] and silanes[86] which are highly substrate-restricted, mussel-inspired catechol attachment is facile, versatile and strong even in wet environment. Messersmith and his coworkers pioneered the work of using mussel-inspired adhesive anchors to immobilize functional moieties onto target surfaces in 2003. In their work, monomethoxy-terminated PEG was

conjugated to a single DOPA residue and a decapeptide analogue of mussel foot proteins respectively. PEGs were immobilized to gold and titanium surfaces through adsorption from the polymer solution, which was confirmed by surface analysis using X-ray photoelectron spectroscopy and time-of-flight secondary ion mass spectroscopy, rendering target surfaces resistant to cell attachment for extended periods of time.[38]
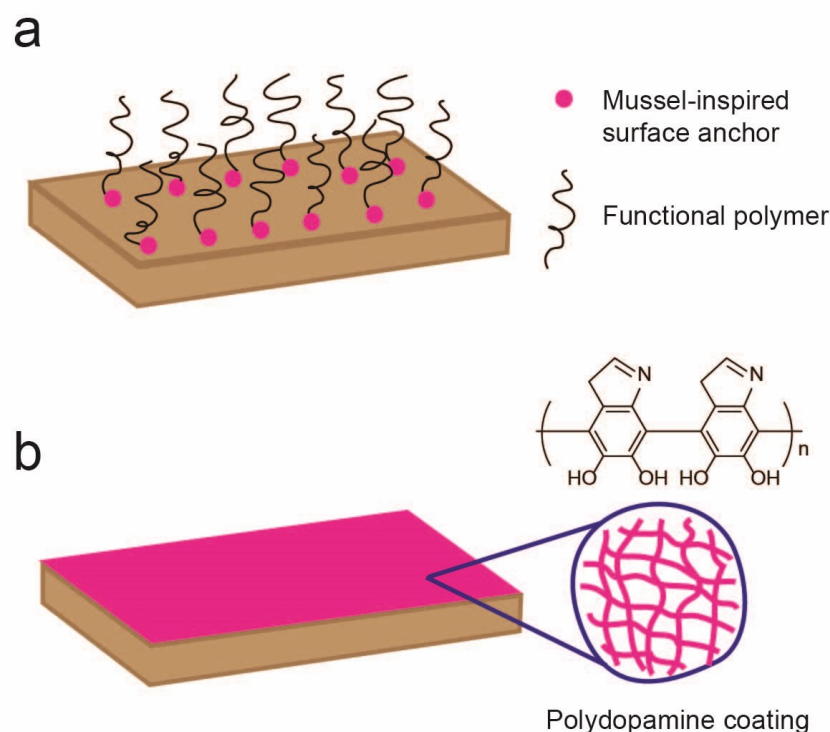
Figure 1.3 Mussel-inspired functional coatings through (a) surface anchors and (b) versatile platform.

Following this idea, numerous DOPA-derivatives especially catechol-containing groups have been applied as adhesive anchors to introduce diverse functionalities.[87] The surface modification is achieved either through a "grafting to" method using functional polymers end-tethered to catechol groups,[88] or through a

"grafting from" method using catechol-containing initiators which facilitate the polymerization from surfaces by means of atom transfer radical polymerization (ATRP)[71, 82], or the conjugation of functional polymers through click chemistry.[89, 90]

1.3.2.2 Versatile platform

Besides surface anchors, the research group headed by Messersmith reported another mussel-inspired universal approach for surface modification in 2007.[70] By immersing the target substrates into aqueous solution of dopamine adjusted to pH 8.5, an adherent layer of polydopamine (PDA) would deposit spontaneously through self-polymerization. This PDA coating can form on virtually all kinds of substrates, regardless of its composition and surface properties, and serve as a versatile platform for secondary functionalization, through diverse reactions related to catechol/quinone groups. The publication of this paper has attracted explosive attention worldwide and provided a general way to fabricate numerous functional surfaces. Various molecules including DNA,[91] proteins,[92, 93] living cells[94], hyaluronic acid, [95] and gold nanoparticles [96] have been immobilized onto PDA-coated surfaces to impart functions such as biomolecule delivery, enhanced tissue affinity and sterilization. Besides acting as adherent platform, PDA itself has proven to be effective coatings to nanoparticles for enhanced stability and biocompatibility. Liu *et al.* used well-controlled PDA nano layers to modify gold nanoparticles (GNPs) and found that the uniform core/shell nanostructures (GNP@PDA) exhibited ultra-stability *in vivo* and could translocate to cancer cells smoothly, which could be attributed to the partial escape from endosomes/lysosomes to cytosol through shielding of PDA. [97] Graphene Quantum Dots (GQDs) coated with

PDA also showed excellent stability of photoluminescent intensity in acidic, neutral and alkaline aqueous environment due to the presence of PDA barrier, thus could be used as long-term optical imaging agent. [98]

1.3.3 Mussel-inspired self-healing materials

The ability of self-healing and regeneration of function upon inflicted damage, such as the healing of bone fracture and the closure of injured blood vessels, are pervasive in biological systems while rare in man-made materials.[99] During the last decade self-healing has enjoyed great popularity in materials science because it can provide reduced material damage during general usage, reduced replacement costs and improved product safety, especially for applications located in poorly accessible areas whereas demanding long-term reliability. Polymers are by far the mostly studied material class in the context of self-healing behavior due to the facile functionalization and modification of polymeric systems. Generally the self-healing polymeric materials can be classified into two kinds: to achieve healing extrinsically based on external healing components or intrinsically by reversible bond formation.[100]

Mussel threads bear an inherent property of self-healing which allows themselves to autonomously recover the initial length and modulus after yield or plastic deformation, confirmed by both natural observation and laboratory cyclic stress-strain tests.[101] It is proposed that some reversible covalent and noncovelent intermolecular cross-links existing in the mussel threads could serve as breakable sacrificial bonds which rupture at elevated strain levels and reform when the load is removed. Through years of endeavors, various interactions contributing to the self-

healing behaviors of mussel threads have been found, including the catechol-metal coordination, catechol-boronate dynamic covalent interaction and catechol-mediated hydrogen bonding, which have inspired the design and development of many self-healing polymeric materials.

1.3.3.1 Catechol-metal coordination

Catechol-Fe^{3+} coordination has been the most widely applied mechanism for preparing mussel-inspired self-healing polymeric materials since the work published in 2011.[30] It was proposed that mussel foot proteins pre-bound Fe^{3+} in mono-dopa-Fe^{3+} complexes in secretory granules at pH≤5, while when released to sea water (pH~8) the thread material would undergo a spontaneous cross-linking via bis- and/or tris-dopa-Fe^{3+} complexes due to the considerable pH drop. It was further testified that the catechol-Fe^{3+} interpolymer cross-linking was readily pH-controlled, with mono-complex dominating at pH < 5.6, bis-complex at 5.6 < pH < 9.1 and tris-complex at pH > 9.1, and the bis- and tris-complexes can act as breakable sacrificial bonds for constructing self-healing materials (Figure 1.4).[30]
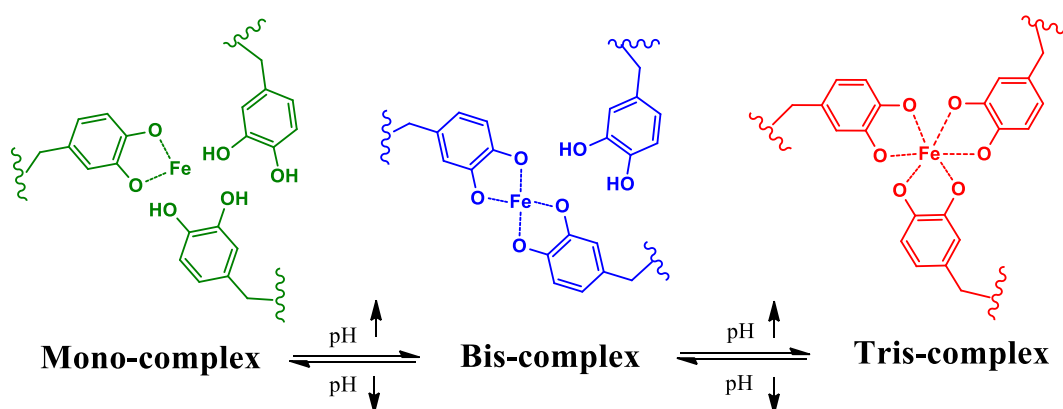
Figure 1.4 Mechanism of pH-dependent catechol-Fe^{3+} coordination.

Based on this mechanism, dopa-containing recombinant mussel adhesive proteins (MAPs) which was mass-produced by *Escherichia coli* and modified by mushroom tyrosinase was used to prepare adhesive hydrogel bearing simultaneously self-healing properties.[56] An in vivo residue-specific incorporation strategy was also adopted to create engineered MAPs in *Escherichia coli* with high DOPA content (16.5 mol%) comparable to that of natural MAPs.[57] However in general, the expression of MAPs via recombinant DNA technology is complicated, troublesome and expensive, which fueled the booming development of polymer mimetics. Generally a two-step process is needed for creating mussel-inspired self-healing polymeric materials, in which various chemical reactions are used first to incorporate the mussel functional moieties into polymer backbones, followed by a cross-linking of these functionalized polymers to 3D networks through various interactions. During the past few years catechol groups have been successfully incorporated into various polymer backbones including polyethylene glycol,[30] polyallylamine,[42] chitosan[102], polyurethane[103] and peptide[104] to form self-healing polymeric networks through catechol-Fe^{3+} coordination, which could be potentially used in biomedical applications as drug delivery platform or tissue adhesives.

Readily synthesized by nitration of dopamine, nitrodopamine reserved all advantages of catechol groups while obtained an additional functionality from onitrophenyl ethyl moiety: the photo-cleavability. Cross-linking of a nitrocatechol polymer prepared by end-functionalizing a four-arm star-poly(ethyleneglycol) with nitrodopamine created self-healing gels and coatings underwater that can be photodegraded upon light exposure,[105] which could be widely used in multiple cell

and medical applications. Birkedal *et al.* devised a very simple and low-cost method to synthesize self-healing hydrogel through the interactions between natural polyphenol tannic acid (TA), iron ions and polyallylamine (PAA), with TA and PAA acting as models for the catechol and lysine-rich Mfp-3 and 5.[106] Due to the very high catechol content in TA, the resulting material transformed into a sticky solid via formation of bis- and tris-complexes at pH above 3, which was much lower than the value (pH~9) obtained from systems involving dopa-functionalized polymers cross-linked by Fe^{3+}.[30, 42] Flexible and lightweight fibers can also be spun from the concentrated Fe^{3+}-TA-PAA mixtures and could be potentially applied as water sensitive mechanical locks.

Recently Andersen and co-workers demonstrated how the mechanical properties of aqueous metal-coordinating polymer network could be controlled by metal-ion identity, using simple catechol-modified PEG polymers and vanadium, iron and aluminum salts as model systems.[107] VCl_3, $FeCl_3$, or $AlCl_3$ salts were all used to construct polymer networks with a catechol: metal ratio of 3: 1. It was found that at fixed pH 8, V^{3+}-catechol polymer networks exhibited a 10-fold higher stability and significantly more solid-like properties than the Fe-catechol networks, mainly due to their difference in crosslink stoichiometry: V^{3+} was more inclined to induce tris-coordination while Fe^{3+} induced primarily bis-coordination at pH 8. Al^{3+}-catechol networks, on the other hand, displayed a 5-fold lower stability than that of Fe^{3+}-catechol networks, due to weaker non-coordinate Al^{3+}-catechol interactions attributed to the non-transition nature of aluminum. Birkedal et al. also reported that the mechanical properties and colors of mussel-inspired self-healing

hydrogels based on DOPA-polyallylamine can be readily adjusted by systematically varying the coordinating metal from Al^{3+}, Ga^{3+} to In^{3+}.[108] These studies demonstrated the possibility of tuning viscoelastic properties and colors of hydrophilic polymer materials over several orders of magnitude purely by the choice of coordinating metal ions, according to different practical applications.

1.3.3.2   Catechol-boronate interaction

Catechol-boronate dynamic covalent interaction has also been commonly employed in preparing self-healing hydrogels. Generally speaking, the strength and reversibility of this interaction in aqueous media is governed by an equilibrium which depends heavily on the media pH and the pKa of the boronic acid component. The formation of this complex is favored at neutral and alkaline pH (above the pKa of the boronic acid component) while a dissociation is favored by the equilibrium in an acidic environment.[109, 110] The reversible formation and dissociation of boronate ester, or the self-healing behavior of the resultant cross-linked network is most effective when the pH is near the pKa.[111]

He *et al.* constructed a self-healing polymeric network by reacting 1,3-benzenediboronic acid (BDBA) with catechol-functionalized 4-arm PEG under basic aqueous condition (pH=9), which was determined between the p*K*a of catechol (9.3) and that of BDBA (8.7).[112] The dynamic tetrahedral borate ester (Figure 1.5a) gave rise to hydrogel networks which could exhibit covalent gel-like behavior and self-heal after mechanical disruption. Harada and co-workers devised pH and sugar-responsive gel assemblies under basic conditions (pH=10), through the formation of cyclic boronate ester (Figure 1.5c) between poly(acrylamide) gels

carrying phenylboronic acid moieties and catechol moieties respectively.[113] As the assembly and disassembly could be controlled by pH or competitive saccharide molecules, this system can potentially work for biomolecule-responsive gel assembly in biomedical field.
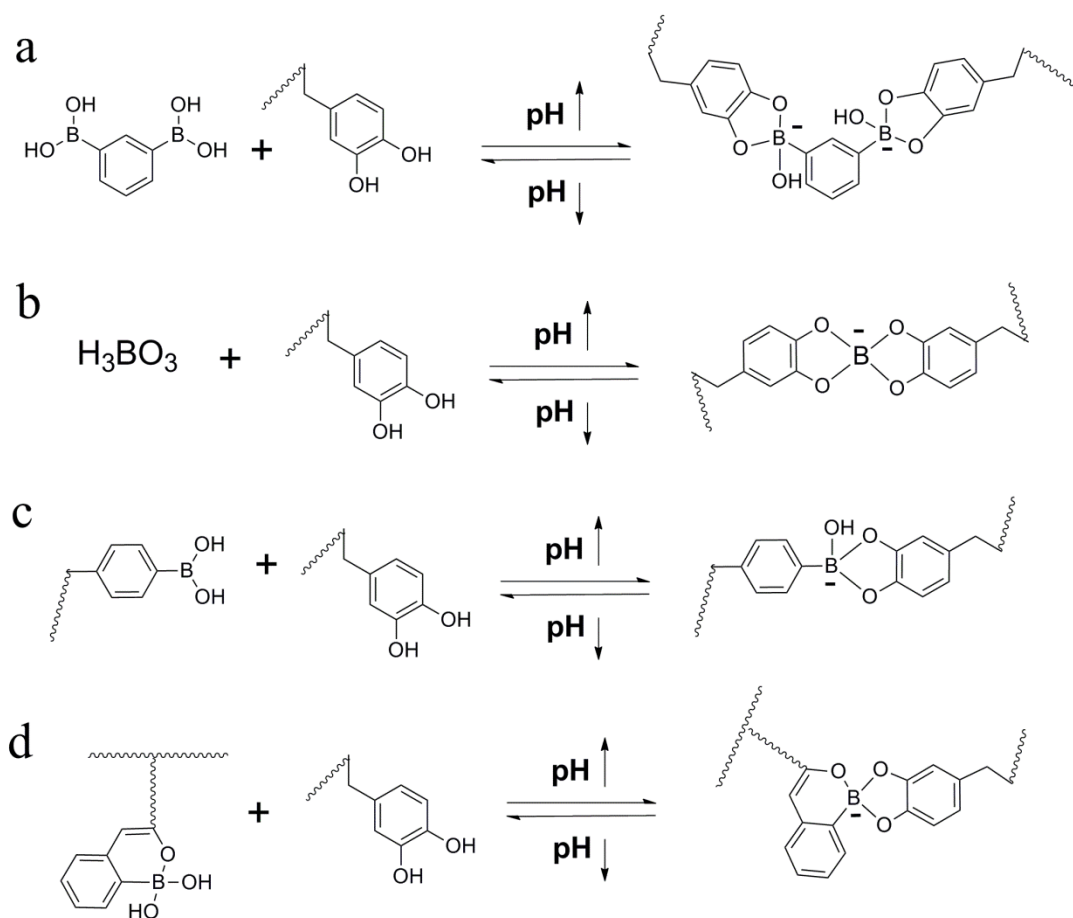
Figure 1.5 Cross-linking mechanism of catechol-functionalized polymers with different boronic acid derivatives: (a) 1,3-benzenediboronic acid (reproduced from reference 112), (b) boronic acid, (c) phenylboronic acid (reproduced from reference 113), (d) 2-acrylamidophenylboronic acid (reproduced from reference 120).

Stadler and co-workers found the difference in the behavior of dry and humid catechol-borate complexes.[114] By complexation of catechol-functionalized polymer with NaBH$_4$ at pH~9, covalent gels were prepared but the network could not restructure dynamically after mechanical disruption. However humidity can be adsorbed by these gels to change the catechol-borate covalent bonds from irreversible to reversible. This finding may be important for several biochemical and pharmaceutical systems utilizing this kind of bond. A rapid self-healing and triple stimuli responsive hydrogel was reported recently based on interactions between poly(dopamine methacrylate-co-N-isopropylacrylamide) and boric acid (H$_3$BO$_3$),[115] and it was found the complexation was strongly dependent on the pH and catechol concentration.

The fact that various dynamic catechol-boronate conjugates formed at high pH would dissociate at low pH endows the above-mentioned materials great potential as drug delivery carriers, as many pathological changes including inflammation or tumor are accompanied with a pH decrease in the local microenvironment.[116] However, if healing can occur in a broad pH range or additional stability at relatively low pH values can be achieved, the possible applications of boronate ester hydrogels would be greatly expanded, especially in acidic environment like the gastrointestinal tract.[117] One method to accomplish this is by using intramolecular coordination that can stabilize the formation of boronate ester at reduced pH.[118, 119] To this end, Sumerlin and co-workers constructed boronate ester-cross-linked hydrogels which can achieve healing over a wide pH range by reacting a catechol-functionalized copolymer with a 2-acrylamidophenylboronic acid (2APBA)

copolymer (Figure 1.5d), where the internal coordination facilitated the stabilization

of cross-links formed at acidic and neutral pH.[120]

1.3.3.3 Hydrogen bonding
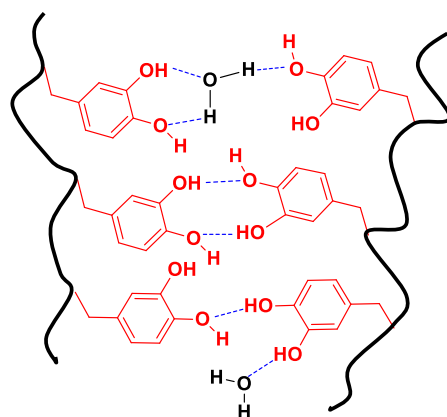
Figure 1.6 Mechanism of catechol-mediated hydrogen bonding.

Despite of the multiple metal-coordination mechanisms mentioned above, biological self-healing in wet conditions, as occurs in self-assembled holdfast proteins in mussels, is generally thought to involve more than reversible metal chelates. Israelachvili, Waite and their co-workers employed synthetic polyacrylate and polymethacrylate materials which were functionalized with mussel-inspired catechols blocked by silyl groups to study their self-healing behavior in metal-free water and it was found that the bisected polymer rods could only self-mend in acid solutions where the catechols were fully revealed due to the removal of silyl groups, while could not self-mend in neutral to basic environment where the catechols were blocked.[43] It was therefore concluded that the underwater self-healing in catechol-functionalized polyacrylates was achieved by hydrogen bonding between interfacial catechol moieties (Figure 1.6). Based on this mechanism, Stadler et al. manipulated

copolymers of *N*-isopropylacrylamide (NIPAM) and dopamine methacrylate to establish a reversible, self-healing 3D network in aprotic solvents based on hydrogen bonding, which could be potentially used in the field of drug delivery.[121]

1.4   Objectives and outline of this thesis

Despite the huge progress made in understanding mussel adhesion and cohesion mechanism, and development in mussel-inspired functional materials, much room for improvement still exist. The overall objective of this thesis is to design, synthesize and characterize novel mussel-inspired polymers (both in structure and in function), and to use them to construct functional materials with potential bioengineering applications such as surface coatings, drug delivery vehicles and wound dressings. The research work presented in this thesis contains three parts. The first part deals with structure, studying the impact of polymer chain conformation on its property. While the second and third parts deal with function, concerning the incorporation of multiple functions into one hydrogel design.

During the past decade, immobilizing functional moieties to target surfaces through mussel-inspired adhesive anchors or versatile polydopamine platform has become a general approach for preparing functional polymeric coatings, most of which bear polymer brushes. However, very little research has been conducted on the preparation and characterization of surfaces bearing polymer loops. The first part of this thesis deals with the polymer loops conformation and their antifouling performance compared with the brush conformation. In chapter 2, an ABA triblock copolymer employing catechol-functionalized PDMA as the mussel-inspired A block and PEG as the middle B block was synthesized through RAFT

polymerization. By simple drop-coating, a single layer of polymer loops was formed with the assistance of two adhesive anchoring blocks, which was compared with a layer of brushes prepared by drop-coating a diblock copolymer with the same anchoring block and half of the middle PEG chain length. In this project, distance and force measurements utilizing surface forces apparatus were applied to determine the formation of polymer loops for the first time. The protein adsorption tests using QCM-D demonstrated that with similar end graft density, the loops-coated surfaces exhibited stronger protein-reduction performance over the brushes-coated ones.

The second and third parts of this thesis concern the development of novel mussel-inspired multifunctional hydrogels with potential bioengineering applications. Injectable hydrogels have been actively applied as drug delivery vehicles due to their capability to carry various bioactive molecules and minimum invasion to human body. However, implanted hydrogels are constantly challenged by external mechanical forces and internal biofouling accumulation, which would severely impair both their structure and property. To address this issue, in chapter 3, we designed a novel injectable self-healing hydrogel with anti-biofouling property. An ABA triblock copolymer with catechol-functionalized PNIPAM as the thermo-sensitive A block and PEO as the middle B block was synthesized through RAFT polymerization. The hydrogel prepared through self-assembly of this triblock copolymer exhibited excellent thermo-sensitivity and antifouling performance. What's more, this hydrogel could heal from repeated deformation and recover its mechanical properties and structure within seconds in metal-free aqueous

environment. Triblock copolymers with slight difference in monomer species were synthesized and prepared into hydrogels. By characterizing recovery perfomance of these hydrogels after external strain, new mussel-inspired self-healing mechanism, catechol-mediated hydrogen bonding and aromatic interactions, were proposed and experiemntally verified.

In designing hydrogels with bioengineering applications, researchers would spare no efforts to introduce as many properties as they could to meet the diverse needs in dynamic biomedical processes. In chapter 4, we designed a thermo-sensitive injectable self-healing hydrogel with antimicrobial and antifouling properties. An ABA triblock copolymer with catechol functionalized PEG-based A block and quaternized B block were synthesized through RAFT polymerization. The hydrogel prepared through self-assembly of this copolymer exhibited excellent sol-gel thermo-reversibility and could effectively inhibit the growth of *E. coli* (>99.8% reduction in bacterial counts) and prevent nonspecific cell attachment. It can also heal autonomously from repeated damage, through the newly-discovered mussel-inspired metal-free self-healing mechanisms: catechol-mediated hydrogen bonding and aromatic interactions.

Finally, conclusions from the three major research projects were given and future research prospects were proposed in chapter 5.

1.5   References

1.   J. H. Kavouras and J. S. Maki, *Invertebr Biol*, 2003, **122**, 138-151.

2.   J. Kavouras and J. Maki, *J Appl Microbiol*, 2004, **97**, 1236-1246.

3.   N. Aldred, L. Ista, M. Callow, J. Callow, G. Lopez and A. Clare, *J R Soc Interface*, 2006, **3**, 37-43.

4.   D. Crisp, G. Walker, G. Young and A. Yule, *J Colloid Interface Sci*, 1985, **104**, 40-50.

5.   V. Haris, *Sessile animals of the sea shore*, Springer Science & Business Media, 1990.

6.   J. H. Waite, *Int J Adhes Adhes*, 1987, **7**, 9-14.

7.   B. P. Lee, P. B. Messersmith, J. N. Israelachvili and J. H. Waite, *Ann Rev Mater Res*, 2011, **41**, 99.

8.   J. H. Waite, in *Structure, cellular synthesis and assembly of biopolymers*, Springer, 1992, pp. 27-54.

9.   D. S. Hwang, H. Zeng, A. Masic, M. J. Harrington, J. N. Israelachvili and J. H. Waite, *J Biol Chem*, 2010, **285**, 25850-25858.

10.   X. Qin and J. H. Waite, *J Exp Biol*, 1995, **198**, 633-644.

11.   N. Holten-Andersen, G. E. Fantner, S. Hohlbauch, J. H. Waite and F. W. Zok, *Nat mater*, 2007, **6**, 669-672.

12.   J. H. Waite, *J Biol Chem*, 1983, **258**, 2911-2915.

13.   D. R. Filpula, S. M. Lee, R. P. Link, S. L. Strausberg and R. L. Strausberg, *Biotechnol Prog*, 1990, **6**, 171-177.

14. S. W. Taylor, J. H. Waite, M. M. Ross, J. Shabanowitz and D. F. Hunt, *J Am Chem Soc*, 1994, **116**, 10803-10804.

15. L. M. Rzepecki, K. M. Hansen and J. H. Waite, *Biol Bull*, 1992, **183**, 123-137.

16. K. Inoue, Y. Takeuchi, D. Miki and S. Odo, *J Biol Chem*, 1995, **270**, 6698-6701.

17. V. V. Papov, T. V. Diamond, K. Biemann and J. H. Waite, *J Biol Chem*, 1995, **270**, 20183-20192.

18. M. A. Even, J. Wang and Z. Chen, *Langmuir*, 2008, **24**, 5795-5801.

19. L. A. Burzio and J. H. Waite, *Biochemistry*, 2000, **39**, 11147-11153.

20. S. Warner and J. Waite, *Mar Biol*, 1999, **134**, 729-734.

21. H. Zhao and J. H. Waite, *Biochemistry-us*, 2006, **45**, 14223-14231.

22. J. H. Waite and X. Qin, *Biochemistry*, 2001, **40**, 2887-2893.

23. H. Zhao and J. H. Waite, *J Biol Chem*, 2006, **281**, 26150-26158.

24. J. Yu, W. Wei, E. Danner, R. K. Ashley, J. N. Israelachvili and J. H. Waite, *Nat chem biol*, 2011, **7**, 588-590.

25. M. Yu, J. Hwang and T. J. Deming, *J Am Chem Soc*, 1999, **121**, 5825-5826.

26. H. Lee, N. F. Scherer and P. B. Messersmith, *Proc Natl Acad Sci*, 2006, **103**, 12999-13003.

27. B. K. Ahn, D. W. Lee, J. N. Israelachvili and J. H. Waite, *Nat Mater*, 2014, **13**, 867-872.

28. Q. Lu, E. Danner, J. H. Waite, J. N. Israelachvili, H. Zeng and D. S. Hwang, *J R Soc Interface*, 2013, **10**, 20120759.

29. H. Zeng, D. S. Hwang, J. N. Israelachvili and J. H. Waite, *Proc Natl Acad Sci*, 2010, **107**, 12850-12853.

30. N. Holten-Andersen, M. J. Harrington, H. Birkedal, B. P. Lee, P. B. Messersmith, K. Y. C. Lee and J. H. Waite, *Proc Natl Acad Sci*, 2011, **108**, 2651-2655.

31. M. Krogsgaard, V. Nue and H. Birkedal, *Chem Eur J*, 2015.

32. C. Fant, K. Sott, H. Elwing and F. Hook, *Biofouling*, 2000, **16**, 119-132.

33. J. Waite and M. Tanzer, *Biochem Biophys Res Commun*, 1980, **96**, 1554-1561.

34. Q. Lu, D. X. Oh, Y. Lee, Y. Jho, D. S. Hwang and H. Zeng, *Angew Chem*, 2013, **125**, 4036-4040.

35. Q. Lu, D. S. Hwang, Y. Liu and H. Zeng, *Biomaterials*, 2012, **33**, 1903-1911.

36. H. Zhang, L. P. Bré, T. Zhao, Y. Zheng, B. Newland and W. Wang, *Biomaterials*, 2014, **35**, 711-719.

37. H. Lee, J. Rho and P. B. Messersmith, *Adv mater (Deerfield Beach, Fla.)*, 2009, **21**, 431.

38. J. L. Dalsin, B.-H. Hu, B. P. Lee and P. B. Messersmith, *J Am Chem Soc*, 2003, **125**, 4253-4258.

39. Y.-Z. Wang, L. Li, F.-S. Du and Z.-C. Li, *Polymer*, 2015.

40. C. E. Brubaker and P. B. Messersmith, *Biomacromolecules*, 2011, **12**, 4326-4334.

41.   W. Zhang, Z. Pan, F. K. Yang and B. Zhao, *Adv Funct Mater*, 2015, **25**, 1588-1597.

42.   M. Krogsgaard, M. A. Behrens, J. S. Pedersen and H. Birkedal, *Biomacromolecules*, 2013, **14**, 297-301.

43.   B. K. Ahn, D. W. Lee, J. N. Israelachvili and J. H. Waite, *Nat mater*, 2014, **13**, 867-872.

44.   L. Li, B. Yan, J. Yang, L. Chen and H. Zeng, *Adv Mater*, 2015, **27**, 1294-1299.

45.   C. E. Brubaker, H. Kissler, L.-J. Wang, D. B. Kaufman and P. B. Messersmith, *Biomaterials*, 2010, **31**, 420-427.

46.   L. Ninan, J. Monahan, R. L. Stroshine, J. J. Wilker and R. Shi, *Biomaterials*, 2003, **24**, 4091-4099.

47.   J. Schnurrer and C.-M. Lehr, *Int J Pharm*, 1996, **141**, 251-256.

48.   R. Chivers and R. Wolowacz, *Int J Adhes Adhes*, 1997, **17**, 127-132.

49.   L. Ninan, R. Stroshine, J. Wilker and R. Shi, *Acta biomater*, 2007, **3**, 687-694.

50.   D. S. Hwang, H. J. Yoo, J. H. Jun, W. K. Moon and H. J. Cha, *Appl Environ Microb*, 2004, **70**, 3352-3359.

51.   D. S. Hwang, Y. Gim and H. J. Cha, *Biotechnol Prog*, 2005, **21**, 965-970.

52.   D. S. Hwang, Y. Gim, H. J. Yoo and H. J. Cha, *Biomaterials*, 2007, **28**, 3560-3568.

53.   D. S. Hwang, S. B. Sim and H. J. Cha, *Biomaterials*, 2007, **28**, 4039-4046.

54. Y. Gim, D. S. Hwang, S. Lim, Y. H. Song and H. J. Cha, *Biotechnol Prog*, 2008, **24**, 1272-1277.

55. S. Lim, Y. S. Choi, D. G. Kang, Y. H. Song and H. J. Cha, *Biomaterials*, 2010, **31**, 3715-3722.

56. B. J. Kim, D. X. Oh, S. Kim, J. H. Seo, D. S. Hwang, A. Masic, D. K. Han and H. J. Cha, *Biomacromolecules*, 2014, **15**, 1579-1585.

57. B. Yang, N. Ayyadurai, H. Yun, Y. S. Choi, B. H. Hwang, J. Huang, Q. Lu, H. Zeng and H. J. Cha, *Angew Chem Int Ed*, 2014, **53**, 13360-13364.

58. H. Yamamoto and T. Hayakawa, *Biopolymers*, 1982, **21**, 1137-1151.

59. M. Yu and T. J. Deming, *Macromolecules*, 1998, **31**, 4739-4745.

60. M. J. Sever and J. J. Wilker, *Tetrahedron*, 2001, **57**, 6139-6146.

61. J. Wang, C. Liu, X. Lu and M. Yin, *Biomaterials*, 2007, **28**, 3456-3468.

62. G. Westwood, T. N. Horton and J. J. Wilker, *Macromol*, 2007, **40**, 3960-3964.

63. Y. Saito, T. Kawano, M. Shimomura and H. Yabu, *Macromolecular rapid commun*, 2013, **34**, 630-634.

64. M. Guvendiren, P. B. Messersmith and K. R. Shull, *Biomacromolecules*, 2007, **9**, 122-128.

65. D. G. Barrett, G. G. Bushnell and P. B. Messersmith, *Adv healthc mater*, 2013, **2**, 745-755.

66. E. Y. Jeon, B. H. Hwang, Y. J. Yang, B. J. Kim, B.-H. Choi, G. Y. Jung and H. J. Cha, *Biomaterials*, 2015.

67. H. JungáChung and T. GwanáPark, *Soft Matter*, 2010, **6**, 977-983.

68.   J. H. Ryu, Y. Lee, W. H. Kong, T. G. Kim, T. G. Park and H. Lee, *Biomacromolecules*, 2011, **12**, 2653-2659.

69.   J. L. Dalsin and P. B. Messersmith, *Mater today*, 2005, **8**, 38-46.

70.   H. Lee, S. M. Dellatore, W. M. Miller and P. B. Messersmith, *science*, 2007, **318**, 426-430.

71.   C. Gao, G. Li, H. Xue, W. Yang, F. Zhang and S. Jiang, *Biomaterials*, 2010, **31**, 1486-1492.

72.   Q. Wei, T. Becherer, R.-C. Mutihac, P.-L. M. Noeske, F. Paulus, R. Haag and I. Grunwald, *Biomacromolecules*, 2014, **15**, 3061-3071.

73.   Y. Dang, M. Quan, C.-M. Xing, Y.-B. Wang and Y.-K. Gong, *J Mater Chem B*, 2015, **3**, 2350-2361.

74.   S. Saxer, C. Portmann, S. Tosatti, K. Gademann, S. Zurcher and M. Textor, *Macromolecules*, 2009, **43**, 1050-1060.

75.   G. Li, G. Cheng, H. Xue, S. Chen, F. Zhang and S. Jiang, *Biomaterials*, 2008, **29**, 4592-4597.

76.   H. Han, J. Wu, C. W. Avery, M. Mizutani, X. Jiang, M. Kamigaito, Z. Chen, C. Xi and K. Kuroda, *Langmuir*, 2011, **27**, 4010-4019.

77.   X. Ding, C. Yang, T. P. Lim, L. Y. Hsu, A. C. Engler, J. L. Hedrick and Y.-Y. Yang, *Biomaterials*, 2012, **33**, 6593-6603.

78.   K. Lim, R. R. Y. Chua, B. Ho, P. A. Tambyah, K. Hadinoto and S. S. J. Leong, *Acta biomater*, 2015, **15**, 127-138.

79.   J. Liu, J. Li, B. Yu, B. Ma, Y. Zhu, X. Song, X. Cao, W. Yang and F. Zhou, *Langmuir*, 2011, **27**, 11324-11331.

80. E. Faure, E. Halusiak, F. Farina, N. Giamblanco, C. Motte, M. Poelman, C. Archambeau, C. c. Van De Weerdt, J. Martial and C. Jérôme, *Langmuir*, 2012, **28**, 2971-2978.

81. F. Yu, S. Chen, Y. Chen, H. Li, L. Yang, Y. Chen and Y. Yin, *J Mol Struct*, 2010, **982**, 152-161.

82. Q. Wei, X. Pei, J. Hao, M. Cai, F. Zhou and W. Liu, *Adv Mater Interfaces*, 2014, **1**.

83. S. M. Kang, I. You, W. K. Cho, H. K. Shon, T. G. Lee, I. S. Choi, J. M. Karp and H. Lee, *Angew Chem Int Ed*, 2010, **49**, 9401-9404.

84. Q. Ye, X. Wang, S. Li and F. Zhou, *Macromolecules*, 2010, **43**, 5554-5560.

85. C. I. Biggs, M. Walker and M. I. Gibson, *Biomacromolecules*, 2016, **17**, 2626-2633.

86. A. Taglietti, C. R. Arciola, A. D'Agostino, G. Dacarro, L. Montanaro, D. Campoccia, L. Cucca, M. Vercellino, A. Poggi, P. Pallavicini and L. Visai, *Biomaterials*, 2014, **35**, 1779-1788.

87. M. Mazur, A. Barras, V. Kuncser, A. Galatanu, V. Zaitzev, K. V. Turcheniuk, P. Woisel, J. Lyskawa, W. Laure and A. Siriwardena, *Nanoscale*, 2013, **5**, 2692-2702.

88. M. Arslan, T. N. Gevrek, J. Lyskawa, S. Szunerits, R. Boukherroub, R. Sanyal, P. Woisel and A. Sanyal, *Macromolecules*, 2014, **47**, 5124-5134.

89. L. Wang, G. Li, Y. Lin, Z. Zhang, Z. Chen and S. Wu, *Polym Chem*, 2016, **7**, 4964-4974.

90.   A. S. Goldmann, C. Schödel, A. Walther, J. Yuan, K. Loos and A. H. Müller, *Macromol rapid commun*, 2010, **31**, 1608-1615.

91.   H. O. Ham, Z. Liu, K. Lau, H. Lee and P. B. Messersmith, *Angew Chem Int Ed*, 2011, **50**, 732-736.

92.   H. Lee, J. Rho and P. B. Messersmith, *Adv Mater*, 2009, **21**, 431-434.

93.   A. Rai and C. C. Perry, *J Mater Chem*, 2012, **22**, 4790-4796.

94.   Y. M. Shin, I. Jun, Y. M. Lim, T. Rhim and H. Shin, *Macromol Mater Eng*, 2013, **298**, 555-564.

95.   B.-H. Choi, Y. S. Choi, D. S. Hwang and H. J. Cha, *Tissue Eng Pt C Methods*, 2011, **18**, 71-79.

96.   Y. Cong, T. Xia, M. Zou, Z. Li, B. Peng, D. Guo and Z. Deng, *J Mater Chem B*, 2014, **2**, 3450-3461.

97.   X. Liu, J. Cao, H. Li, J. Li, Q. Jin, K. Ren and J. Ji, *Acs Nano*, 2013, **7**, 9384-9395.

98.   M. Nurunnabi, Z. Khatun, M. Nafiujjaman, D.-g. Lee and Y.-k. Lee, *ACS appl mater interfaces*, 2013, **5**, 8246-8253.

99.   M. D. Hager, P. Greil, C. Leyens, S. van der Zwaag and U. S. Schubert, *Adv Mater*, 2010, **22**, 5424-5430.

100.   B. Blaiszik, S. Kramer, S. Olugebefola, J. S. Moore, N. R. Sottos and S. R. White, *Ann Rev Mater Res*, 2010, **40**, 179-211.

101.   E. Vaccaro and J. H. Waite, *Biomacromolecules*, 2001, **2**, 906-911.

102.   P. S. Yavvari and A. Srivastava, *J Mater Chem B*, 2015, **3**, 899-910.

103. P. Sun, J. Wang, X. Yao, Y. Peng, X. Tu, P. Du, Z. Zheng and X. Wang, *ACS appl mater interfaces*, 2014, **6**, 12495-12504.

104. H. Ceylan, M. Urel, T. S. Erkal, A. B. Tekinay, A. Dana and M. O. Guler, *Adv Funct Mater*, 2013, **23**, 2081-2090.

105. Z. Shafiq, J. Cui, L. Pastor-Pérez, V. San Miguel, R. A. Gropeanu, C. Serrano and A. del Campo, *Angew Chem*, 2012, **124**, 4408-4411.

106. M. Krogsgaard, A. Andersen and H. Birkedal, *Chem Commun*, 2014, **50**, 13278-13281.

107. N. Holten-Andersen, A. Jaishankar, M. J. Harrington, D. E. Fullenkamp, G. DiMarco, L. He, G. H. McKinley, P. B. Messersmith and K. Y. C. Lee, *J Mater Chem B*, 2014, **2**, 2467-2472.

108. M. Krogsgaard, M. R. Hansen and H. Birkedal, *J Mater Chem B*, 2014, **2**, 8292-8297.

109. D. Roy, J. N. Cambre and B. S. Sumerlin, *Chem Commun*, 2009, DOI: 10.1039/B900374F, 2106-2108.

110. J. N. Cambre, D. Roy and B. S. Sumerlin, *J Polym Sci A Polyme Chem*, 2012, **50**, 3373-3382.

111. J. Yan, G. Springsteen, S. Deeter and B. Wang, *Tetrahedron*, 2004, **60**, 11205-11209.

112. L. He, D. E. Fullenkamp, J. G. Rivera and P. B. Messersmith, *Chem Commun*, 2011, **47**, 7497-7499.

113. M. Nakahata, S. Mori, Y. Takashima, A. Hashidzume, H. Yamaguchi and A. Harada, *ACS Macro Lett*, 2014, **3**, 337-340.

114. M. Vatankhah-Varnoosfaderani, A. GhavamiNejad, S. Hashmi and F. J. Stadler, *ChemCommun*, 2013, **49**, 4685-4687.

115. M. Vatankhah-Varnoosfaderani, S. Hashmi, A. GhavamiNejad and F. J. Stadler, *Polym Chem*, 2014, **5**, 512-523.

116. J. Su, F. Chen, V. L. Cryns and P. B. Messersmith, *J Am Chem Soc*, 2011, **133**, 11850-11853.

117. D. Tarus, E. Hachet, L. Messager, B. Catargi, V. Ravaine and R. Auzély-Velty, *Macromol Rapid Commun*, 2014, **35**, 2089-2095.

118. D. Roy and B. S. Sumerlin, *ACS Macro Lett*, 2012, **1**, 529-532.

119. K. T. Kim, J. J. L. M. Cornelissen, R. J. M. Nolte and J. C. M. v. Hest, *J Am Chem Soc*, 2009, **131**, 13908-13909.

120. C. C. Deng, W. L. Brooks, K. A. Abboud and B. S. Sumerlin, *ACS Macro Lett*, 2015, **4**, 220-224.

121. M. Vatankhah-Varnoosfaderani, A. GhavamiNejad, S. Hashmi and F. J. Stadler, *Macromol Rapid Commun*, 2015, 36, 447-452.

2 Mussel-inspired antifouling coatings bearing polymer loops[2]

2.1 Introduction

Nonspecific protein adsorption to material surfaces is generally considered as the first stage in a "successional" process of fouling community development, which would facilitate the subsequential adsorption of bacteria and cells to form biofouling films, hindering the effectiveness of various medical devices and inducing further inflammatory responses and infection.[1-3] Therefore, improving the antifouling properties of material surfaces is of great significance to biomedical applications. Various strategies have been developed for surface modification, among which antifouling polymer coatings have been extensively studied because the easy control of their chemistry and architecture can provide great mechanical and chemical robustness with desired long-term stability.[4-9] Self-assembly, grafting-to method via physical adsorption or chemical linkage, and grafting-from method via surface-initiated polymerization have been commonly applied for preparing antifouling polymer coatings.[10-14] The latter method allows a closer control of the architecture of the coated polymer layer; however, the multi-step treatment involving surface pre-treatment, immobilization of surface initiators and controlled polymerization normally leads to increased production cost. On this aspect, grafting-to method enjoys great superiority

---

due to its ease of operation, especially for antifouling polymers conjugated with stable and generally applicable surface anchors.

Inspired by mussel's remarkable underwater adhesion capability to various surfaces by secreting adhesive proteins in which 3,4-Dihydroxyphenyl-L-alanine (DOPA) plays a significant role,[15-20] much effort has been dedicated to the preparation of antifouling polymers conjugated to mussel-mimetic polymeric anchors.[21-26] End-tethered to target surfaces through stable anchoring, the polymer chains tend to be extended and partially oriented to avoid excluded volume effects, forming a layer of polymer brushes. Due to the strong hydration and steric repulsion of polymer chains, the surfaces bearing polymer brushes generally exhibit considerable antifouling performance. When polymers possessing adhesive anchors on both chain ends come into contact with a surface, loops are expected to be formed. However, very limited research has been conducted on polymer loops, among which emphasis has been placed on understanding loop formation process through experiments or theoretical modelling.[27, 28] To the best of our knowledge, no experimental research has been reported on studying the antifouling performance of surface bearing polymer loops, especially the ones formed using mussel-mimetic adhesive anchors, nor has the comparison of antifouling performance between loops-bearing surface and brushes-bearing surface been studied.
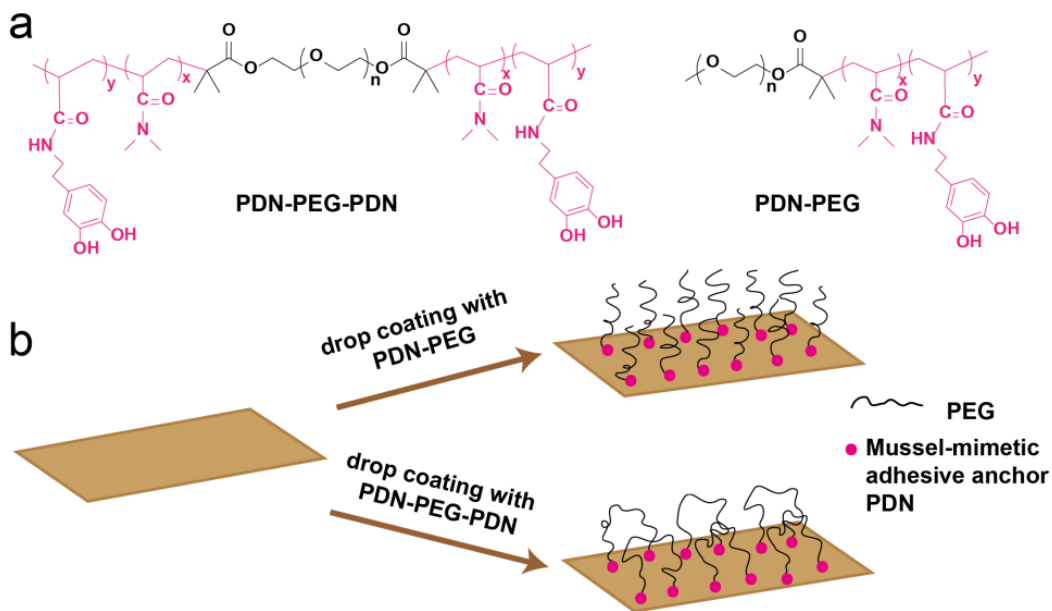
Figure 2.1 (a) Chemical structure of the triblock copolymer PDN-PEG-PDN and the diblock copolymer PDN-PEG. (b) Schematics of the preparation of surfaces bearing polymer brushes and polymer loops using drop coating method.

Herein we report the preparation of antifouling coatings bearing polymer loops using an *ABA* triblock copolymer by simple drop coating method. Mussel-inspired catechol-functionalized poly(*N,N*-dimethylacrylamide) and poly(ethylene glycol) (PEG) were selected as the adhesive *A* block and antifouling *B* block, respectively. This copolymer poly[(*N,N*-dimethylacrylamide)$_{15}$-*co*-(*N*-3,4-dihydroxyphenethyl acrylamine)$_2$]-*b*-poly(ethylene glycol)$_{90}$-*b*-poly[(*N,N*-dimethylacrylamide)$_{15}$-*co*-(*N*-3,4-dihydroxyphenethyl acrylamine)$_2$] (PDN-PEG-PDN, Figure 2.1) was synthesized by reversible addditional fragment transfer (RAFT) polymerization. By simple drop coating, this triblock copolymer can form a layer of loops onto substrate surface with the assistance of two adhesive

anchoring blocks, which is compared with a layer of brushes prepared by drop-coating a diblock copolymer poly[(*N,N*-dimethylacrylamide)$_{15}$-*co*-(*N*-3,4-dihydroxyphenethyl acrylamine)$_2$]-*b*-poly(ethylene glycol)$_{45}$ (PDN-PEG, Figure 2.1) with the same anchoring block and half of the middle PEG chain length.

2.2   Materials and methods

2.2.1   Polymer synthesis

N,N-Dimethylacrylamide (DMA) was purchased from Sigma-Aldrich and passed through a short column of basic Aluminum oxide. Macro-RAFT agents RAFT-PEG$_{90}$-RAFT **(2)** and PEG$_{45}$-RAFT**(3)** were synthesized by attaching the chain transfer agent (S)-1-dodecyl-(S')-(α,α'-dimethyl-α''-acetic acid) trithiocarbonate **(1)** to ends of PEG precursors following a reported procedure.[29] *N*-(3,4-Dihydroxyphenylethyl)acrylamide **(4)** was synthesized according to a modified procedure reported.[30] All the other chemicals were purchased from Aldrich and used as received.

Macro-RAFT agent RAFT-PEG$_{90}$-RAFT (0.2365 g, 0.05 mmol), *N*-(3,4-Dihydroxyphenyl-ethyl)acrylamide (0.0828 g, 0.4 mmol), DMA (0.1782 g, 1.8 mmol) and azobisisobutyronitrile (AIBN) (0.0041 g, 0.025 mmol) were dissolved in 1 ml dioxane. After purging N$_2$ for 15 min, the whole system was stirred at 78 °C for 1 h. The final reaction mixture was dissolved in a small amount of dichloromethane and precipitated twice in ethyl ether. The resulting polymer was collected by filtration and dried in vacuum as a white solid of 0.3933 g. The composition of the resulting polymer was characterized by ^{1}H NMR and was

determined as poly{DMA$_{15}$-*co*-[*N*-(3,4-dihydroxyphenethyl)acrylamide]$_2$}-*b*-PEG$_{90}$-*b*-poly{DMA$_{15}$-*co*-[*N*-(3,4-dihydroxyphenethyl) -acrylamide]$_2$}(denoted as PDN-PEG-PDN**(5)**, Figure 2.2).
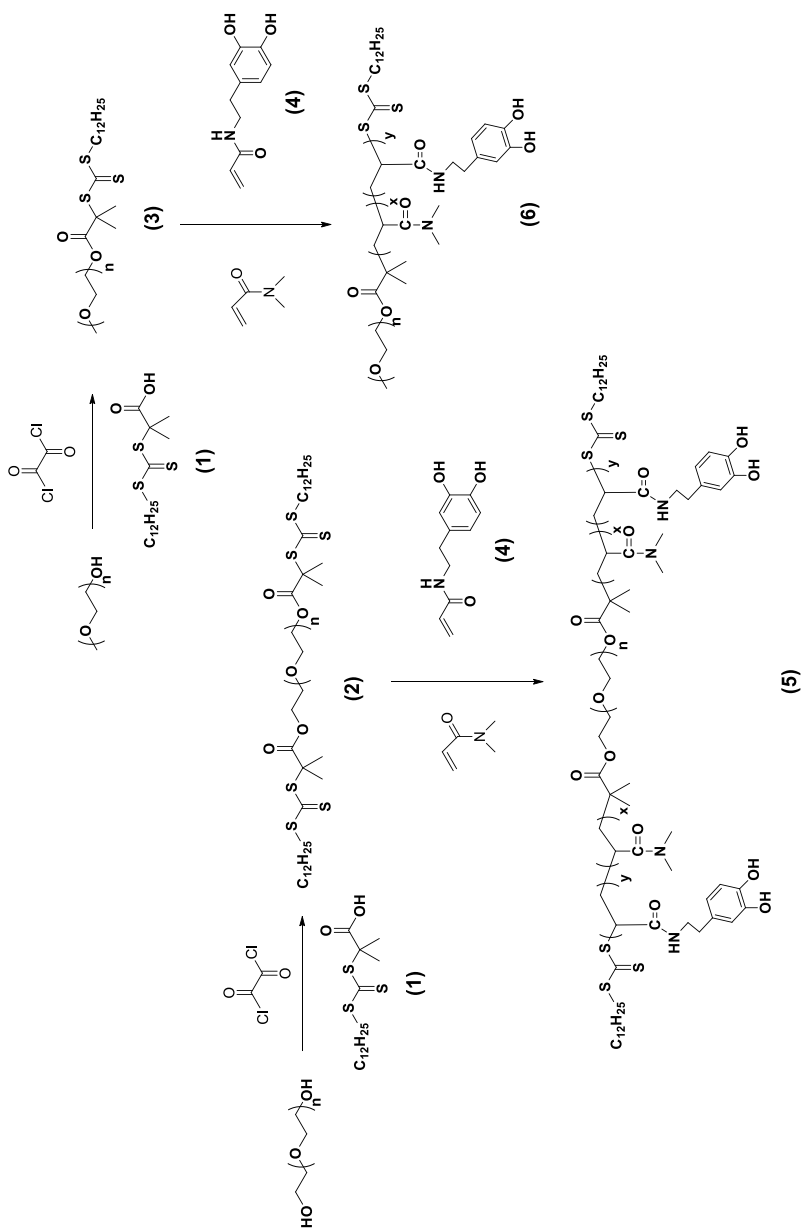
Figure 2.2 Synthesis routes for PDN-PEG-PDN(5) and PDN-PEG(6).

Similar procedures as those described above were used to prepare diblock copolymer PDN-PEG. A typical example was shown as follows: PEG$_{45}$-RAFT

(0.2365 g, 0.1 mmol), *N*-(3,4-Dihydroxyphenylethyl)acrylamide (0.0828 g, 0.4 mmol), DMA (0.1782 g, 1.8 mmol) and AIBN (0.0041 g, 0.025 mmol) were dissolved in 1 ml dioxane. The whole system was purged with N_2 for 15 min and then stirred at 78 °C for 1 h. The resulting polymer was precipitated twice with ethyl ether and vacuum-dried to obtain a white solid of 0.2786 g. The composition of the resulting polymer was characterized by ^{1}H NMR and was determined as poly{DMA$_{15}$-*co*-[*N*-(3,4-dihydroxyphenethyl)acrylamide]$_2$}-*b*-PEG$_{45}$ (denoted as PDN-PEG**(6)**, Figure 2.2). Raw NMR data and GPC curves were illustrated as Figure S2.1 and S2.2 in Appendix.

2.2.2   Surface preparation

The polymer films for surface force measurement were prepared by drop coating method on mica surface. Several drops of polymer solution (1 mg/ml in acetate buffer, pH 5.0) were placed on the mica surface in a water vapor saturated petri dish. After 30 minutes of adsorption the surface was rinsed with a capacious amount of acetate buffer and deionized (DI) water for several times and dried in vacuum. The same procedure was applied for the preparation of bovine serum albumin (BSA) film on mica. Several drops of 5 wt% BSA in phosphate buffer saline (PBS, pH 7.4) were placed onto the mica surface. After 30 minutes of adsorption the surface was rinsed with DI water and dried in vacuum.

Dry film thickness of the polymer film was measured in situ using multiple beam interferometry employing fringes of equal chromatic order (FECO) coupled with the surface forces apparatus (SFA). The polymer film thickness was also confirmed by drop-coating a film on silicon wafer cleaned with ethanol and

UV/ozone using a Sopra GESP-5 spectroscopic ellipsometer (France).

2.2.3   Surface force measurements in aqueous solution using SFA

In this study the interactions between prepared surfaces were measured in NaCl solution using an SFA. Two back-silvered mica sheets of the same thickness (1-5 µm) were separately glued onto two cylindrical silica disks (radius R = 2 cm). After drop-coated with the synthetic polymers, the two prepared surfaces were mounted in the SFA chamber in a crossed-cylinder conformation, of which the interactions was locally equivalent to a sphere of radius R interacting with a flat surface or two spheres of radius 2R when the surface separation D was much smaller than R (D « R). In this study, the interaction forces between two polymer-bearing surfaces and between a polymer-bearing surface and a protein-bearing surface were measured in NaCl solution. For each fixed experimental condition, the surface force measurements were repeated for at least three different positions of each pair of surfaces with at least two pairs of surfaces to ensure the reproducibility.

2.2.4   AFM imaging

Surface morphology of the mica surface coated with polymers or BSA were characterized using an atomic force microscope (AFM) (MFP-3D, Asylum, Santa Barbara, CA). The sample surfaces were imaged using tapping mode in air. For each AFM imaging, at least three samples were imaged at different (>3) positions of each sample and typical images were presented.

2.2.5   Protein adsorption tests using QCM-D

Antifouling properties of the polymer surfaces were examined using a QCM-D (Q-sense E4, Sweden). A typical procedure for a QCM-D measurement is shown as

follows. Before the experiment, silica sensors were placed in a UV/Ozone cleaning chamber (UV/Ozone ProCleaner, BioForce Nanosciences Inc, Iowa, USA) for 10 minutes followed by an immersion in 2% sodium dodecyl sulphate (SDS) for 20 minutes. After rinsed with DI water and dried with nitrogen, the sensors were placed in the UV/Ozone chamber for another 10 minutes. Then the cleaned silica sensors were drop coated with different polymers (1 mg/ml in acetate buffer, pH 5.0) and mounted into the QCM-D chamber. The system was firstly run in a PBS buffer to attain a stable baseline, then the sensor was exposed to BSA solution (5 wt% in PBS buffer, pH 7.4) introduced at a flow rate of 50 μL/min before rinsed with pure PBS buffer. The shifts in resonance frequency and the changes in energy dissipation, corresponding to the 3rd, 5th and 7thovertones, were recorded and fitted to the Voigt viscoelastic model in the QTools software to obtain the mass of adsorbed proteins. All the experiments were performed at 25°C and repeated for at least three times.

2.3   Results and discussion

2.3.1   Characterization of surfaces bearing polymer loops and polymer brushes

Mica surfaces coated with PDN-PEG and PDN-PEG-PDN were imaged with AFM and their surface morphologies are shown in Figure 2.3b and d. Both surfaces were rather smooth with a root-mean-square (rms) roughness of ~0.2 nm and ~0.3 nm, respectively. The Flory radius (R_F) of PEG chain for PDN-PEG was calculated using equation (i),where a is the monomer length (0.35 nm),[31] N is the number of monomers per polymer chain and υ is 0.6 for

a good solvent.[32] The average distance between grafted sites S was calculated using a dry film thickness measured by SFA through equation (ii),[33] where σ is the graft density, ρ is the polymer density (~1.2 g/cm^3), l is the dry film thickness (3.3 nm), N_A is the Avogadro's constant and M is the molecular weight of the polymer. As R_F (3.4 nm) was larger than S (1.3 nm), the coated PDN-PEG was in a brush regime.[33]

$$R_F = aN^{\upsilon} \qquad \text{(i)}$$

$$\sigma = \frac{\rho l N_A}{M} = \frac{1}{S^2} \qquad \text{(ii)}$$
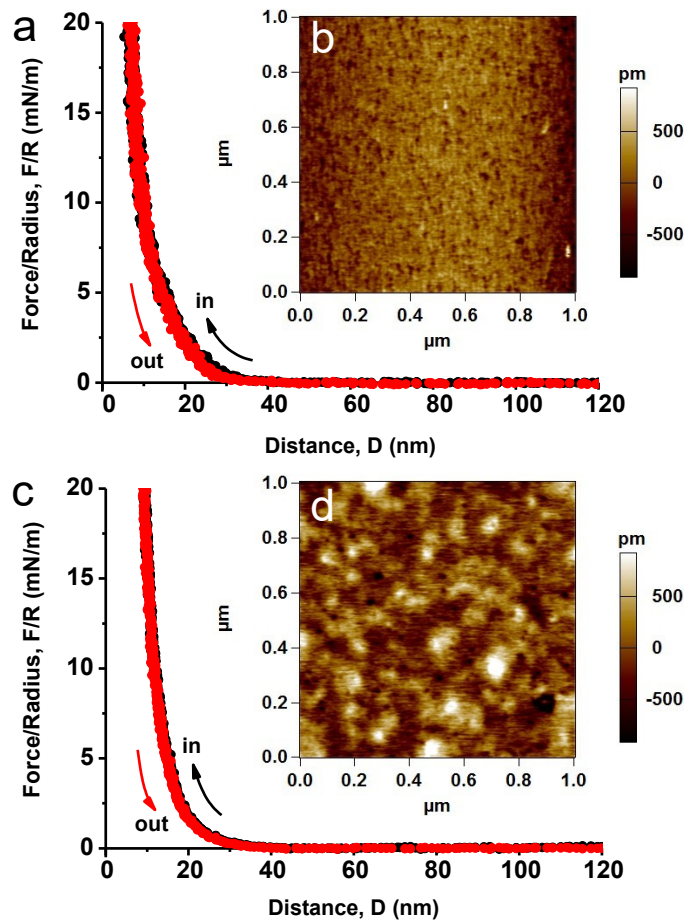
Figure 2.3 (a) Force-distance profiles measured between symmetric surfaces coated with PDN-PEG in 1mM NaCl solution and (b) AFM topographic image showing

the surface morphology of PDN-PEG film. (c) Force-distance profiles measured between symmetric surfaces coated with PDN-PEG-PDN in 1mM NaCl solution and (d) surface morphology of the PDN-PEG-PDN film.

SFA has been widely used for direct force measurements of numerous material surfaces as a function of the absolute surface separation distance D as determined using an optical technique called multiple beam interferometry by employing fringes of equal chromatic order (FECO).[34-39] In this study, force-distance profiles measured between symmetric surfaces coated with PDN-PEG (Figure 2.3a) and with PDN-PEG-PDN (Figure 2.3c) in 1mM NaCl solution were obtained using SFA in experimental configurations shown in Figure 2.4, which were also used to confirm the successful formation of polymer loops. For a typical force measurement, the two surfaces were first brought together to reach a "hard wall", and after contacting for a certain period of time, the two surfaces were separated apart. Here "hard wall" refers to a confined distance between two mica surfaces which did not change significantly with increasing normal load. The reference distance (D=0) was set as the adhesive contact between two bare mica surfaces in air. As shown in Figure 2.3a and c, for both PDN-PEG and PDN-PEG-PDN surfaces, pure repulsive forces were measured and the force curves obtained during approach and separation almost overlapped, showing no adhesion hysteresis.[40] This interaction behaviour could be explained by the interpenetration hindrance due to large excluded volume of the hydrated PEG chains which led to the steric repulsion between opposing swollen PEG

chains. Previous studies showed that if the doubly bound chain ends were not strongly adsorbed to the same substrate, the formation of bridges across the layer gap would be favoured due to the entropic advantage, thus attraction would be measured during the loops-loops interaction.[41-44] However it was also proposed that by applying triblocks with longer or more strongly adsorbed end blocks, the formation of bridges could be avoided.[45] In the present work, the mussel-mimetic adhesive anchors can hold sufficiently fast to the mica surfaces so no bridging occurred, resulting in the pure repulsion measured. It is noted that for the opposing loops-bearing surfaces of PDN-PEG-PDN, if thick coatings were prepared by spin coating using relatively high concentration of polymer solution, there would inevitably be free adhesive anchors that led to strong adhesion measured during separation (Figure S2.3 in Appendix). Therefore, for all the surface forces measurements shown in the main text, single-layered coating was achieved by drop coating method using a relatively low concentration of polymer (1mg/ml) in acetate buffer solution (as further discussed below).
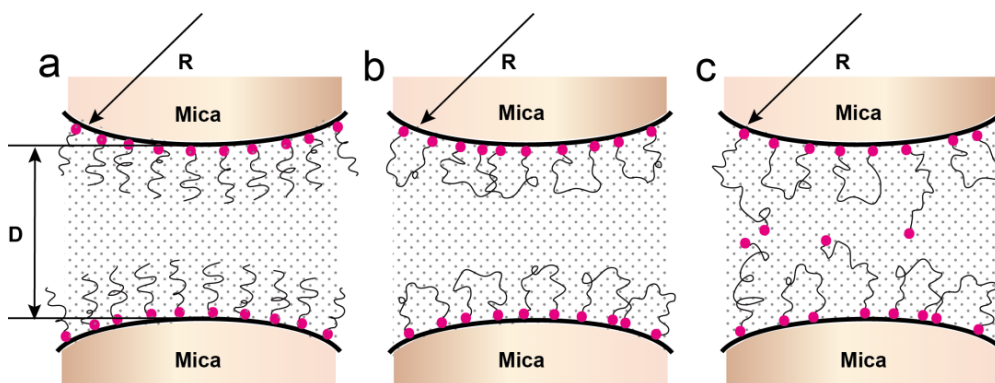
Figure 2.4 Simplified schematics of experimental configurations for opposing polymer layers in SFA measurements: (a) brushes formed by PDN-PEG, (b) loops

formed by PDN-PEG-PDN, (c) combination of brushes and loops with free adhesive anchors formed by PDN-PEG-PDN.

The chain length of the extended PEG part for PDN-PEG was calculated as 15.8 nm using equation $L=N \times a$, where N is the number of monomers per polymer chain and $a \approx 0.35$ nm[31] is the effective monomer length. For interactions measured between symmetric surfaces bearing polymer brushes (Figure 2.3a), repulsion started from a distance of around 30 nm which was roughly twice of the extended PEG chain length (15.8 nm), proving that the coated PDN-PEG were single layered. For interactions measured between symmetric surfaces bearing polymer loops (Figure 2.3c), if the two mussel-mimetic adhesive anchors (shown as red dots in Figure 2.4) were not tethered to the same mica surface (in other words there were free adhesive anchors swaying as illustrated in Figure 2.4c), adhesive force caused by the bridging effect would be measured as aforementioned or the repulsion would appear at a much longer distance than 30 nm if only one free adhesive anchor was fixed on the substrate surface. However, in Figure 2.3c only pure repulsion starting at ~30 nm was measured, confirming the successful formation of a single layered polymer loops with PDN-PEG-PDN.

The dry film thickness of PDN-PEG-PDN and PDN-PEG layer were both measured as 3.3 nm by SFA, and the graft density of PDN-PEG-PDN chains was calculated using equation (2) and found to be half of the value of PDN-PEG (~0. 6 chains/nm^2) due to the doubled molecular weight of PDN-PEG-PDN. When the graft density of chain ends (or so-called end graft

density) was referred to, the prepared loops-bearing coating and brushes-bearing coating had the same end graft density. With identical end graft density, a layer of loops could be viewed as closely equivalent to a layer of regular brushes with half of the loop chain length, if seen by "cutting" the loops at their midpoint.[46] Thusly the loops-bearing coating formed by PDN-PEG-PDN could be comparable with the brushes-bearing coating formed by PDN-PEG, facilitating the further meaningful comparison of their antifouling performance.

2.3.2 Antifouling performance of surfaces bearing polymer loops and polymer brushes

Polymers were then drop coated to silica sensors to study the antifouling performance of different coatings against BSA using a QCM-D. As shown in Figure 2.5a, for bare silica or silica sensors coated with different polymers, a strong negative frequency shift and a positive dissipation shift were observed upon the introduction of a 5wt% BSA solution in PBS into the QCM-D chamber, indicating the adsorption of BSA on all tested surfaces. After stable frequency and dissipation shift curves were attained, PBS was introduced into the chamber to remove the loosely-bound proteins, resulting in an increase in frequency and a decrease in dissipation. The QCM-D data were fitted using the Voigt viscoelastic model to obtain the mass of proteins adsorbed on the different surfaces before and after rinsing with PBS. As shown in Figure 2.5b, less proteins were absorbed on the polymer brushes-coated sensor (1980.0 ± 210.6 ng/cm^2) than on bare silica surface (3775.2 ± 326.4 ng/cm^2), while the

protein adsorption was the least on polymer loops-coated sensor (567.6 ± 61.6 ng/cm^2). After rinsed with PBS, a significant portion of the BSA proteins was washed off and the remanent BSA on the loops-coated and brushes-coated sensor were 31.7 ± 2.9 ng/cm^2 and 277.2 ± 32.4 ng/cm^2, respectively; while for the uncoated silica sensor, the BSA remained on the surface was 937.2 ± 82.3 ng/cm^2. The dry film thickness of the polymer coatings on silica sensors was measured to be 3.3 nm using ellipsometry, which is consistent with the thickness determined using SFA. This result is expected as silica possesses very similar surface chemistry as mica and the surface coatings for SFA and QCM-D experiments were prepared under the same conditions. Therefore, the end graft density of PDN-PEG-PDN and PDN-PEG was very similar on silica, and the protein adsorption results indicate that the loops-coated surface shows better protein reduction (or antifouling) performance (94.4%) than the brushes-coated sensor (86.0%). It is expected that optimizing the graft density would further enhance the protein-reduction performance of the loops-coated surfaces.

Polyethylene glycol monomethylether PEG$_{45}$ and polyethylene glycol PEG$_{90}$ were also coated onto silica sensors (mainly through hydrogen bonding) for comparison. Evaluated following the same QCM-D measurements for protein adsorption as that in Figure 2.5a, the physisorbed PEG layers only demonstrated slightly enhanced antifouling properties as compared to the bare silica surfaces, showing weaker antifouling performance than that of brushes-coated and loops-coated surfaces (Figure S2.4 in Appendix) which was most likely attributed to the

random conformation of the physisorbed PEG chains with smaller excluded volume, and less steric hindrance as compared to the chemically grafted PDN-PEG brushes and PDN-PEG-PDN loops assisted by the PDN adhesive anchors.
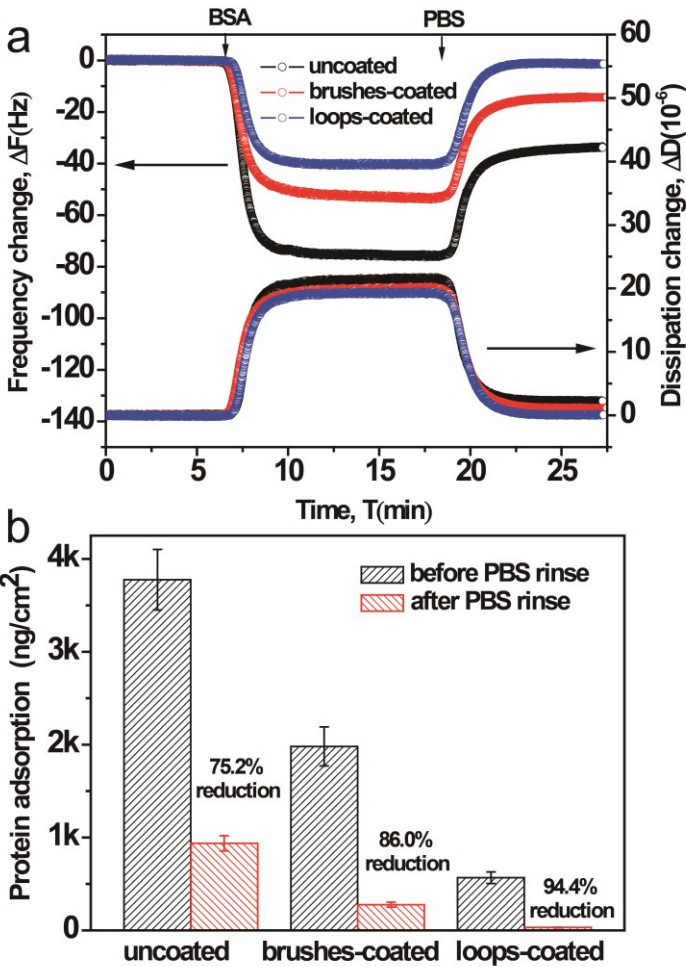
Figure 2.5 (a) Changes in frequency and dissipation associated with the adsorption of protein BSA on bare silica sensor, silica sensors coated with PDN-PEG brushes and PDN-PEG-PDN loops using a QCM-D. (b) Protein adsorption on the three substrate surfaces.

2.3.3 Antifouling mechanism of surfaces bearing polymer loops

The interactions between a PDN-PEG-PDN loop layer and a BSA film coated on mica were measured in 1 mM NaCl solution using the SFA. As illustrated in Figure 2.6a, the hard wall separation was found to be 10 nm, which was close to that observed in the symmetric loops-loops interaction, indicating the successful deposition of BSA on mica as also confirmed by AFM imaging shown in Figure 2.6b. Previous studies have shown that weak attraction could be measured when proteins were pressed into a layer of polymer brushes at relatively high load, most likely due to the rearrangements in polymer conformation and protein penetration into the polymer core.[47] Figure 2.6a shows that pure repulsive forces were measured between PDN-PEG-PDN loops and BSA during both approach and separation and no adhesion hysteresis was detected. These results indicate that the polymer loops could better adapt external compression and reduce the protein penetration, exhibiting great potential in antifouling applications. The interactions between symmetric loops-bearing surfaces in aqueous solutions of different salt concentrations (0.001 M, 0.01 M and 0.1 M NaCl) were also measured and similar force-distance profiles were obtained (Figure S2.5 in Appendix), which indicates that the PDN-PEG-PDN loop coating was neutrally charged and the repulsive forces between the loops-bearing coating and proteins arose from the steric hindrance of the extended PEG loops.
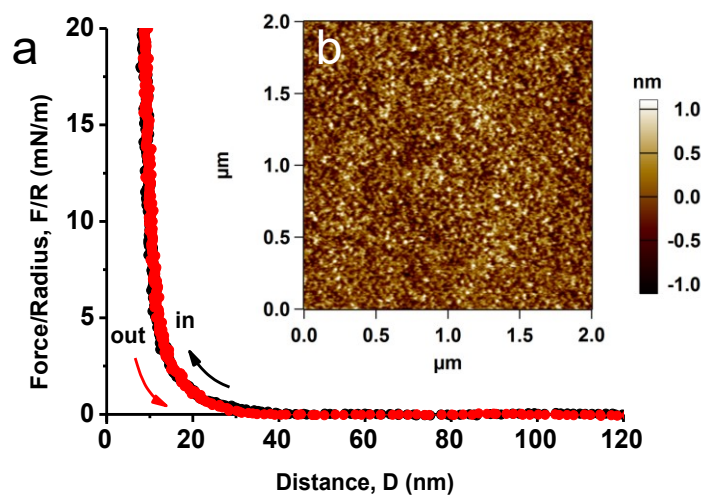
Figure 2.6 (a) Force-distance profile between a PDN-PEG-PDN film and a BSA film in 1 mM NaCl solution. (b) Topographic AFM image of BSA absorbed on mica surface.

2.4 Conclusion

In summary, a mussel-inspired *ABA* triblock copolymer PDN-PEG-PDN was synthesized and used to prepare surfaces bearing polymer loops. By direct drop coating, this triblock copolymer can form a layer of loops onto substrate surfaces with the assistance of two adhesive anchoring blocks. The mussel-inspired adhesive anchors can provide stable anchoring points and facilitate the grafting of PEG chains to achieve large excluded volume. A diblock copolymer PDN-PEG was also synthesized which could form a brush layer on substrate surfaces by drop coating. The QCM-D protein adsorption tests demonstrate that the loops-coated surfaces show stronger protein-reduction performance over the brushes-coated surface with similar end graft density. The superior antifouling property of PDN-PEG-PDN loops is mainly

attributed to the strong steric hindrance of the neutrally charged polymer loops as confirmed by direct force measurements.

2.5 References

1.   C. Werner, M. F. Maitz and C. Sperling, *J Mater Chem*, 2007, **17**, 3376-3384.

2.   H. Otsuka, Y. Nagasaki and K. Kataoka, *Adv Drug Delivery Rev*, 2003, **55**, 403-419.

3.   L. Li, B. Yan, J. Yang, L. Chen and H. Zeng, *Adv Mater*, 2015, **27**, 1294-1299.

4.   M. Krishnamoorthy, S. Hakobyan, M. Ramstedt and J. E. Gautrot, *Chem Rev*, 2014, **114**, 10976-11026.

5.   S. J. Sofia, V. Premnath and E. W. Merrill, *Macromolecules*, 1998, **31**, 5059-5070.

6.   B. Dong, S. Manolache, A. C. Wong and F. S. Denes, *Polym Bull*, 2011, **66**, 517-528.

7.   W. Norde and D. Gage, *Langmuir*, 2004, **20**, 4162-4167.

8.   L. D. Unsworth, H. Sheardown and J. L. Brash, *Langmuir*, 2008, **24**, 1924-1929.

9.   W. Zhao, Q. Ye, H. Hu, X. Wang and F. Zhou, *J Mater Chem B*, 2014, **2**, 5352-5357.

10.   S. Maity, S. Nir, T. Zada and M. Reches, *Chem Commun*, 2014, **50**, 11154-11157.

11.   J. H. Cho, K. Shanmuganathan and C. J. Ellison, *Acs Appl Mater Interfaces*, 2013, **5**, 3794-3802.

12.   X. Ding, C. Yang, T. P. Lim, L. Y. Hsu, A. C. Engler, J. L. Hedrick and Y.-Y. Yang, *Biomaterials*, 2012, **33**, 6593-6603.

13.   J. Kuang and P. B. Messersmith, *Langmuir*, 2012, **28**, 7258-7266.

14.   M. Kobayashi, Y. Terayama, H. Yamaguchi, M. Terada, D. Murakami, K. Ishihara and A. Takahara, *Langmuir*, 2012, **28**, 7212-7222.

15.   B. P. Lee, P. B. Messersmith, J. N. Israelachvili and J. H. Waite, *Ann Rev Mater Res*, 2011, **41**, 99.

16.   M. Yu, J. Hwang and T. J. Deming, *J Am Chem Soc*, 1999, **121**, 5825-5826.

17.   H. Zeng, D. S. Hwang, J. N. Israelachvili and J. H. Waite, *Proc Natl Acad Sci*, 2010, **107**, 12850-12853.

18.   Q. Lu, D. S. Hwang, Y. Liu and H. Zeng, *Biomaterials*, 2012, **33**, 1903-1911.

19.   Q. Lu, D. X. Oh, Y. Lee, Y. Jho, D. S. Hwang and H. Zeng, *Angew Chem*, 2013, **125**, 4036-4040.

20.   A. Ma, Y. Xie, J. Xu, H. Zeng and H. Xu, *Chem Commun*, 2015, **51**, 1469-1471.

21.   A. R. Statz, R. J. Meagher, A. E. Barron and P. B. Messersmith, *J Am Chem Soc*, 2005, **127**, 7972-7973.

22.   J. L. Dalsin, B.-H. Hu, B. P. Lee and P. B. Messersmith, *J Am Chem Soc*, 2003, **125**, 4253-4258.

23. O. Pop-Georgievski, D. Verreault, M.-O. Diesner, V. Proks, S. Heissler, F. e. Rypáček and P. Koelsch, *Langmuir*, 2012, **28**, 14273-14283.

24. G. Li, G. Cheng, H. Xue, S. Chen, F. Zhang and S. Jiang, *Biomaterials*, 2008, **29**, 4592-4597.

25. D. Hong, K. Bae, S.-P. Hong, J. H. Park, I. S. Choi and W. K. Cho, *Chem Commun*, 2014, **50**, 11649-11652.

26. L. Li, W. Smitthipong and H. Zeng, *Polym Chem*, 2015, **6**, 353-358.

27. Z. Haung, H. Ji, J. Mays, M. Dadmun, G. Smith, D. Bedrov and Y. Zhang, *Langmuir*, 2009, **26**, 202-209.

28. Z. Huang, H. Ji, J. W. Mays and M. D. Dadmun, *Macromolecules*, 2008, **41**, 1009-1018.

29. Y. He and T. P. Lodge, *Macromolecules*, 2008, **41**, 167-174.

30. J. Nishida, M. Kobayashi and A. Takahara, *ACS Macro Lett*, 2013, **2**, 112-115.

31. P. L. Hansen, J. A. Cohen, R. Podgornik and V. A. Parsegian, *Biophys J*, 2003, **84**, 350-355.

32. I. Teraoka, *Polymer solutions: an introduction to physical properties*, Wiley. com, 2002.

33. P. De Gennes, *Adv Colloid Interface*, 1987, **27**, 189-209.

34. J. N. Israelachvili and G. E. Adams, *J Chem Soc Faraday Trans 1*, 1978, **74**, 975-1001.

35. G. Luengo, F.-J. Schmitt, R. Hill and J. Israelachvili, *Macromolecules*, 1997, **30**, 2482-2494.

36. H. Zeng, Y. Tian, T. H. Anderson, M. Tirrell and J. N. Israelachvili, *Langmuir*, 2007, **24**, 1173-1182.

37. Q. Lu, J. Wang, A. Faghihnejad, H. Zeng and Y. Liu, *Soft Matter*, 2011, **7**, 9366-9379.

38. D. S. Hwang, H. Zeng, A. Srivastava, D. V. Krogstad, M. Tirrell, J. N. Israelachvili and J. H. Waite, *Soft Matter*, 2010, **6**, 3232-3236.

39. J. Israelachvili, Y. Min, M. Akbulut, A. Alig, G. Carver, W. Greene, K. Kristiansen, E. Meyer, N. Pesika and K. Rosenberg, *Rep Prog Phys*, 2010, **73**, 036601.

40. L. Zhang, H. Zeng and Q. Liu, *J Phys Chem C*, 2012, **116**, 17554-17562.

41. L. Dai and C. Toprakcioglu, *Macromolecules*, 1992, **25**, 6000-6006.

42. D. Cao and J. Wu, *Langmuir*, 2006, **22**, 2712-2718.

43. L. Dai, C. Toprakcioglu and G. Hadziioannou, *Macromolecules*, 1995, **28**, 5512-5517.

44. E. Eiser, J. Klein, T. A. Witten and L. J. Fetters, *Phys Rev Lett*, 1999, **82**, 5076.

45. S. R. Bhatia and W. B. Russel, *Macromolecules*, 2000, **33**, 5713-5720.

46. J. Klein, *J Phys Condens Matter*, 2000, **12**, A19.

47. S. Sheth and D. Leckband, *Proc Natl Acad Sci*, 1997, **94**, 8399-8404.

3 Novel mussel-inspired injectable self-healing hydrogel with anti-biofouling property[3]

3.1 Introduction

Injectable hydrogels are emerging as promising materials for biomedical applications like drug delivery because of their biocompatibility, ease of administration and minimal invasion due to their high resemblance with natural extracellular matrices.[1, 2] Bioactive molecules like drugs, proteins, DNA and antibodies can be easily mixed with precursor solutions and loaded at target site via an *in-situ* gelation right after the injection.[3-9] The release of these bioactive molecules can be performed in a sustainable or burst way on demand in response to external stimuli such as change in temperature or pH,[10, 11] introduction of redox or biomolecules,[12-14] and exposure to light or electric field.[15, 16] Encapsulated in hydrogel matrix, the loaded molecules can be maximally protected from unnecessary enzymatic degradation or hydrolyzation to retain their bioactivity, before triggered for releasing to target cells or tissues by external stimuli to fulfil their therapeutical potential. However, proteins or microorganisms could easily adhere to implanted hydrogels and form biofouling films, not only blocking the circulation of loaded biomolecules but also triggering an immune response or inflammation.[17-19]

---

[3] The content of this chapter was published in *Adv Mater*, **2015**, 27, 1294-1299.

A common means to address this challenging issue is to confer the developed hydrogels antifouling or antimicrobial properties to minimize accumulation of biofouling films on their surfaces.[20] Nonetheless, the outcome of this approach is quite limited because implanted hydrogels after injection suffer from constant external mechanical force, which could lead to certain deformation or damage of the hydrogels. Once disruption takes place *in vivo*, body fluids will intrude and simultaneously introduce nutrients and microorganisms to build up detrimental biofoulings, consequently shortening the lifespan of the hydrogel materials used and inducing further inflammatory responses. In this circumstance, a hydrogel possessing autonomous healing capability after inflicted damage will be of great significance to extend its application and lifespan, because the integrity of the broken hydrogel fragments after injection could be recovered at the target site under physiological conditions, preventing a burst release of the loaded biomolecules and enhancing delivery efficiency. The healable networks are usually constructed through interactions such as dynamic covalent bonding, noncovalent linkages, host-guest interactions and hydrogen bonding.[21-28] Recently marine mussel has inspired various applications in diverse fields,[29-32] among which the preparation of self-healing hydrogels inspired by the self-repair of mussel threads are of great significance.[33-37] Marine mussels secrete foot proteins which after a curing process can form byssus consisting of proteinaceous thread and adhesive plaque to adhere to various substrates underwater.[38] The self-repair of mussel byssal threads is mainly attributed to

the reversible metal-catechol coordination between metals like Fe^{3+} and catechol groups from an amino acid called 3,4-Dihydroxyphenyl-L-alanine (DOPA), and other interactions like cation-π interaction can also play a role.[33, 39-42] Very recently, self-repair was also demonstrated in metal-free water of synthetic polyacrylate and polymethacrylate surface-functionalized with catechols through catechol-mediated interfacial hydrogen bonds.[43]

Herein we report a new type of injectable hydrogel based on self-assembly of an *ABA* triblock copolymer with rapid self-healing properties through mussel-inspired catechol-mediated hydrogen bonding interactions and aromatic interactions and with anti-biofouling capability. Mussel-inspired catechol-functionalized poly(*N*-isopropylacrylamide) (PNIPAM) and poly(ethylene oxide) (PEO) were selected as the thermo-sensitive *A* block and hydrophilic *B* block of the copolymer, respectively. This triblock copolymer poly[(*N*-isopropylacrylamide)-*co*-(*N*-3,4-dihydroxyphenethyl acrylamide)]-*b*-poly(ethylene oxide)-*b*-poly[(*N*-isopropylacrylamide)-*co*-(*N*-3,4-dihydroxyphenethyl acrylamide)] (DNODN) was synthesized by a combination of reversible additional fragment transfer (RAFT) polymerization and a sequent replacement between an active ester and dopamine following a modified procedure reported.[44] In this work, we demonstrated that the hydrogel prepared through self-assembly of this DNODN triblock copolymer exhibited a fast thermo-responsive sol-to-gel transition and could heal autonomously from repeated damage. In addition, the DNODN hydrogel exhibited an excellent antifouling performance against nonspecific cell attachment due to the presence of a major component PEO possessing strong antifouling property. It is

also interesting to note that the catechol-functionalized PNIPAM *A* block provides a hydrophobic microenvironment which effectively retards the oxidation of catechol groups, a tricky and smart strategy adopted by marine mussels. [45]

3.2 Materials and methods

3.2.1 Polymer synthesis

All chemicals for polymer synthesis were purchased from Sigma Aldrich and were used as received. Perfluorophenyl acrylate (PFPA) was synthesized according to a reported procedure.[46] Macro-RAFT agent RAFT-PEO$_{455}$-RAFT was synthesized by attaching the chain transfer agent (S)-1-dodecyl-(S')-(α,α'-dimethyl-α''-acetic acid) trithiocarbonate to ends of PEO$_{455}$ precursor following a reported procedure.[44] The synthesis routes of all tri-block polymers were demonstrated in MessersmithRAFT-PEO$_{455}$-RAFT agent (0.518 g, 0.025 mmol), *N*-isopropylacrylamide (1.130 g, 10 mmol), pentafluorophenyl acrylate (0.238 g, 1 mmol) and azobisisobutyronitrile (0.002 g, 0.0125 mmol) were dissolved in 3 ml dioxane. After purging N$_2$ for 15 min, the whole system was stirred at 78 °C for 2 h. The polymerization was quenched by adding 5 mL tetrahydrofuran (THF) into the above mixture and the resulted solution was added dropwise into a great amount of ethyl ether to precipitate the polymer out. Afterwards the filtered polymer was redissolved in THF and precipitated twice into an excess amount of ethyl ether. The polymer was dried under vacuum overnight and 1.681g of the polymer was obtained. The composition of the resulting polymer was characterized by ^{1}H NMR and was obtained as poly[(NIPAM$_{227}$-*co*-PFPA$_{56}$)]-*b*-PEO$_{455}$-poly[(NIPAM$_{227}$-*co*-PFPA$_{56}$)]. ^{1}H NMR (CDCl$_3$, 400 MHz): δ$_H$ (ppm) = 4.0 (s, O=C-NH-C**H**-(CH$_3$)$_2$),

3.64 (m, -**CH₂CH₂**O-), 2.49 (br, -CH₂-**CH**(CONH)-), 1.68-1.4 (br, -**CH₂**-CH(CONH)-,**CH₂**-**CH**COO), 1.1 (s, O=C-NH-CH-(**CH₃**)₂).

PNIPAM-*b*-PEO-*b*-PNIPAM (NON) was synthesized following the same procedure shown above except that no PFPA was added during polymerization. The obtained polymer was characterized as PNIPAM*₃₀₀*-*b*-PEO*₄₅₅*-*b*-PNIPAM*₃₀₀*. ¹H NMR (CDCl₃, 400 MHz): δ_H (ppm) = 4.0 (s, O=C-NH-**CH**-(CH₃)₂), 3.64 (m, -**CH₂CH₂**O-), 2.49 (br, -CH₂-**CH**(CONH)-), 1.68 (br, -**CH₂**-CH(CONH)-), 1.1 (s, O=C-NH-CH-(**CH₃**)₂).

Poly[(NIPAM-*co*-N-3,4-dihydroxyphenethyl acrylamide)]-*b*-PEO-*b*-poly[(NIPAM-*co*-N-3,4-dihydroxyphenethyl acrylamide)] (DNODN) and poly[(NIPAM-*co*-phenethyl acrylamide)]-*b*-PEO-*b*-poly[(NIPAM-*co*-phenethyl acrylamide)] (BNOBN) were synthesized by substituting pentafluorophenyl group with the corresponding amine groups such as *N*-3,4-dihydroxyphenethylamine and phenethylamine. A typical example of DNODN was given as follows: poly[(NIPAM*₂₂₇*-*co*-PFPA*₅₆*)]-*b*-PEO*₄₅₅*-poly[(NIPAM*₂₂₇*-*co*-PFPA*₅₆*)] (1.681 g) and dopamine hydrochloride (0.380 g, 2 mmol) were mixed in 20 mL dichloromethane. After 20 min Argon purging, triethylamine (0.202 g, 2 mmol) was added and the whole mixture was stirred overnight at 50 °C. The resulting polymer was precipitated with ethyl ether twice and obtained as a white solid. The catechol functionalized polymer DNODN was obtained as poly[(NIPAM*₂₂₇*)-*co*-(*N*-3,4-dihydroxyphenethyl acrylamide*₅₆*)]-*b*-PEO*₄₅₅*-*b*-poly[(NIPAM*₂₂₇*)-*co*-(*N*-3,4-dihydroxyphenethyl acrylamide*₅₆*)]. ¹H NMR (CDCl₃, 400 MHz): δ_H (ppm) = 6.8-6.5 (m, CH₂C₆**H**₃(OH)₂), 4.0 (s, O=C-NH-**CH**-(CH₃)₂), 3.64 (m, -**CH₂CH₂**O-), 3.4

(q, CH_2–NHC(O)), 2.6 (m, CH_2- $C_6H_3(OH)_2$) 2.49 (br, -CH_2-CH(CONH)-), 1.68 (br, -CH_2-CH(CONH)-), 1.1 (s, O=C-NH-CH-(CH_3)$_2$).
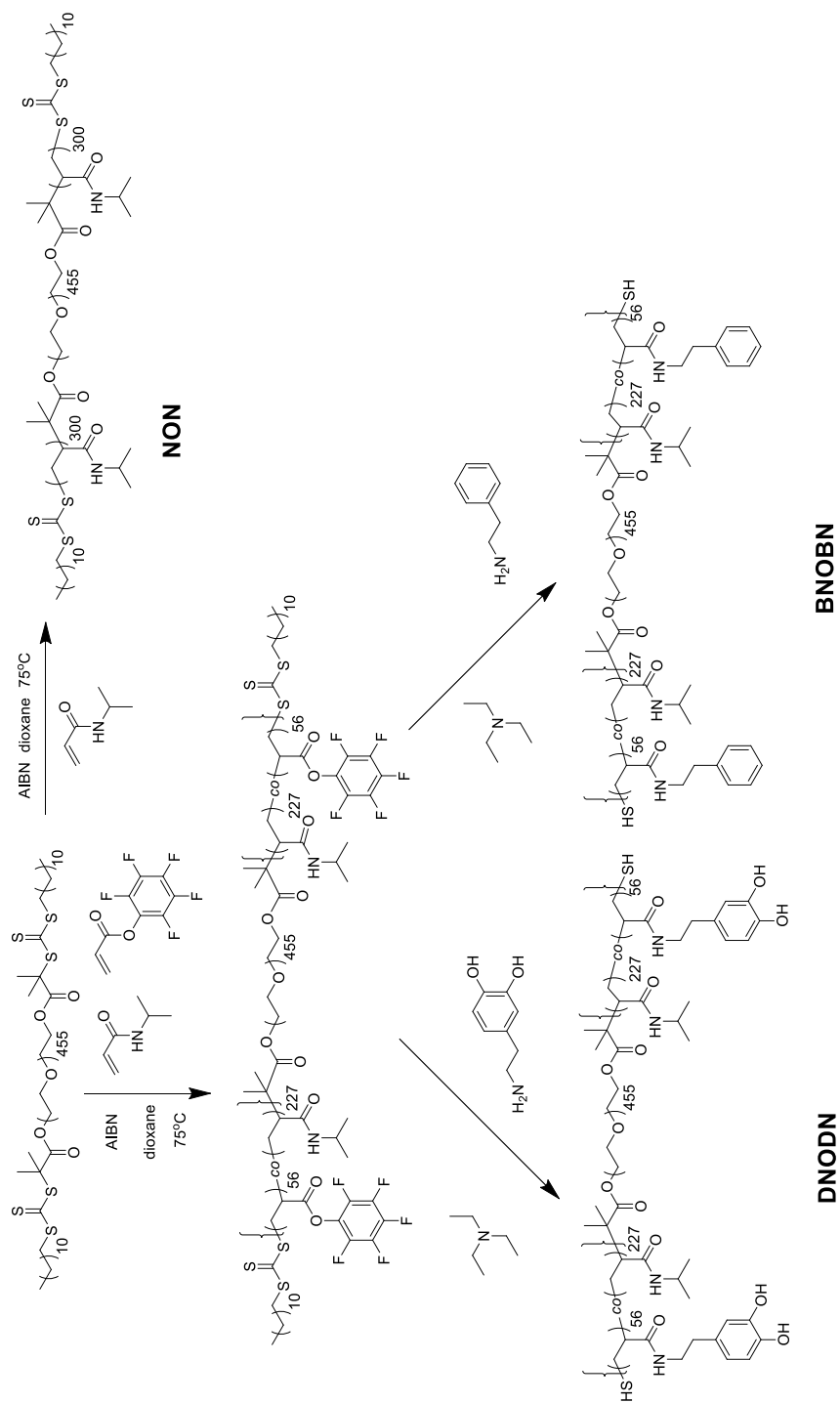
Figure 3.1 Synthesis routes of triblock copolymers NON, DNODN and BNODN.

As a control to investigate the effect of catechol on the self-healing properties of the obtained hydrogels, BNOBN was synthesized using phenethylamine in the above procedure and obtained as poly[(NIPAM$_{227}$)-*co*-(phenylethylacrylamide$_{56}$)]-*b*-PEO$_{455}$-*b*-poly[(NIPAM$_{227}$)-*co*-(phenylethylacrylamide$_{56}$)]. ^{1}H NMR (CDCl$_3$, 400 MHz): δ$_H$ (ppm) = 6.8-6.5 (m, CH$_2$C$_6$**H$_5$**), 4.0 (s, O=C-NH-C**H**-(CH$_3$)$_2$), 3.64 (m, -**CH$_2$CH$_2$**O-), 3.4 (q, **CH$_2$**–NHC(O)), 2.6 (m, CH$_2$-C$_6$**H$_3$**(OH)$_2$) 2.49 (br, -CH$_2$-CH(CONH)-), 1.68 (br, -**CH$_2$**-CH(CONH)-), 1.1 (s, O=C-NH-CH-(C**H$_3$**)$_2$).

3.2.2 Hydrogel preparation

All hydrogels were prepared by dissolving corresponding polymers to DI water with a concentration of 10 wt%. The polymer solutions were stored in 4 °C before following characterizations.

3.2.3 Dynamic light scattering study

The hydrodynamic diameters of the copolymer at different temperatures between 0-40 °C were measured using a zetasizer (Malvern, Zetasizer Nano ZSP). The temperature where a sudden increase in particle size occurred was determined as the lower critical solution temperature (LCST).

3.2.4 UV-Vis spectrometry

UV-Vis absorption spectra of a DNODN solution (1 mg/ml) at room temperature under air atmosphere were tracked for 48 h using a UV-Vis spectrometer (Thermo Fisher Scientific, EVO300).

3.2.5　Oscillatory rheology

SFA was used to study the rheological properties of all prepared hydrogels with a 20-mm parallel-plate configuration. For 10 wt% DNODN hydrogel, the plate was set at 0 °C before the polymer solution was dropped. Temperature ramp experiments were conducted within the range of 4-37 °C to study its thermo-sensitive sol-gel transition behavior, with a heating rate of 1 °C/min. A temperature cyclic step tests between 12 °C and 37 °C was also carried out, with angular frequency (ω) and strain (γ) held constant at 10 rad/s and 5 %, respectively. The amplitude oscillation was conducted at 37 °C and 10 rad/s, the strain was raised from 0.1 % to 1000 % to achieve a strain failure, followed by a time-dependent modulus observation at 1 % strain. Finally a strain step cycled between 1 % and 500 % was performed at 37 °C and 10 rad/s.

For the 10 wt% NON hydrogel, temperature ramp experiments were conducted within the range of 15-45 °C (due to a higher LCST transition temperature than the other two hydrogels) with a heating and cooling rate of 1 °C/min. The amplitude oscillation was conducted at 45 °C and 10 rad/s, the strain was raised from 0.1 % to 1000 % to achieve a strain failure, followed by a time-dependent modulus observation at 1 % strain. For 10 wt% BNOBN hydrogel, temperature ramp experiments were conducted within the range of 4-37 °C with a heating and cooling rate at 1 °C/min. The amplitude oscillation was conducted at 37 °C and 10 rad/s, the strain was raised from 0.1 % to 1000 % to achieve a strain failure, followed by a time-dependent modulus observation at 1 % strain.

3.2.6 Antifouling assay

Alexa Fluor dyes and 4,6-diamidino-2-phenylindole (DAPI) were purchased from Life Technologies (burlington, ON, Canada). Human intestinal Caco-2 cell line, the Caco-2 cell basel medium, the Caco-2 cell growth kit (low serum), Trypsin-EDTA and Trypsin neutralizing solution were purchased from the American Type Culture Collection (ATCC, Manassas, VA, USA).

A thin layer of DNODN hydrogel was formed on the glass bottom of the microwell dish (P35G-1.5-14-C, MatTek Corp., USA). Normal glass bottom microwell dishes without hydrogel were used as control test. Caco-2 cells were seeded onto the dishes and cultured for 2 days until a confluent cell layer was developed. The cells were then washed with PBS and fixed with 4% paraformaldehyde (w/v in PBS). Then Alexa Fluor 488 and DAPI were used to stain the cell membrane and the nuclei respectively. The hydrogel-coated microwell dish and the control were observed under a confocal laser scanning microscopy (CLSM 510 Meta, Carl Zeiss, Jena, Germany) equipped with a ZEN 2009LE software.

3.2.7 Cytotoxicity assay

The cytotoxicity of the DNODN polymer was evaluated by MTT assay. Caco-2 cells were seeded into 96-well plates at a density of 8×10^3 cells/well in 100 μL medium. These cells were allowed to grow for 24 h before the assay. Then different volumes of diluted DNODN polymer solutions were added to each well to reach a final concentration of 5.00, 2.50, 1.25, 0.63, 0.32 and 0.16 mg/ml, respectively. DNODN polymer and cells were incubated together for 24 h before 10 μL MTT

solvent (5 mg/ml in PBS) was added to each well. After incubation for 4 h, medium was removed from each well and 100 μL of DMSO was added to dissolve the purple MTT formazan crystals. The intensity of the color was read at 570 nm using a microplate reader (SpectraMax, Molecular Devices, USA) and the viability was defined as the percentage of living cells with respect to that in the control test.

3.3 Results and discussion

3.3.1 Characterization of the injectable self-healing DNODN hydrogel
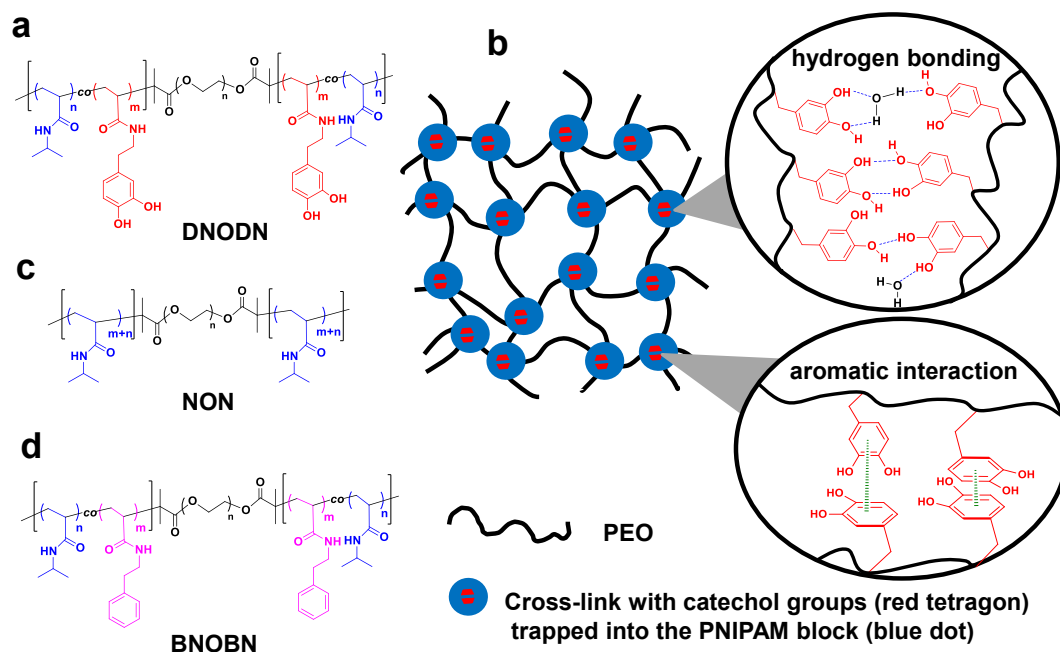
Figure 3.2 (a) Chemical structure of the ABA triblock copolymer DNODN. (b) Schematic of a proposed structure of the DNODN hydrogel. (c-d) Chemical structure of tri-block copolymer NON (c) and tri-block copolymer BNOBN (d) for comparison with DNODN.
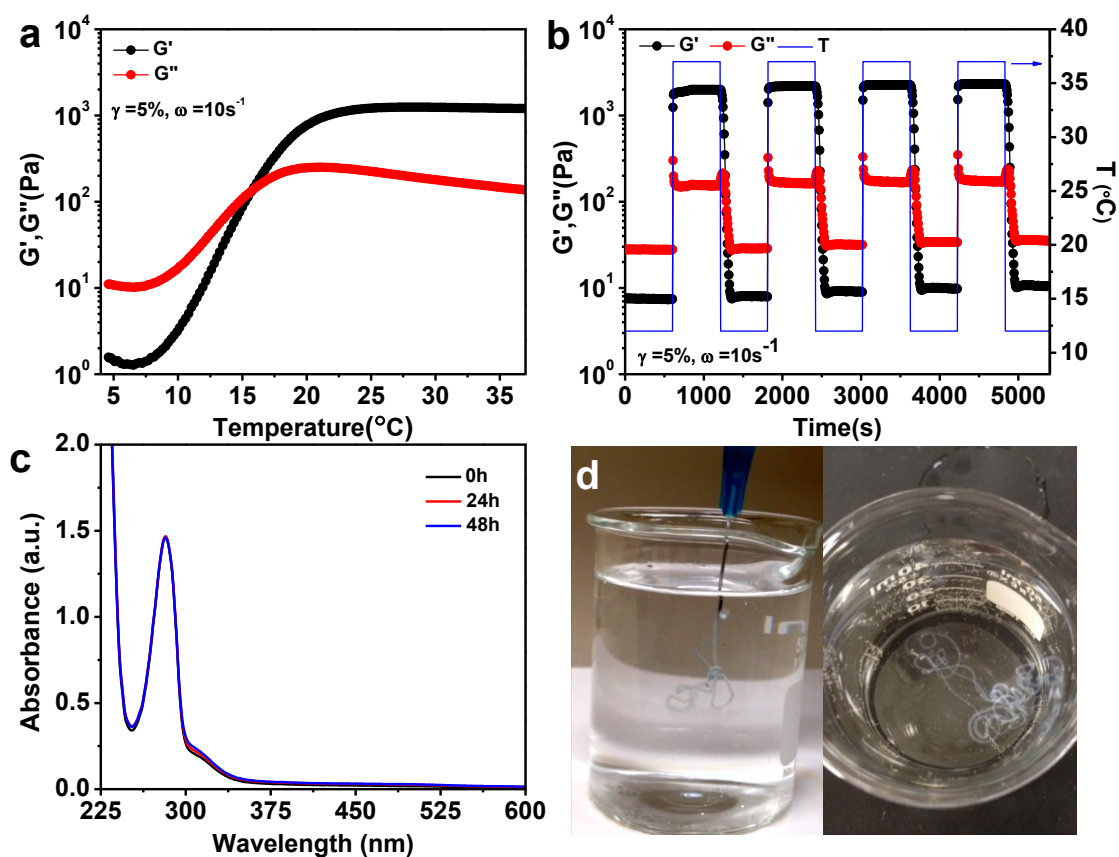
Figure 3.3 (a) Temperature-responsive storage (G') and loss (G") modulus changes of a 10 wt% DNODN hydrogel. (b) Modulus changes of a 10 wt% DNODN hydrogel with thermal cycles of heating (37 °C) and cooling (12 °C) for four rounds. (c) UV/Vis spectra of a DNODN solution (1mg/ml in DI water) tracked within 48h at room temperature under air atmosphere. (d) Injection of a liquefied 10 wt% DNODN sample (colored in light blue) into 37 °C DI water.

Since *A* blocks are thermosensitive and B blocks are permanently water-soluble, increasing solution temperature would lead to the formation of a three-dimensional network with the dehydrated *A* blocks associating into micellar cores and the central *B* blocks forming bridges (Figure 3.2b).[47, 48] A sample of 10 wt%

DNODN is a free-flow viscous liquid at a lower temperature (i.e. 4 °C) but becomes a free-standing gel when warmed to room temperature (Figure S3.1 in Appendix). The thermo-sensitivity of the DNODN hydrogel was first characterized with a temperature ramp test using a rheometer, in which storage modulus G' and loss modulus G" were recorded from 4 °C to 37 °C at a heating rate of 1 °C /min, as shown in Figure 3.3a. At lower temperatures, G'' was greater than G', signifying a liquid-like property. While with the heating process, G' increased significantly faster than G" and became much larger than G" at higher temperature, indicating a gel-like property. The crossover between G' and G" at 16 °C was identified as the sol-gel transition temperature.[49] To rule out the possibility that thermal-induced gelation was due to cathechols' coupling reactions after oxidation, dynamic temperature sweep measurements between 12 °C and 37 °C were conducted (Figure 3.3b). It was observed that the sol-gel-sol transitions were totally reversible during the cyclic tests, indicating that the hydrogel is not constructed through irreversible quinone cross-linking but through hydrophobic interactions arisen from PNIPAM at high temperature. UV-Vis absorption spectra of DNODN solution (1 mg/ml) at room temperature (22 °C) under air atmosphere were tracked within 48 h and shown in Figure 3.3c. Characteristic absorption peak of catechol groups at 280 nm was clearly observed and remained unchanged, demonstrating the catechol groups remained unoxidized, which was consistent with the fact that the DNODN solution (1 mg/ml) retained clear within the experimental period (Figure S3.2a in Appendix). Since the lower critical solution temperature (LCST) of DNODN was measured as 15 °C by dynamic light scattering (Figure S3.3 in Appendix), the polymer chains

aggregated into micelles with hydrodynamic diameter ~43 nm at room temperature, indicating an encapsulation of catechol groups in the micellar cores. For comparison, a dopamine hydrochloride solution (0.23 mg/ml) with same concentration of catechol groups as that of DNODN solution was prepared and it was found that its catechol groups were easily oxidized within 5 h with visible color change (Figure S3.2b in Appendix). The DNODN hydrogel's insusceptibility to oxidation is mainly attributed to the local hydrophobic microenvironment provided by the catechol functionalized poly(N-isopropyl acrylamide) A blocks at temperature above the sol-gel transition temperature. Such a protection mechanism is consistent with previous study that DOPA in mussel foot protein 3 (mfp3) is less prone to oxidation because the high proportion of hydrophobic amino acid residues in mfp3 sequence provides DOPA with a microenvironment that retards oxidation by shielding the amino acids from external oxidants.[45] The excellent thermo-reversibility together with the low modulus (<10 Pa) at low temperature endow the novel DNODN hydrogel injectable properties: as shown in Figure 3.3d, the 4 °C-preserved polymer solution was injected into a water bath at 37 °C using a 23G×3/4" syringe and immediately turned into stable hydrogel.

For an injectable hydrogel as a qualified drug delivery depot, it is essential that the hydrogel could rapidly self-heal and restore to its original gel state after inflicted damage. Therefore, strain sweep measurements were conducted on the DNODN hydrogel (10 wt%) to test its responsive behaviour upon external strains. Figure 3.4a shows that G' and G" remained constant until the strain reached 100%, suggesting the formed free-standing hydrogel

could withstand relatively large deformations. However when the applied strain γ was further increased, a dramatic drop was observed for both G' and G" values and a crossover occurred at around strain γ=400%, indicating that beyond this critical strain point severe dislocation of polymer chains occurred and disrupted the hydrogel network which turned into a sol state. It was found that the mechanical properties of the hydrogel could be fully recovered if a 1% strain test was immediately followed after severe strain deformation (γ=1000%) in Figure 3.4a. Meanwhile, repeated dynamic strain step tests (γ =1% or 500%) were applied on the DNODN (10 wt%) hydrogel. As presented in Figure 3.4b, when subjected to a 500% strain, G' immediately dropped from ~1200 Pa to around 20 Pa. Upon the strain returned to 1 %, both G' and G" were able to recover the initial values without any loss. This recovery process was completed instantly, within the time interval (6 seconds) of data obtaining (Figure S3.4 in Appendix). This recovery behaviour was totally reversible and reproducible during the cyclic tests. This self-healing property of the novel DNODN hydrogel was further demonstrated in Figure 3.4c-f, where two hydrogel fragments could adhere to each other instantly when brought into contact and automatically heal into one integral piece. The healed hydrogel could withstand vigorous shaking and maintain its integrity. Viscosity measurement on a 10 wt% DNODN hydrogel at 37 °C and 5% strain was conducted and a reduction in viscosity with increasing shear rate was observed (Figure 3.4g). This shearing thinning behaviour resulting from the disruption of physical cross-links would provide broken segments with

higher mobility within the hydrogel matrix, which may be an explanation to this self-healing property.
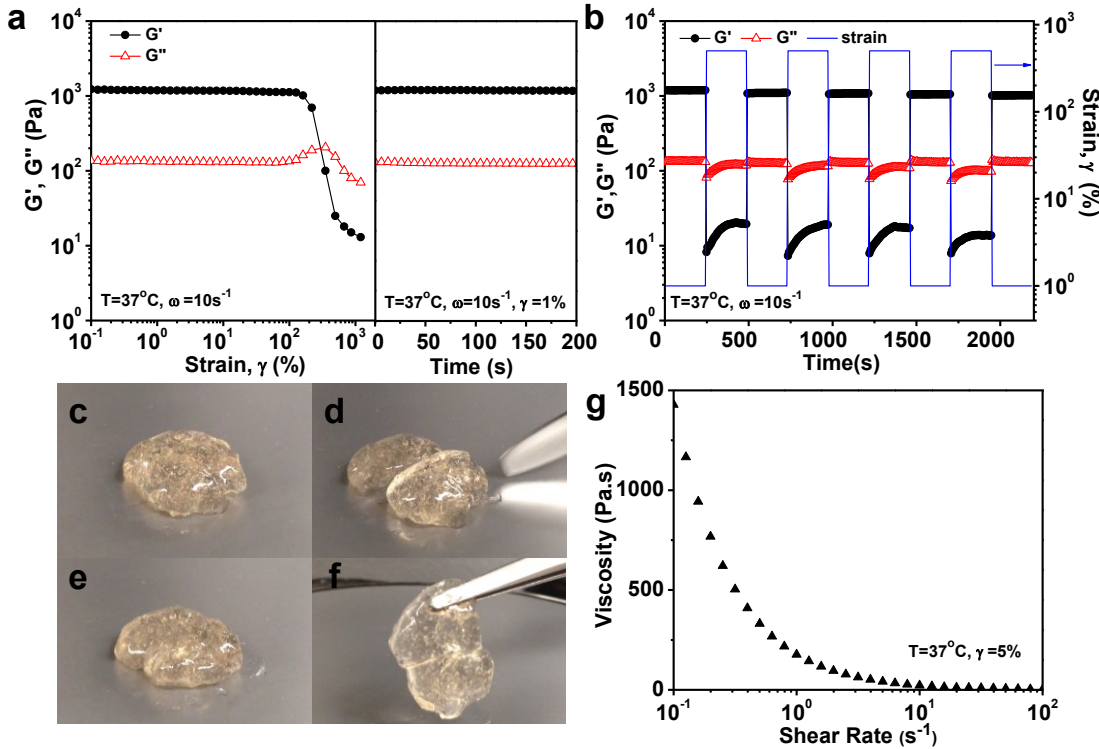
Figure 3.4 (a) Strain sweep measurements of a 10 wt% DNODN hydrogel at 37 °C (storage modulus G' and loss modulus G" as a function of strain γ) (left) and an immediate recovery from the 1000% strain deformation (right). (b) Dynamic strain amplitude cyclic test (γ =1% or 500%) of 10 wt% DNODN hydrogel at 37 °C showing self-healing behavior. (c-f) Optical evidence of self-healing: (c) initial hydrogel sample, (d) sample hydrogel was cut into two pieces, (e) separated pieces were brought together and the self-healing process occurred instantaneously, (f) the healed hydrogel supported its own weight. (g) Viscosity measurement on a 10 wt% DNODN hydrogel at 37 °C.

3.3.2 Study the self-healing mechanism of the DNODN hydrogel

To better understand the self-healing mechanism of the DNODN hydrogel, a fully oxidized hydrogel was prepared by adding $NaIO_4$ to freshly-prepared DNODN hydrogel (Figure S3.5 in Appendix). The treated hydrogel sample lost its thermo-reversibility and self-healing property, and turned into a permanent hydrogel due to the irreversible quinone cross-linking. Meanwhile, an *ABA* triblock copolymer without functionalization of catechol groups (NON, Figure 3.2c) with PNIPAM as *A* block and PEO as the middle *B* block was synthesized. A 10 wt% NON hydrogel showed good thermo-reversibility (Figure 3.5a) but its modulus recovery from severe strain deformation (γ=1000%) was only 25% (Figure 3.5b). It is evident from the above results that the unoxidized catechol groups play an important role in achieving the remarkable self-healing performance through hydrogen bonding (Figure 3.2b). Such a proposed mechanism agrees with the recent results by Israelachvili, Waite and co-workers[43] on interfacial self-healing of synthetic polyacrylate and polymethacrylate surface-functionalized with catechols.
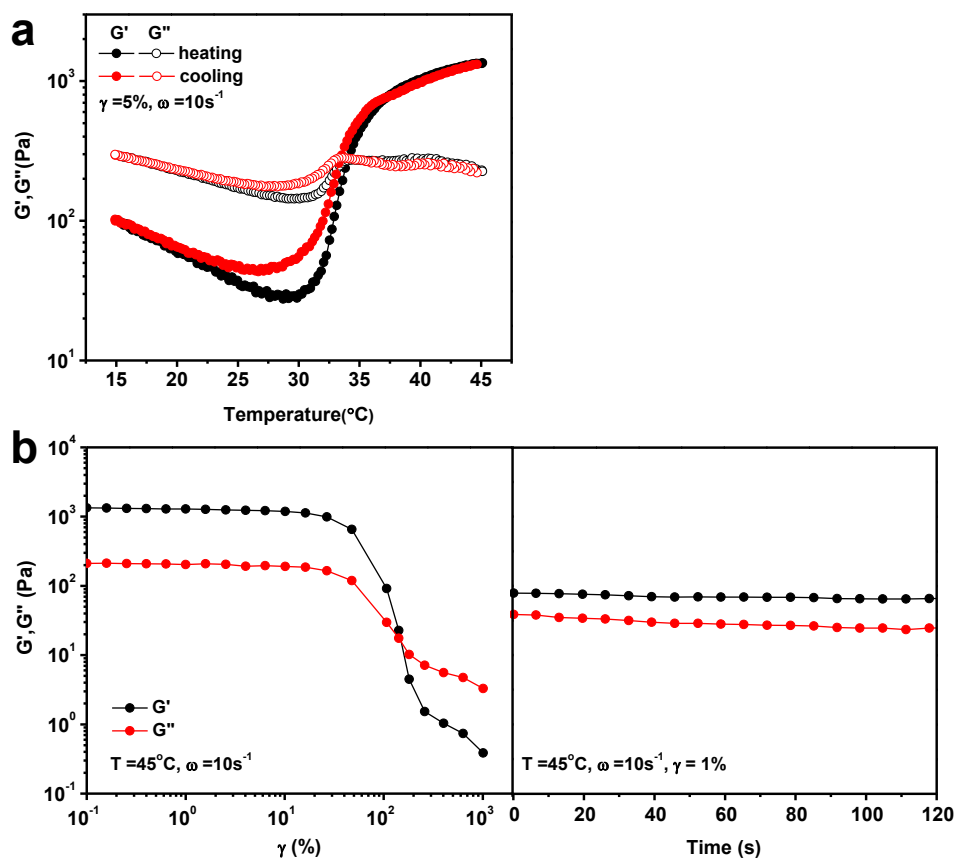
Figure 3.5 (a) Temperature-responsive storage (G') and loss (G") modulus changes of a 10 wt% NON hydrogel. (b) Strain sweep measurements of a 10 wt% NON hydrogel at 45 °C (left) and time-dependent recovery from the strain failure (right). The modulus recovery was ~ 25%.
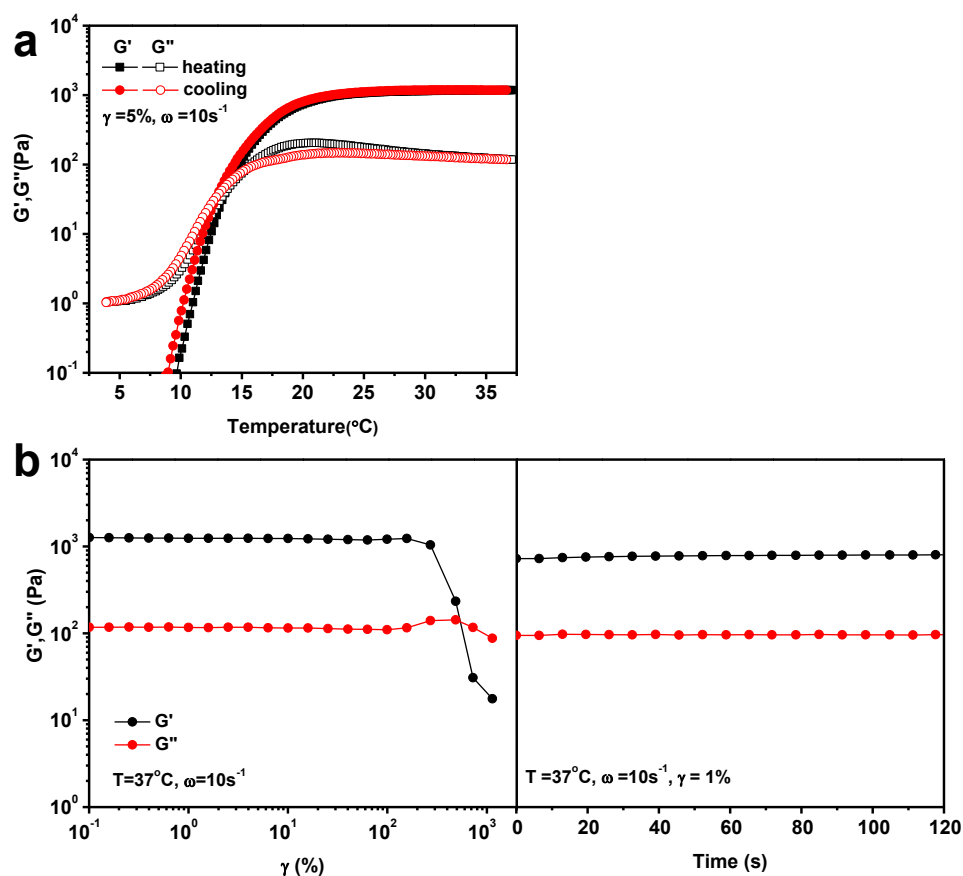
Figure 3.6 (a) Temperature-responsive storage (G') and loss (G") modulus changes of a 10 wt% BNOBN hydrogel. (b) Strain sweep measurements of a 10 wt% BNOBN hydrogel at 37 °C (left) and time-dependent recovery from the strain failure (right). The modulus recovery was ~57%.

However, it should be noted that whether hydrogen bonding between interfacial catechol moieties plays the sole role in the self-healing of the DNODN hydrogel still remains unclear. To fully elucidate the mechanism, another *ABA* tri-block copolymer (BNOBN, Figure 3.2d) with *A* block from random copolymerization of phenylethylacrylamide and NIPAM and *B* block PEO was also synthesized. A 10 wt% BNOBN hydrogel showed good

thermo-reversibility (Figure 3.6a) and the modulus recovery from severe strain deformation (γ=1000%) could reach 57% (Figure 3.6b), indicating that aromatic interactions including quadrupolar interactions (edge-to-face) and π-π stacking interactions [50] could also contribute to the self-healing mechanism (Figure 3.2b). A freshly-prepared DNODN gel piece and a periodate-oxidized one (with excess periodate removed) were brought together for healing. It was found that the two gel pieces could adhere to each other readily but be separated right from the contact interface by a tiny force (Figure S3.6 in Appendix), indicating a largely reduced healing performance compared with that between two freshly-prepared DNODN hydrogel pieces. Since the strength of hydrogen bonding between asymmetric catechol-quinone surfaces was comparable to or stronger than that between symmetric catechol-catechol surfaces,[43] and the strength of π-π stacking interactions could be considered unchanged, the reduced healing performance of BNOBN hydrogel compared with that of DNODN hydrogel could be attributed to weaker quadrupolar interactions between quinones and catechols and a restrained chain mobility due to oxidized cross-linking. This experiment further suggested that quadrupolar and π-π stacking interactions all played roles in achieving this self-healing property. To sum up, it is evident from the above results that (i) the shear-thinning behaviour of the DNODN hydrogel enhances the mobility of polymer chains and catechol groups to interact with each other during self-healing, and (ii) both hydrogen bonding and aromatic interactions including

quadrupolar and π-π stacking interactions between interfacial catechol groups play important roles in achieving this remarkable self-healing performance.

3.3.3 Antifouling performance of the DNODN hydrogel
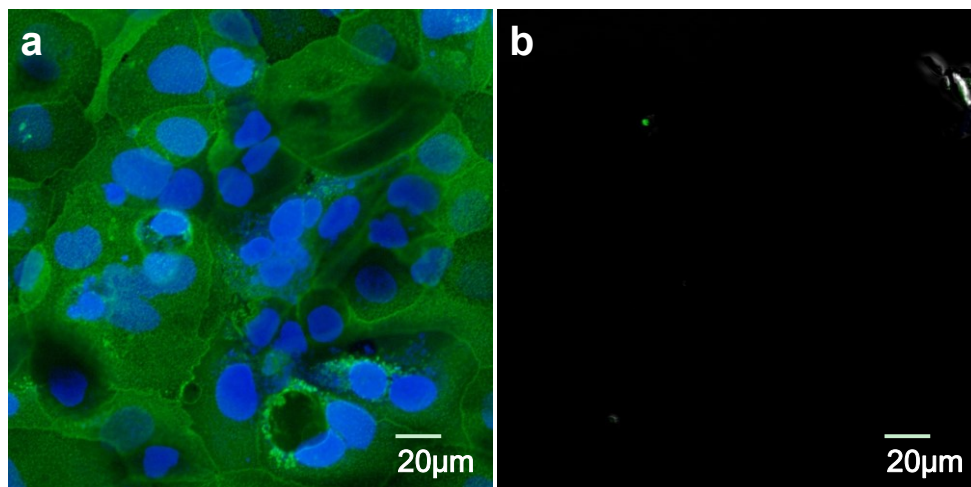
Figure 3.7 Representative fluorescence microscopy images of (a) uncoated and (b) DNODN hydrogel coated microwell dishes after exposure to Caco-2 cells for 48 h. Alexa Fluor 488 and 4,6-diamidino-2-phenylindole (DAPI) were used to stain the cell membrane and the nuclei respectively.

The novel DNODN hydrogel also shows exceptional antifouling performance against cell attachment, studied by seeding human intestinal Caco-2 cells directly onto the hydrogel-coated microwell dishes followed by fluorescence imaging. Representative fluorescence microscopy images of uncoated and DNODN hydrogel coated microwell dishes after exposure to Caco-2 cells for 48 h are shown in Figure 3.7a and b, respectively. Caco-2 cells attached to the glass bottom of the microwell dishes readily, forming a dense cell layer. In contrast, DNODN hydrogel coated microwell dishes showed exceptional resistance to cell attachment, which could be attributed to the presence of a major component PEO[51, 52] and the inherent structure

of the whole hydrogel. The tri-block copolymer DNODN also exhibited good biocompatibility within the experimental concentrations (up to 5 mg/ml, Figure S3.7 in Appendix).

3.4   Conclusion

In summary, we have developed a novel injectable thermo-sensitive self-healing hydrogel DNODN with anti-biofouling property, based on self-assembly of a mussel-inspired triblock copolymer in metal-free aqueous environment. The thermo-sensitive propery and shearing thinning behavior of the hydrogel allow it injectable *in vivo* at body temperature, and the anti-biofouling properties can effectively inhibit the formation of biofilms. The self-mending DNODN hydrogel can withstand high strain and repeated deformation and quickly recover its mechanical properties and structure through the catechol-mediated reconstruction of hydrogen bonding and aromatic interactions, thus reducing the inflammation risk in bioengineering applications because of the body fluids' intrusion to damaged gel matrix in injection and burst release of loaded bio-active molecues. Compared with the conventional mussel-inspired self-healing hydrogel constructed through catechol-metal coordination,[29, 30, 33] which may cause certain cytotoxicity when brought *in vivo*, our novel DNODN hydrogel exhibits great potential in various bioengineering applications (e.g. drug delivery), due to its inherent metal-free self-healing nature, and a combination of thermo-sensitivity, injectability, and anti-biofouling properties.

3.5 References

1.   L. Yu and J. Ding, *Chem Soc Rev*, 2008, **37**, 1473-1481.

2.   N. A. Peppas, J. Z. Hilt, A. Khademhosseini and R. Langer, *Adv Mater*, 2006, **18**, 1345-1360.

3.   H. Park, J. S. Temenoff, Y. Tabata, A. I. Caplan and A. G. Mikos, *Biomaterials*, 2007, **28**, 3217-3227.

4.   D. Sivakumaran, D. Maitland and T. Hoare, *Biomacromolecules*, 2011, **12**, 4112-4120.

5.   A. Parisi-Amon, W. Mulyasasmita, C. Chung and S. C. Heilshorn, *Adv Healthc Mater*, 2013, **2**, 428-432.

6.   T. Nakai, T. Hirakura, Y. Sakurai, T. Shimoboji, M. Ishigai and K. Akiyoshi, *Macromol Biosci*, 2012, **12**, 475-483.

7.   A. Paul, A. Hasan, H. A. Kindi, A. K. Gaharwar, V. T. Rao, M. Nikkhah, S. R. Shin, D. Krafft, M. R. Dokmeci and D. Shum-Tim, *ACS nano*, 2014, **8**, 8050-8062.

8.   A. L. Lee, V. W. Ng, S. Gao, J. L. Hedrick and Y. Y. Yang, *Adv Funct Mater*, 2014, **24**, 1538-1550.

9.   B. F. Lin, K. A. Megley, N. Viswanathan, D. V. Krogstad, L. B. Drews, M. J. Kade, Y. Qian and M. V. Tirrell, *J Mater Chem*, 2012, **22**, 19447-19454.

10.   A. López-Noriega, C. L. Hastings, B. Ozbakir, K. E. O'Donnell, F. J. O'Brien, G. Storm, W. E. Hennink, G. P. Duffy and E. Ruiz-Hernández, *Adv healthc mater*, 2014.

11. C. Ding, L. Zhao, F. Liu, J. Cheng, J. Gu, S.-. Dan, C. Liu, X. Qu and Z. Yang, *Biomacromolecules*, 2010, **11**, 1043-1051.

12. J. Yu, H. Fan, J. Huang and J. Chen, *Soft Matter*, 2011, **7**, 7386-7394.

13. Y. Zhang, Y. Sun, X. Yang, J. Hilborn, A. Heerschap and D. A. Ossipov, *Macromol Biosci*, 2014.

14. L. Tan, Y. Liu, W. Ha, L.-S. Ding, S.-L. Peng, S. Zhang and B.-J. Li, *Soft Matter*, 2012, **8**, 5746-5749.

15. X. Jiang, S. Jin, Q. Zhong, M. D. Dadmun and B. Zhao, *Macromolecules*, 2009, **42**, 8468-8476.

16. A. Servant, V. Leon, D. Jasim, L. Methven, P. Limousin, E. V. Fernandez-Pacheco, M. Prato and K. Kostarelos, *Adv healthc mater*, 2014.

17. E. Brynda, N. A. Cepalova and M. Štol, *J Biomed Mater Res*, 1984, **18**, 685-693.

18. B. Wehrle-Haller, *Curr Opin Cell Biol*, 2012, **24**, 569-581.

19. M. Black, A. Trent, Y. Kostenko, J. S. Lee, C. Olive and M. Tirrell, *Adv Mater*, 2012, **24**, 3845-3849.

20. L. Mi and S. Jiang, *Angew Chem Int Ed*, 2014, **53**, 1746-1754.

21. T. Kakuta, Y. Takashima, M. Nakahata, M. Otsubo, H. Yamaguchi and A. Harada, *Adv Mater*, 2013, **25**, 2849-2853.

22. A. Phadke, C. Zhang, B. Arman, C.-C. Hsu, R. A. Mashelkar, A. K. Lele, M. J. Tauber, G. Arya and S. Varghese, *Proc Natl Acad Sci*, 2012, **109**, 4383-4388.

23.   Y. Amamoto, J. Kamada, H. Otsuka, A. Takahara and K. Matyjaszewski, *Angew Chem*, 2011, **123**, 1698-1701.

24.   Y. Amamoto, H. Otsuka, A. Takahara and K. Matyjaszewski, *Adv Mater*, 2012, **24**, 3975-3980.

25.   P. Cordier, F. Tournilhac, C. Soulie-Ziakovic and L. Leibler, *Nature*, 2008, **451**, 977-980.

26.   S. Rose, A. Prevoteau, P. Elzière, D. Hourdet, A. Marcellan and L. Leibler, *Nature*, 2013.

27.   A. Faghihnejad, K. E. Feldman, J. Yu, M. V. Tirrell, J. N. Israelachvili, C. J. Hawker, E. J. Kramer and H. Zeng, *Adv Funct Mater*, 2014, **24**, 2322-2333.

28.   D. Liu, D. Wang, M. Wang, Y. Zheng, K. Koynov, G. K. Auernhammer, H.-J. Butt and T. Ikeda, *Macromolecules*, 2013, **46**, 4617-4625.

29.   J. Sedó, J. Saiz-Poseu, F. Busqué and D. Ruiz-Molina, *Adv Mater*, 2013, **25**, 653-701.

30.   Y. Zhao, F. Sakai, L. Su, Y. Liu, K. Wei, G. Chen and M. Jiang, *Adv Mater*, 2013, **25**, 5215-5256.

31.   Y. Liu, K. Ai and L. Lu, *Chem Rev*, 2014.

32.   B. Yang, N. Ayyadurai, H. Yun, Y. S. Choi, B. H. Hwang, J. Huang, Q. Lu, H. Zeng and H. J. Cha, *Angew Chem Int Ed*, 2014.

33.   N. Holten-Andersen, M. J. Harrington, H. Birkedal, B. P. Lee, P. B. Messersmith, K. Y. C. Lee and J. H. Waite, *Proc Natl Acad Sci*, 2011, **108**, 2651-2655.

34. M. Krogsgaard, M. A. Behrens, J. S. Pedersen and H. Birkedal, *Biomacromolecules*, 2013, **14**, 297-301.

35. L. He, D. E. Fullenkamp, J. G. Rivera and P. B. Messersmith, *Chem Commun*, 2011, **47**, 7497-7499.

36. M. Vatankhah-Varnoosfaderani, S. Hashmi, A. GhavamiNejad and F. J. Stadler, *Polym Chem*, 2014, **5**, 512-523.

37. B. J. Kim, D. X. Oh, S. Kim, J. H. Seo, D. S. Hwang, A. Masic, D. K. Han and H. J. Cha, *Biomacromolecules*, 2014, **15**, 1579-1585.

38. B. P. Lee, P. B. Messersmith, J. N. Israelachvili and J. H. Waite, *Ann Rev Mater Res*, 2011, **41**, 99.

39. H. Zeng, D. S. Hwang, J. N. Israelachvili and J. H. Waite, *Proc Natl Acad Sci*, 2010, **107**, 12850-12853.

40. Q. Lu, D. S. Hwang, Y. Liu and H. Zeng, *Biomaterials*, 2012, **33**, 1903-1911.

41. Q. Lu, D. X. Oh, Y. Lee, Y. Jho, D. S. Hwang and H. Zeng, *Angew Chem Int Ed*, 2013, **52**, 3944-3948.

42. D. S. Hwang, H. Zeng, A. Masic, M. J. Harrington, J. N. Israelachvili and J. H. Waite, *J Biol Chem*, 2010, **285**, 25850-25858.

43. B. K. Ahn, D. W. Lee, J. N. Israelachvili and J. H. Waite, *Nat mater*, 2014, **13**, 867-872.

44. Y. He and T. P. Lodge, *Macromolecules*, 2008, **41**, 167-174.

45. W. Wei, J. Yu, C. Broomell, J. N. Israelachvili and J. H. Waite, *J Am Chem Soc*, 2012, **135**, 377-383.

46.   M. Eberhardt, R. Mruk, R. Zentel and P. Théato, *Eur Polym J*, 2005, **41**, 1569-1575.

47.   T. G. O'Lenick, N. Jin, J. W. Woodcock and B. Zhao, *J Phys Chem B*, 2011, **115**, 2870-2881.

48.   A. Vagias, P. Košovan, K. Koynov, C. Holm, H.-J. r. Butt and G. Fytas, *Macromolecules*, 2014, **47**, 5303-5312.

49.   R. Bodvik, L. Karlson, K. Edwards, J. Eriksson, E. Thormann and P. M. Claesson, *Langmuir*, 2012, **28**, 13562-13569.

50.   L. M. Salonen, M. Ellermann and F. Diederich, *Angew Chem Int Ed*, 2011, **50**, 4808-4842.

51.   S. Herrwerth, W. Eck, S. Reinhardt and M. Grunze, *J Am Chem Soc*, 2003, **125**, 9359-9366.

52.   E. Ostuni, R. G. Chapman, R. E. Holmlin, S. Takayama and G. M. Whitesides, *Langmuir*, 2001, **17**, 5605-5620.

4 Injectable self-healing hydrogel with antimicrobial and antifouling properties[4]

4.1 Introduction

Injectable hydrogels have attracted considerable research interests in biomedical fields such as drug delivery and tissue engineering due to their desirable biocompatibility, ease of operation and minimum tissue invasion.[1] Besides the embedding of bioactive molecules such as drugs, proteins and antibodies into precursor solution to achieve target delivery via an in-situ gelation right after injection, the capability of obtaining diverse functionalities by employing various polymers in constructing hydrogel networks have also made this type of material highly competitive in bioengineering applications.[2-4] Soaked in complex body fluid environment, the hydrogel materials implanted *in vivo* are vulnerable to proteins and microorganism accumulation, which would not only block circulation of metabolites and embedded biomolecules, but also lead to possible inflammatory responses.[5, 6] To address this issue, several approaches have been adopted to endow hydrogel materials with simultaneous antimicrobial and antifouling properties, such as the switching between cationic active hunting state and zwitterionic/mixed charged nonfouling state,[7, 8] the releasing of antibiotics/silver nanoparticles while maintaining nonfouling

---

[4] The content of this chapter was submitted to *ACS Appl Mater Interfaces*.

nature,[9-13] and the inclusion of nonfouling and antimicrobial ingredients into one structure through cross-linking or copolymerization.[14, 15]

However implanted hydrogels are subject to constant mechanical forces from daily body movement which would lead to gel deformation or even damage, not only increasing the risk of infection due to the microorganism intrusion, but also weakening other functional performances due to the rupture of the hydrogel structure. Thus the key point to ensure both the structural and functional integrity is to confer the hydrogel materials autonomously self-healing, a property pervasive in biological systems while rare in man-made materials.[16] Generally intrinsic self-healable hydrogel networks are constructed through reversible non-covalent bonds such as hydrogen bonding, ionic interactions, π-π stacking and metal-ligand coordination.[17-19] Mussel-inspired catechol-metal coordination has been widely employed in preparing self-healing hydrogels.[20] However, their bioengineering applications are restrained by the *in vivo* cytotoxicity of metal ions. Recently using mussel-inspired catechol-mediated hydrogen bonding and aromatic interactions as novel self-healing mechanism to construct reversible hydrogel networks has attracted much attention, and the prepared materials exhibit great superiority over those constructed through catechol-metal coordination in bioengineering applications, due to their reduced cytotoxicity and enhanced transparency attributed to the metal-free nature.[21, 22]

To satisfy the different needs in dynamic biomedical processes, a multifunctional hydrogel with features including the in-situ gelation capability and injectability to facilitate operation, the antimicrobial and antifouling property to prevent bacterial growth and biofilm accumulation, and the self-healing property to ensure structural and functional integrity, would be of significant potential for bioengineering applications. However, to the best of our knowledge, combining all the above-mentioned features into one single hydrogel design has not been achieved. In this work, we report a new type of multi-functional hydrogel based on the self-assembly of an *ABA* tri-block copolymer comprising catechol functionalized polyethylene glycol(PEG)-based *A* block and quaternized *B* block, as illustrated in Figure 4.1a. This tri-block copolymer poly{[2-(2-methoxyethoxy)ethyl methacrylate]-*co*-[oligo(ethylene glycol) methacrylate]-*co*-(*N*-3,4-dihydroxyphenethyl acrylamide)}-*b*-poly{[2-(methacryloyloxy)- ethyl] trimethyl ammonium iodide}-*b*-poly{[2-(2-methoxyethoxy)ethyl methacrylate]-*co*-[oligo(ethylene glycol) methacrylate]-*co*-(*N*-3,4-dihydroxyphenethyl acrylamide)}, deviated as P(MEO$_2$MA-*co*-OEGMA-*co*-DOPA)-*b*-PMETA-*b*-P(MEO$_2$MA-*co*-OEGMA-*co*-DOPA), was synthesized by reversible additional fragment transfer (RAFT) polymerization, followed successively by the replacement between an active ester and dopamine and the quaternization of the middle *B* block. As the PEG-based *A* blocks are thermo-sensitive and the quaternized *B* blocks are permanently hydrophilic, the tri-block copolymer can be hydrated and adopt an extended conformation

in water at lower temperature, exhibiting a liquid-like behaviour. However, temperature increase can lead to gelation with *A* blocks dehydrating and associating into micellar core-like crosslinks and middle *B* blocks acting as network bridges,[23-25] as illustrated in Figure 4.1b.
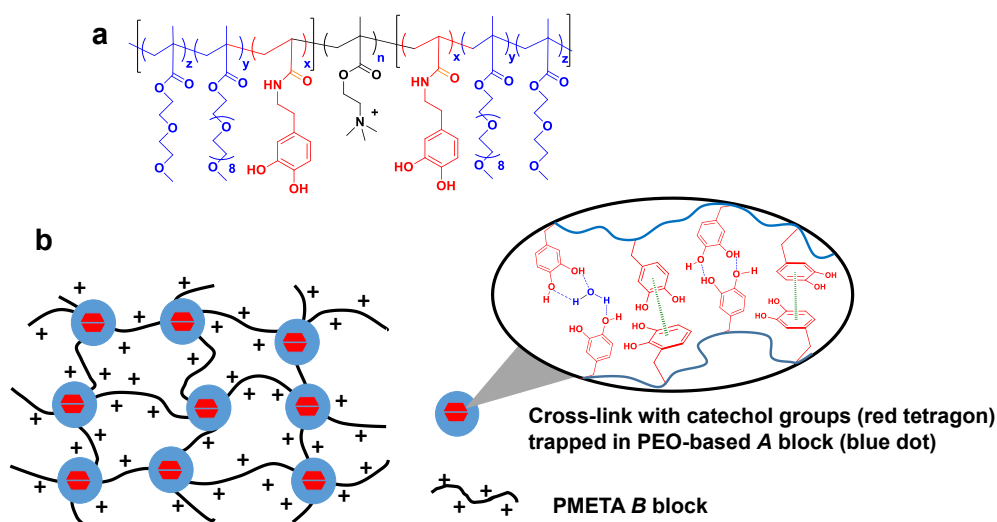
Figure 4.1 (a) Structure of the tri-block copolymer synthesized. (b) Schematic of a proposed structure of the resulting hydrogel and the mussel-inspired self-healing mechanism.

4.2   Materials and methods

4.2.1   Polymer synthesis

Monomers 2-(dimethylamino)ethyl methacrylate (DMAEMA), oligo(ethylene glycol) methacrylate (OEGMA) with a molecular weight of around 500, 2-(2-methoxyethoxy)ethyl methacrylate (MEO_2MA) were purchased from Sigma-Aldrich and passed through a short column of basic Aluminum oxide to remove inhibitors before use. Perfluorophenyl acrylate (PFPA) was synthesized according to a reported procedure.[26] All other chemicals for polymer synthesis were purchased

from Sigma Aldrich and were used as received. The chain transfer agent **(1)** was synthesized using 4-Cyano-4-[(dodecylsulfanylthiocarbonyl)sulfanyl]pentanoic acid and 1,6-hexanediamine following a modified procedure.

In a typical synthesis route, chain transfer agent **(1)** (0.081 g, 0.1 mmol), DMAEMA (3.144 g, 20 mmol) and azobisisobutyronitrile (AIBN, 0.008 g, 0.05 mmol) were dissolved in 10 ml dioxane. The mixture was stirred at 72 °C for 4 h after purging Argon for 15 min. The resulting solution was added dropwise into a great amount of hexane to precipitate the polymer out. The filtered polymer was redissolved in dioxane and precipitated again into an excess amount of hexane. The polymer was dried under vacuum overnight to obtain p(DMAEMA)$_{135}$ macro RAFT agent **(2)**. ^{1}H NMR (CDCl$_3$, 400 MHz): δ_H (ppm) = 0.78-1.10 (m, -CH$_2$-C(CO)-CH$_3$), 1.69-2.02 (m, -**CH$_2$**-C(CO)-CH$_3$), 4.05 (s, -COO-**CH$_2$**-CH$_2$-N(CH$_3$)$_2$), 2.56 (s, -COO-CH$_2$-**CH$_2$**-N(CH$_3$)$_2$), 2.25 (s, -COO-CH$_2$-CH$_2$-N(**CH$_3$**)$_2$). PDI=1.2.

P(DMAEMA) macro RAFT agent (0.4046g, 0.02mmol), pentafluorophenyl acrylate (PFPA, 0.19g, 0.8mmol), MEO$_2$MA (0.5715g, 3.04mmol), OEGMA (0.08g, 0.16mmol), AIBN (0.0016g, 0.01mmol) were dissolved in 5 ml dioxane and the whole mixture was stirred at 72 °C for 4 h after purging Argon for 15 min. The resulted solution was precipitated twice into an excess amount of hexane. The resulting polymer was filtered and dried in vacuum overnight to obtain p(MEO$_2$MA-*co*-OEGMA-*co*-PFPA)-*b*-p(DMAEMA)$_{135}$-*b*-p(MEO$_2$MA-*co*-OEGMA-*co*-PFPA) **(3)**.

Product **(2)** (0.6g, 0.01mmol) and *N*-3,4-dihydroxyphenethylamine (0.152g, 0.8mmol) were dissolved in 3ml dichloromethane (DCM). After purging Argon for

15 min, triethylamine (0.081 g, 0.8 mmol) was added dropwise and the whole mixture was stirred at room temperature for 2 days. The final mixture was diluted with DCM and centrifuged to remove salt. The rest solution was precipitated twice into hexane and dried overnight to obtain p(MEO$_2$MA-*co*-OEGMA-*co*-DOPA)-*b*-p(DMAEMA)$_{135}$-*b*-p(MEO$_2$MA-*co*-OEGMA-*co*-DOPA) **(4)**.

Product **(3)** (0.6g, 0.01mmol) and methyl iodide (0.568g, 4mmol) were dissolved in 3ml dichloromethane. After purging Argon for 15 min, the mixture was stirred at room temperature for 4 h. The final mixture was diluted with DCM and centrifuged to obtain the precipitated polymer. The final product was dried in vacuum overnight and characterized as p[(MEO$_2$MA)$_{14}$-*co*-(OEGMA)$_2$-*co*-(DOPA)$_2$]-*b*-p(META)$_{135}$-*b*-p[(MEO$_2$MA)$_{14}$-*co*-(OEGMA)$_2$-*co*-(DOPA)$_2$] **(5)**. ^{1}H NMR (D$_2$O, 400 MHz): δ_H (ppm) = 0.85-1.22 (m, -CH$_2$-C(CO)-CH$_3$), 1.83-2.24 (m, -CH$_2$-C(CO)-CH$_3$), 4.50 (s, -COO-CH$_2$-CH$_2$-N(CH$_3$)$_3$), 3.28 (s, -COO-CH$_2$-CH$_2$-N(CH$_3$)$_3$), 6.58-6.86 (m, -CH$_2$C$_6$H$_3$(OH)$_2$), 3.50-4.00 (m, -CH$_2$-CH$_2$O-). PDI=1.3.
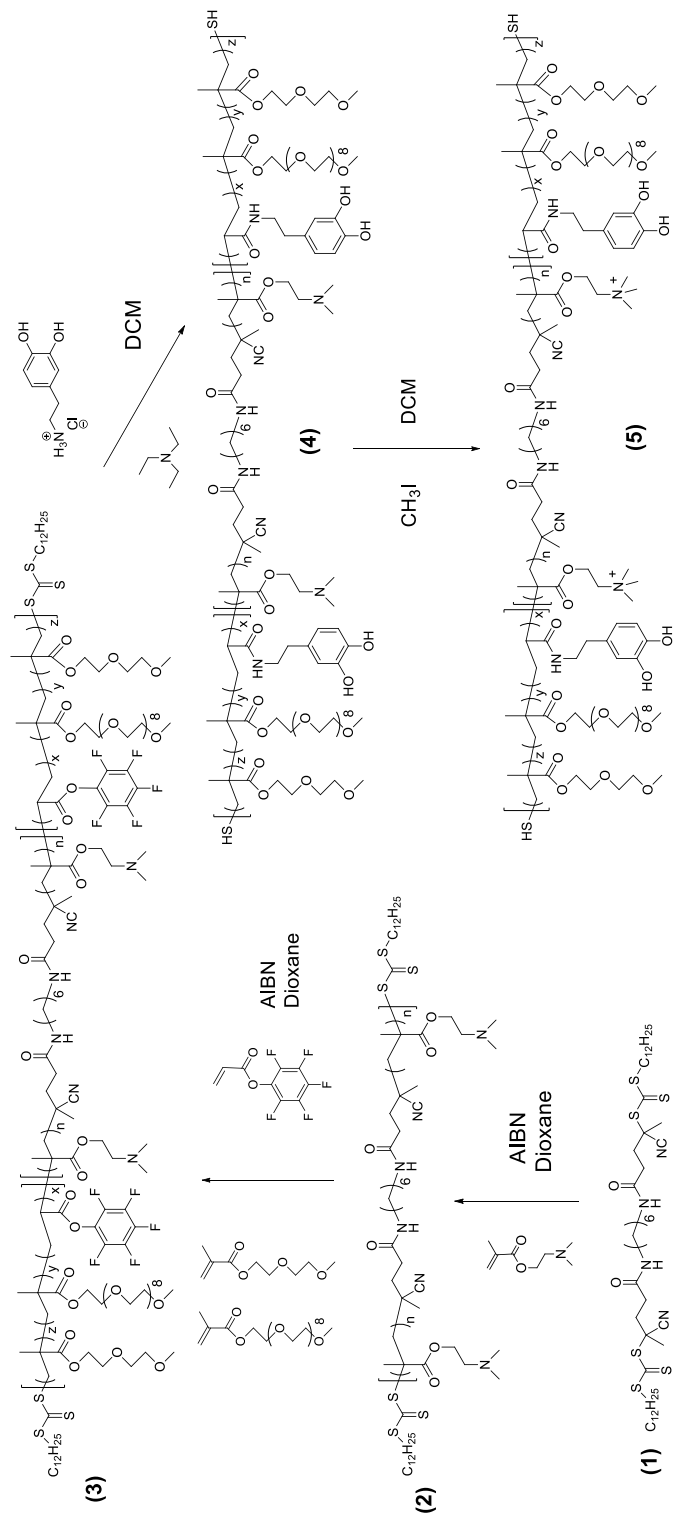
Figure 4.2 Synthesis routes

4.2.2   Oscillatory rheology

A rheometer (TA instruments, AR-G2) equipped with a 20-mm parallel-plate configuration was used to study the thermo-sensitivity and self-healing performance of the prepared hydrogel. Temperature ramp between 0-40 °C with a heating rate of 1 °C/min was conducted on a 20 wt% sample. A temperature cyclic step test alternating between 0 °C and 37 °C with 10 rad/s angular frequency and 1 % strain was also applied. The changes of storage and loss modulus with temperature and time were recorded. To characterize the self-healing performance of the prepared hydrogel, external strain increasing from 0.1% to 1000% was applied to a 20 wt% sample at 37 °C and 10 rad/s, followed by an immediate return of strain to 1%. A strain step cycled between 1 % and 500 % was also performed at 37 °C and 10 rad/s. Changes of storage and loss modulus with strain amplitude and time were recorded.

4.2.3   Antifouling assay

Human intestinal Caco-2 cell line, the Caco-2 cell base medium, growth kit (low serum), Trypsin-EDTA and Trypsin neutralizing solution were purchased from the American Type Culture Collection (ATCC, Manassas, VA, USA). Alexa Fluor dyes and 4,6-diamidino-2-phenylindole (DAPI) were purchased from Life Technologies (burlington, ON, Canada). Caco-2 cells were seeded onto the 15 wt% hydrogel-coated dishes and bare control dishes and cultured for 2 days. The cells were washed with PBS and fixed with 4% paraformaldehyde (w/v in PBS) before Alexa Fluor 488 and DAPI were used to stain the cell membrane and the nuclei respectively. The hydrogel-coated microwell dishes and the control dishes were

observed under a confocal laser scanning microscopy (CLSM 510 Meta, Carl Zeiss, Jena, Germany) equipped with a ZEN 2009LE software.

4.2.4   Antimicrobial assay

Escherichia coli aw1.7 strain line was purchased from the American Type Culture Collection (ATCC, Manassas, VA, USA). Luria-Bertani (LB) and agar were purchased from BD Difco[TM]. LB broth was prepared by mixing LB (25g) in 1000 mL distilled water and then sterilized in a reusable media storage bottle (PYREX™) at 121°C for 30 min. *E. coli* was transferred to a tube containing LB broth and incubated at 37°C for 24 h with shake to prepare *E. coli* suspension. Then 100 µL *E. coli* suspension was transferred to a tube containing 2.5 mL LB broth and 400 µL 1 wt% polymer sample and incubate at 37°C for 24h with shake. 100 µL *E. coli* suspension was also transferred to a tube containing pure LB broth as a control.

By mixing LB (25 g) and agar (15 g) in 1000 mL distilled water and autoclaving the mixture in a conical flask at 121°C for 30 min, nutrient agar media was prepared and added (15mL, 70°C) into a sterilized petri dish (diameter=10cm). After cooling and solidification, 100 µL of polymer-treated and non-treated *E. coli* suspension dilute solutions were transferred to cover the entire agar plates, respectively. The agar plates were incubated at 37°C for 24h before *E. coli* colony forming units were counted and calculated.

4.3 Results and discussion
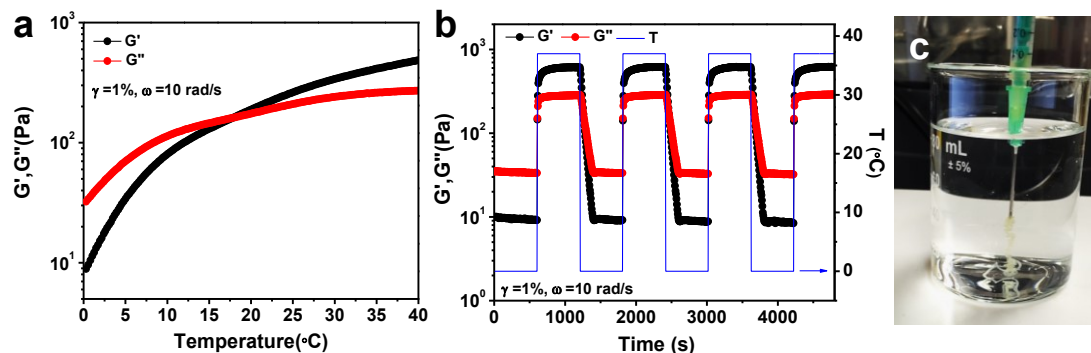
Figure 4.3 (a) Storage (G') and loss (G") modulus changes of a 20 wt% hydrogel with temperature. (b) Modulus changes of a 20 wt% hydrogel with thermal cycles of heating (37 °C) and cooling (0 °C) for four rounds. (c) Injection of a 4 °C-preserved polymer solution sample into 37 °C DI water.

To quantitatively characterize the thermo-sensitivity of the prepared hydrogel, rheological tests were conducted on a 20 wt% sample to measure the changes of its storage modulus (G') and loss modulus (G") with temperature. As shown in Figure 4.3a, at lower temperatures, G" was larger than G', indicating a liquid-like sol state. While with the heating process, G' increased significantly faster than G" and surpassed G" at higher temperature, indicating a solid-like gel state. The cross-over point at 18 °C was defined as the gelation temperature. The temperature was then cycled between 0 °C and 37 °C and the tested hydrogel demonstrated a fully reversible sol-gel transition behaviour within the 90 min test duration (Figure 4.3b), indicating that the hydrogel was constructed mainly through hydrophobic interactions arisen from the PEG-based analogues, rather than through irreversible

covalent quinone cross-linking arisen from the catechol moieties. The excellent thermo-reversibility endows this novel hydrogel a mouldable property, that a low-temperature preserved precursor solution when transferred to target location can form gel tailored to the specific surface morphology. To facilitate operation, it would be desirable that the transferring process can be achieved through injection using a syringe. As shown in Figure 4.3c, when a 4 °C-preserved 20 wt% polymer solution was injected to a 37 °C-water bath using a 23G× 3/4" syringe, robust hydrogel formed instantaneously.
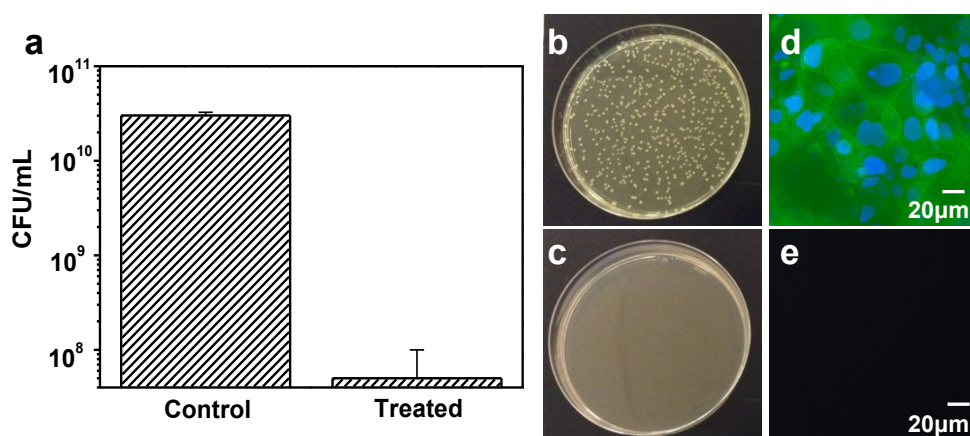
Figure 4.4 (a) Colony forming units (CFUs) of *E. coli* in control broth and 1wt% polymer treated broth after 24 h incubation. (b-c) Images of *E. coli* colonies on agar plates from diluted bacterial suspension without treatment (b) and treated with 1 wt% polymer (c). (d-e) Representative fluorescence microscopy images of uncoated (d) and hydrogel coated (e) microwell dish after exposure to Caco-2 cells for 48 h.

Gram-negative *Escherichia coli* aw1.7 (*E. coli*) was used as a model bacterial strain to evaluate the antimicrobial properties of our sample. *E. coli*

suspensions were incubated with control Luria-Bertani (L-B) broth and 1 wt% polymer treated L-B broth respectively, at 37 °C for 24h. The resulting bacterial suspensions were used for agar plating and colony counting to determine the viable bacterial numbers. As shown in Figure 4.4a-c, 1 wt% polymer sample was able to kill *E. coli* with more than 99.8% reduction in bacterial counts, as compared with the control L-B broth, which was attributed to the electrostatic targeting of the negatively-charged microorganism lipid membrane followed by a lysis resulting in cell death.[27] Compared with antibiotics-releasing materials, cationic polymers are less likely to select and promote the emergence of new resistant strains due to their contact-killing mechanism, which is important for some chronic biomedical processes.[28]Human intestinal Caco-2 cell was used as a model cell strain to evaluate the antifouling performance of the prepared hydrogel. Caco-2 cells were cultured in uncoated and hydrogel-coated microwell dishes respectively for 48 h before they were rinsed and stained followed by fluorescence imaging. As shown in Figure 4.4d, a dense layer of cells attached to the glass bottom of the uncoated microwell dish, with green fluorescence indicating cell membranes and blue fluorescence indicating nuclei. In contrast, the hydrogel-coated microwell dish (Figure 4.4e) exhibited great resistance against cell attachment, which could be attributed to the presence of PEG-based component and the inherent hydrophilic nature of the prepared hydrogel.[29, 30]
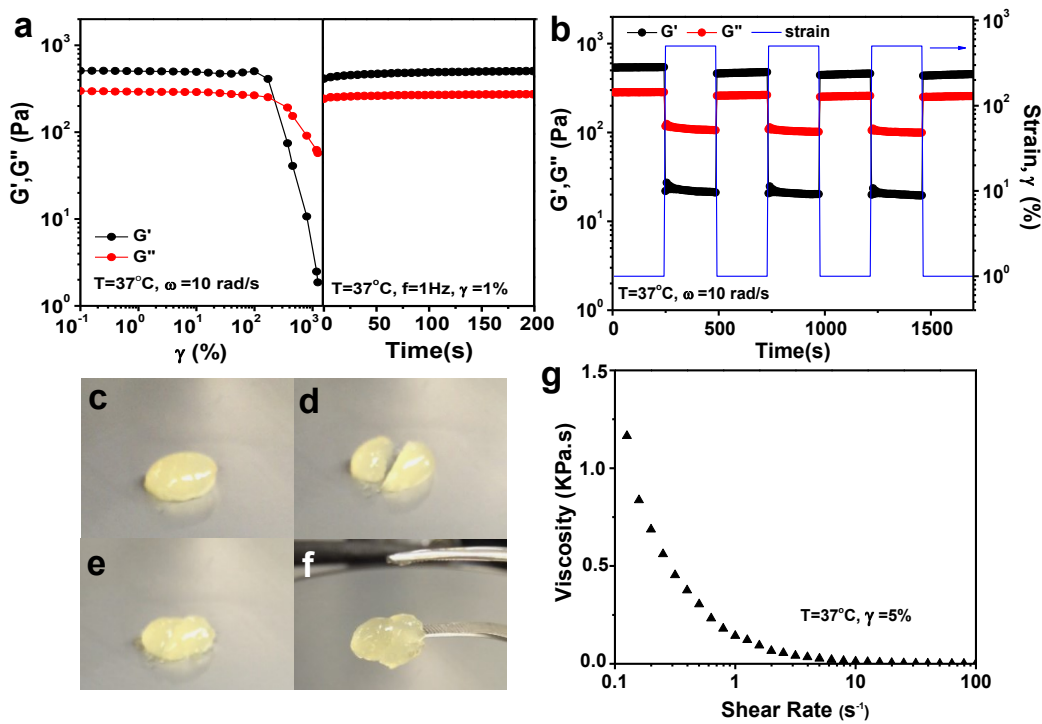
Figure 4.5 (a) Storage (G') and loss (G") modulus changes of a 20 wt% hydrogel upon enhanced external strains at 37°C (left) and an instantaneous recovery from the 1000% strain deformation (right). (b) Dynamic strain cyclic tests (γ =1% or 500%) of 20 wt% hydrogel at 37°C showing self-healing behaviour. (c-f) Visual evidence of self-healing: a hydrogel sample (c) was cut in half (d), and the two fragments after brought together to contact for several seconds (e) could heal into one integral piece (f). (g) Viscosity measurement of a 20 wt% hydrogel sample with shear rate.

For hydrogels working as bioengineering functions, it's important that they can spontaneously recover from inflicted damage to maintain both structural and functional integrity. Rheological strain sweep measurements were conducted on a 20 wt% hydrogel to quantitatively investigate its

responsive behaviour upon external strains. As shown in Figure 4.5a, when applied strain was increased from 0.1% to 100%, both G' and G" values maintained unchanged, suggesting the hydrogel could withstand relatively large deformation. However, a further increase of the strain till 1000% resulted in a dramatic drop of both G' and G" values with a crossover point occurring at around 250%, suggesting that beyond this critical strain limit the hydrogel network got ruptured and turned into a liquid-like sol state due to the severe dislocation of polymer chains. However when a 1% strain was applied immediately after the gel failure (γ=1000%), the mechanical properties of the hydrogel sample got almost fully recovered. Dynamic strain cyclic tests with strain alternating between 1% and 500% were also applied to a 20 wt% hydrogel sample, as illustrated in Figure 4.5b. G' dropped from ~550 Pa to ~20 Pa when subjected to the 500% strain, while achieved over 90% recovery within seconds upon the strain returning to 1%. This recovery behaviour was fully reversible and reproducible during the cyclic tests, indicating excellent self-healing performance of our hydrogel. Visual evidence of the self-healing property was demonstrated in Figure 4.5c-f, where a hydrogel sample was cut into half and the two fragments could automatically heal into one integral piece within seconds when brought into contact. The self-healing mechanism was attributed to catechol-mediated hydrogen bonding and aromatic interactions (Figure 4.1b), which agrees well with recent discovery of the metal-free self-healing mechanism of mussel-inspired catechol-functionalized materials.[21, 22] Viscosity measurement of a

20wt% hydrogel sample was conducted and a dramatic drop of sample viscosity with increasing shear rate was observed (Figure 4.5g). This shear-thinning behaviour provides the broken polymer segments (e.g. catechol groups) at the disrupted interface with enhanced mobility to interact with each other to reconstruct the physical cross-links, and further to restore the hydrogel network.[31]

4.4   Conclusion

In summary, we have developed a novel injectable thermo-sensitive self-healing hydrogel with antimicrobial and antifouling properties, based on the self-assembly of an *ABA* tri-block copolymer in metal-free aqueous solution. This hydrogel can effectively inhibit the growth of *E. coli* due to the presence of cationic quaternary amine, and prevent nonspecific cell attachment due to the presence of a major component PEO. The hydrogel can also heal autonomously from repeated damage, through mussel-inspired catechol-mediated hydrogen bonding and aromatic interactions. The combination of features including thermo-sensitivity, injectability, self-healing, antimicrobial and antifouling into one single design endows this hydrogel with great potential in various bioengineering applications.

4.5   Reference

1.   S. Lü, C. Gao, X. Xu, X. Bai, H. Duan, N. Gao, C. Feng, Y. Xiong and M. Liu, *ACS Appl Mater Interfaces*, 2015, **7**, 13029-13037.

2.   T. T. Reddy and A. Takahara, *Polymer*, 2009, **50**, 3537-3546.

3.   Y. Zhang, J. Zhang, M. Chen, H. Gong, S. Thamphiwatana, L. Eckmann, W. Gao and L. Zhang, *ACS Appl Mater Interfaces*, 2016, **8**, 18367-18374.

4.   F. Yu, X. Cao, J. Du, G. Wang and X. Chen, *ACS Appl Mater Interfaces*, 2015, **7**, 24023-24031.

5.   B. Wehrle-Haller, *Curr Opin Cell Biol*, 2012, **24**, 569-581.

6.   M. Black, A. Trent, Y. Kostenko, J. S. Lee, C. Olive and M. Tirrell, *Adv Mater*, 2012, **24**, 3845-3849.

7.   G. Cheng, H. Xue, G. Li and S. Jiang, *Langmuir*, 2010, **26**, 10425-10428.

8.   B. Cao, Q. Tang, L. Li, J. Humble, H. Wu, L. Liu and G. Cheng, *Adv healthc mater*, 2013, **2**, 1096-1102.

9.   L. Mi and S. Jiang, *Biomaterials*, 2012, **33**, 8928-8933.

10. K. Baek, J. Liang, W. T. Lim, H. Zhao, D. H. Kim and H. Kong, *Acs Appl Mater Interfaces*, 2015, **7**, 15359-15367.

11. C. Zhao, X. Li, L. Li, G. Cheng, X. Gong and J. Zheng, *Langmuir*, 2013, **29**, 1517-1524.

12. A. GhavamiNejad, C.-H. Park and C. S. Kim, *Biomacromolecules*, 2016.

13. D. E. Fullenkamp, J. G. Rivera, Y.-k. Gong, K. H. A. Lau, L. He, R. Varshney and P. B. Messersmith, *Biomaterials*, 2012, **33**, 3783-3791.

14. S. Q. Liu, C. Yang, Y. Huang, X. Ding, Y. Li, W. M. Fan, J. L. Hedrick and Y. Y. Yang, *Adv Mater*, 2012, **24**, 6484-6489.

15. Y.-H. La, B. D. McCloskey, R. Sooriyakumaran, A. Vora, B. Freeman, M. Nassar, J. Hedrick, A. Nelson and R. Allen, *J Membrane Sci*, 2011, **372**, 285-291.

16.   L. Yu, G. Y. Chen, H. Xu and X. Liu, *ACS Nano*, 2016, **10**, 1076-1085.

17.   H.-P. Cong, P. Wang and S.-H. Yu, *Chem Mater*, 2013, **25**, 3357-3362.

18.   S. Burattini, B. W. Greenland, D. H. Merino, W. Weng, J. Seppala, H. M. Colquhoun, W. Hayes, M. E. Mackay, I. W. Hamley and S. J. Rowan, *J Am Chem Soc*, 2010, **132**, 12051-12058.

19.   H. Zeng, D. S. Hwang, J. N. Israelachvili and J. H. Waite, *Proc Natl Acad Sci*, 2010, **107**, 12850-12853.

20.   L. Li, W. Smitthipong and H. Zeng, *Polym Chem*, 2015, **6**, 353-358.

21.   B. K. Ahn, D. W. Lee, J. N. Israelachvili and J. H. Waite, *Nat Mater*, 2014, **13**, 867-872.

22.   L. Li, B. Yan, J. Yang, L. Chen and H. Zeng, *Adv Mater*, 2015, **27**, 1294-1299.

23.   J.-F. Lutz, K. Weichenhan, Ö. Akdemir and A. Hoth, *Macromolecules*, 2007, **40**, 2503-2508.

24.   J. E. St. Dennis, Q. Meng, R. Zheng, N. S. Pesika, G. L. McPherson, J. He, H. S. Ashbaugh, V. T. John, M. B. Dowling and S. R. Raghavan, *Soft Matter*, 2011, **7**, 4170-4173.

25.   Y. He, W. He, D. Liu, T. Gu, R. Wei and X. Wang, *Polym Chem*, 2013, **4**, 402-406.

26.   M. Eberhardt, R. Mruk, R. Zentel and P. Théato, *Eur Polym J*, 2005, **41**, 1569-1575.

27.   A. Strassburg, F. Kracke, J. Wenners, A. Jemeljanova, J. Kuepper, H. Petersen and J. C. Tiller, *Macromol Biosci*, 2015, **15**, 1710-1723.

28. D. Campoccia, L. Montanaro and C. R. Arciola, *Biomaterials*, 2013, **34**, 8533-8554.

29. L. Li, B. Yan, L. Zhang, Y. Tian and H. Zeng, *Chem Commun*, 2015, **51**, 15780-15783.

30. T. Ekblad, G. Bergström, T. Ederth, S. L. Conlan, R. Mutton, A. S. Clare, S. Wang, Y. Liu, Q. Zhao, F. D'Souza, G. T. Donnelly, P. R. Willemsen, M. E. Pettitt, M. E. Callow, J. A. Callow and B. Liedberg, *Biomacromolecules*, 2008, **9**, 2775-2783.

31. M. Guvendiren, H. D. Lu and J. A. Burdick, *Soft Matter*, 2012, **8**, 260-272.

5 Conclusions and prospects

The research work presented in this thesis aimed at developing new designs for mussel-inspired polymeric materials, both in structure and in functionality. Our efforts have been mainly dedicated to synthesizing block copolymers comprising catechol and other functional moieties through RAFT polymerization, and preparing them into functional materials with various potential bioengineering applications. The research works described in Chapter 2-4 have addressed some unresolved issues in polymer chemistry and materials science. One issue is the impact of polymer chain conformation (loops vs brushes) on the antifouling performance of polymeric surface coatings. To address this issue, an ABA tri-block copolymer employing catechol-functionalized PDMA as the adhesive anchoring A block and PEG as the antifouling middle B block was synthesized and used to prepare surfaces bearing polymer loops by simple drop-coating method. The formation of a layer of polymer loops was confirmed by comparing with a layer of polymer brushes prepared by coating an AB di-block copolymer with the same adhesive A block and half of the middle PEG chain length. A key novelty of this project is the determination of loops formation through distance and force measurements utilizing SFA. Protein adsorption tests using QCM-D demonstrated that at similar end graft densities, loops-bearing surfaces exhibited enhanced antifouling performance compared with brushes-bearing surfaces, which could be attributed to the strong steric hindrance and reduced chance of interpenetration of neutrally charged polymer loops as confirmed by direct force measurements.

Another issue is how to maintain both the structural and functional integrity of the implanted hydrogel materials (e.g. drug delivery vehicles) under constant external mechanical forces and internal biofouling accumulation to achieve a desirable *in vivo* performance. To address this issue, an injectable self-healing hydrogel with anti-biofouling property was prepared, based on the self-assembly of an ABA tri-block copolymer with mussel-inspired catechol functionalized PNIPAM as A block and PEO as B block. The prepared hydrogel exhibited excellent thermo-reversibility and a 4°C-preserved precursor solution could gelate immediately upon injection to body temperature. Besides effectively preventing cell attachment, this hydrogel could heal autonomously from repeated damage and recover its mechanical properties and physical structure within seconds in metal-free aqueous environment, guaranteeing both functional and structural integrity in practical application. Our major contribution is the successful unveiling and experimental verification of a novel mussel-inspired self-healing mechanism, catechol-mediated hydrogen bonding and aromatic interactions, by quantitatively characterizing recovery performance of different hydrogels after external strain. This project not only demonstrates a successful case of injectable multifunctional hydrogel working as potential drug delivery vehicles, but also offers inspirations of developing novel bio-inspired self-healing materials by proposing a new self-healing mechanism.

The third issue is how to develop multifunctional hydrogel materials to meet diverse needs in dynamic biomedical processes. To address this issue, a thermos-sensitive injectable self-healing hydrogel with antimicrobial and antifouling properties was developed, based on the self-assembly of an ABA triblock

copolymer with catechol functionalized PEG-based A block and quaternized B block. The excellent sol-gel thermo-reversibility endowed this hydrogel with capabilities of in-situ gelation and injectability, to accommodate to specific surface morphology and facilitate operation. Bearing simultaneously antimicrobial and antifouling properties, this hydrogel could effectively prevent bacterial growth and biofilm accumulation, reducing the risk of infection during biomedical process. What's more, this hydrogel could heal autonomously from repeated damage through the newly-discovered mussel-inspired self-healing mechanism, catechol-mediated hydrogen bonding and aromatic interactions, which was of great significance for implanted hydrogel materials subject to constant mechanical forces from daily body movements. In this project, the key novelty lies in the polymer design. The incorporation of multiple functions including thermos-sensitivity, injectability, antimicrobial, antifouling and self-healing into one hydrogel design has been successfully achieved for the first time.

In summary, based on the versatile DOPA chemistry, novel mussel-inspired functional polymeric materials with diverse potential bioengineering applications have been successfully designed and developed in research works presented in this thesis. For the future studies, one possible direction is optimizing polymer structure and employing *in vivo* tests to apply these functional materials into practical application. The designs proposed in this thesis can be further improved by adopting functional monomers with enhanced biocompatibility and biodegradability to achieve better *in vivo* performance. Another direction is designing and developing more mussel-inspired functional materials such as smart adhesives

which can switch reversibly between adhesive and non-adhesive states, and therapeutic adhesives which can seal surgical wounds as well as provide stimuli-responsive drug release to prevent wound infection or kill residual disease cells.

Bibliography

1.   J. H. Kavouras and J. S. Maki, *Invertebr Biol*, 2003, **122**, 138-151.

2.   J. Kavouras and J. Maki, *J Appl Microbiol*, 2004, **97**, 1236-1246.

3.   N. Aldred, L. Ista, M. Callow, J. Callow, G. Lopez and A. Clare, *J R Soc Interface*, 2006, **3**, 37-43.

4.   D. Crisp, G. Walker, G. Young and A. Yule, *J Colloid Interface Sci*, 1985, **104**, 40-50.

5.   V. Haris, *Sessile animals of the sea shore*, Springer Science & Business Media, 1990.

6.   J. H. Waite, *Int J Adhes Adhes*, 1987, **7**, 9-14.

7.   B. P. Lee, P. B. Messersmith, J. N. Israelachvili and J. H. Waite, *Ann Rev Mater Res*, 2011, **41**, 99.

8.   J. H. Waite, in *Structure, cellular synthesis and assembly of biopolymers*, Springer, 1992, pp. 27-54.

9.   D. S. Hwang, H. Zeng, A. Masic, M. J. Harrington, J. N. Israelachvili and J. H. Waite, *J Biol Chem*, 2010, **285**, 25850-25858.

10.   X. Qin and J. H. Waite, *J Exp Biol*, 1995, **198**, 633-644.

11.   N. Holten-Andersen, G. E. Fantner, S. Hohlbauch, J. H. Waite and F. W. Zok, *Nat mater*, 2007, **6**, 669-672.

12.   J. H. Waite, *J Biol Chem*, 1983, **258**, 2911-2915.

13.   D. R. Filpula, S. M. Lee, R. P. Link, S. L. Strausberg and R. L. Strausberg, *Biotechnol Prog*, 1990, **6**, 171-177.

14. S. W. Taylor, J. H. Waite, M. M. Ross, J. Shabanowitz and D. F. Hunt, *J Am Chem Soc*, 1994, **116**, 10803-10804.

15. L. M. Rzepecki, K. M. Hansen and J. H. Waite, *Biol Bull*, 1992, **183**, 123-137.

16. K. Inoue, Y. Takeuchi, D. Miki and S. Odo, *J Biol Chem*, 1995, **270**, 6698-6701.

17. V. V. Papov, T. V. Diamond, K. Biemann and J. H. Waite, *J Biol Chem*, 1995, **270**, 20183-20192.

18. M. A. Even, J. Wang and Z. Chen, *Langmuir*, 2008, **24**, 5795-5801.

19. L. A. Burzio and J. H. Waite, *Biochemistry*, 2000, **39**, 11147-11153.

20. S. Warner and J. Waite, *Mar Biol*, 1999, **134**, 729-734.

21. H. Zhao and J. H. Waite, *Biochemistry-us*, 2006, **45**, 14223-14231.

22. J. H. Waite and X. Qin, *Biochemistry*, 2001, **40**, 2887-2893.

23. H. Zhao and J. H. Waite, *J Biol Chem*, 2006, **281**, 26150-26158.

24. J. Yu, W. Wei, E. Danner, R. K. Ashley, J. N. Israelachvili and J. H. Waite, *Nat chem biol*, 2011, **7**, 588-590.

25. M. Yu, J. Hwang and T. J. Deming, *J Am Chem Soc*, 1999, **121**, 5825-5826.

26. H. Lee, N. F. Scherer and P. B. Messersmith, *Proc Natl Acad Sci*, 2006, **103**, 12999-13003.

27. B. K. Ahn, D. W. Lee, J. N. Israelachvili and J. H. Waite, *Nat Mater*, 2014, **13**, 867-872.

28. Q. Lu, E. Danner, J. H. Waite, J. N. Israelachvili, H. Zeng and D. S. Hwang, *J R Soc Interface*, 2013, **10**, 20120759.

29.   H. Zeng, D. S. Hwang, J. N. Israelachvili and J. H. Waite, *Proc Natl Acad Sci*, 2010, **107**, 12850-12853.

30.   N. Holten-Andersen, M. J. Harrington, H. Birkedal, B. P. Lee, P. B. Messersmith, K. Y. C. Lee and J. H. Waite, *Proc Natl Acad Sci*, 2011, **108**, 2651-2655.

31.   M. Krogsgaard, V. Nue and H. Birkedal, *Chem Eur J*, 2015.

32.   C. Fant, K. Sott, H. Elwing and F. Hook, *Biofouling*, 2000, **16**, 119-132.

33.   J. Waite and M. Tanzer, *Biochem Biophys Res Commun*, 1980, **96**, 1554-1561.

34.   Q. Lu, D. X. Oh, Y. Lee, Y. Jho, D. S. Hwang and H. Zeng, *Angew Chem*, 2013, **125**, 4036-4040.

35.   Q. Lu, D. S. Hwang, Y. Liu and H. Zeng, *Biomaterials*, 2012, **33**, 1903-1911.

36.   H. Zhang, L. P. Bré, T. Zhao, Y. Zheng, B. Newland and W. Wang, *Biomaterials*, 2014, **35**, 711-719.

37.   H. Lee, J. Rho and P. B. Messersmith, *Adv mater (Deerfield Beach, Fla.)*, 2009, **21**, 431.

38.   J. L. Dalsin, B.-H. Hu, B. P. Lee and P. B. Messersmith, *J Am Chem Soc*, 2003, **125**, 4253-4258.

39.   Y.-Z. Wang, L. Li, F.-S. Du and Z.-C. Li, *Polymer*, 2015.

40.   C. E. Brubaker and P. B. Messersmith, *Biomacromolecules*, 2011, **12**, 4326-4334.

41.   W. Zhang, Z. Pan, F. K. Yang and B. Zhao, *Adv Funct Mater*, 2015, **25**, 1588-1597.

42.   M. Krogsgaard, M. A. Behrens, J. S. Pedersen and H. Birkedal, *Biomacromolecules*, 2013, **14**, 297-301.

43.   B. K. Ahn, D. W. Lee, J. N. Israelachvili and J. H. Waite, *Nat mater*, 2014, **13**, 867-872.

44.   L. Li, B. Yan, J. Yang, L. Chen and H. Zeng, *Adv Mater*, 2015, **27**, 1294-1299.

45.   C. E. Brubaker, H. Kissler, L.-J. Wang, D. B. Kaufman and P. B. Messersmith, *Biomaterials*, 2010, **31**, 420-427.

46.   L. Ninan, J. Monahan, R. L. Stroshine, J. J. Wilker and R. Shi, *Biomaterials*, 2003, **24**, 4091-4099.

47.   J. Schnurrer and C.-M. Lehr, *Int J Pharm*, 1996, **141**, 251-256.

48.   R. Chivers and R. Wolowacz, *Int J Adhes Adhes*, 1997, **17**, 127-132.

49.   L. Ninan, R. Stroshine, J. Wilker and R. Shi, *Acta biomater*, 2007, **3**, 687-694.

50.   D. S. Hwang, H. J. Yoo, J. H. Jun, W. K. Moon and H. J. Cha, *Appl Environ Microb*, 2004, **70**, 3352-3359.

51.   D. S. Hwang, Y. Gim and H. J. Cha, *Biotechnol Prog*, 2005, **21**, 965-970.

52.   D. S. Hwang, Y. Gim, H. J. Yoo and H. J. Cha, *Biomaterials*, 2007, **28**, 3560-3568.

53.   D. S. Hwang, S. B. Sim and H. J. Cha, *Biomaterials*, 2007, **28**, 4039-4046.

54.   Y. Gim, D. S. Hwang, S. Lim, Y. H. Song and H. J. Cha, *Biotechnol Prog*, 2008, **24**, 1272-1277.

55.   S. Lim, Y. S. Choi, D. G. Kang, Y. H. Song and H. J. Cha, *Biomaterials*, 2010, **31**, 3715-3722.

56.   B. J. Kim, D. X. Oh, S. Kim, J. H. Seo, D. S. Hwang, A. Masic, D. K. Han and H. J. Cha, *Biomacromolecules*, 2014, **15**, 1579-1585.

57.   B. Yang, N. Ayyadurai, H. Yun, Y. S. Choi, B. H. Hwang, J. Huang, Q. Lu, H. Zeng and H. J. Cha, *Angew Chem Int Ed*, 2014, **53**, 13360-13364.

58.   H. Yamamoto and T. Hayakawa, *Biopolymers*, 1982, **21**, 1137-1151.

59.   M. Yu and T. J. Deming, *Macromolecules*, 1998, **31**, 4739-4745.

60.   M. J. Sever and J. J. Wilker, *Tetrahedron*, 2001, **57**, 6139-6146.

61.   J. Wang, C. Liu, X. Lu and M. Yin, *Biomaterials*, 2007, **28**, 3456-3468.

62.   G. Westwood, T. N. Horton and J. J. Wilker, *Macromol*, 2007, **40**, 3960-3964.

63.   Y. Saito, T. Kawano, M. Shimomura and H. Yabu, *Macromolecular rapid commun*, 2013, **34**, 630-634.

64.   M. Guvendiren, P. B. Messersmith and K. R. Shull, *Biomacromolecules*, 2007, **9**, 122-128.

65.   D. G. Barrett, G. G. Bushnell and P. B. Messersmith, *Adv healthc mater*, 2013, **2**, 745-755.

66.   E. Y. Jeon, B. H. Hwang, Y. J. Yang, B. J. Kim, B.-H. Choi, G. Y. Jung and H. J. Cha, *Biomaterials*, 2015.

67.   H. JungáChung and T. GwanáPark, *Soft Matter*, 2010, **6**, 977-983.

68. J. H. Ryu, Y. Lee, W. H. Kong, T. G. Kim, T. G. Park and H. Lee, *Biomacromolecules*, 2011, **12**, 2653-2659.

69. J. L. Dalsin and P. B. Messersmith, *Mater today*, 2005, **8**, 38-46.

70. H. Lee, S. M. Dellatore, W. M. Miller and P. B. Messersmith, *science*, 2007, **318**, 426-430.

71. C. Gao, G. Li, H. Xue, W. Yang, F. Zhang and S. Jiang, *Biomaterials*, 2010, **31**, 1486-1492.

72. Q. Wei, T. Becherer, R.-C. Mutihac, P.-L. M. Noeske, F. Paulus, R. Haag and I. Grunwald, *Biomacromolecules*, 2014, **15**, 3061-3071.

73. Y. Dang, M. Quan, C.-M. Xing, Y.-B. Wang and Y.-K. Gong, *J Mater Chem B*, 2015, **3**, 2350-2361.

74. S. Saxer, C. Portmann, S. Tosatti, K. Gademann, S. Zurcher and M. Textor, *Macromolecules*, 2009, **43**, 1050-1060.

75. G. Li, G. Cheng, H. Xue, S. Chen, F. Zhang and S. Jiang, *Biomaterials*, 2008, **29**, 4592-4597.

76. H. Han, J. Wu, C. W. Avery, M. Mizutani, X. Jiang, M. Kamigaito, Z. Chen, C. Xi and K. Kuroda, *Langmuir*, 2011, **27**, 4010-4019.

77. X. Ding, C. Yang, T. P. Lim, L. Y. Hsu, A. C. Engler, J. L. Hedrick and Y.-Y. Yang, *Biomaterials*, 2012, **33**, 6593-6603.

78. K. Lim, R. R. Y. Chua, B. Ho, P. A. Tambyah, K. Hadinoto and S. S. J. Leong, *Acta biomater*, 2015, **15**, 127-138.

79. J. Liu, J. Li, B. Yu, B. Ma, Y. Zhu, X. Song, X. Cao, W. Yang and F. Zhou, *Langmuir*, 2011, **27**, 11324-11331.

80.   E. Faure, E. Halusiak, F. Farina, N. Giamblanco, C. Motte, M. Poelman, C. Archambeau, C. c. Van De Weerdt, J. Martial and C. Jérôme, *Langmuir*, 2012, **28**, 2971-2978.

81.   F. Yu, S. Chen, Y. Chen, H. Li, L. Yang, Y. Chen and Y. Yin, *J Mol Struct*, 2010, **982**, 152-161.

82.   Q. Wei, X. Pei, J. Hao, M. Cai, F. Zhou and W. Liu, *Adv Mater Interfaces*, 2014, **1**.

83.   S. M. Kang, I. You, W. K. Cho, H. K. Shon, T. G. Lee, I. S. Choi, J. M. Karp and H. Lee, *Angew Chem Int Ed*, 2010, **49**, 9401-9404.

84.   Q. Ye, X. Wang, S. Li and F. Zhou, *Macromolecules*, 2010, **43**, 5554-5560.

85.   C. I. Biggs, M. Walker and M. I. Gibson, *Biomacromolecules*, 2016, **17**, 2626-2633.

86.   A. Taglietti, C. R. Arciola, A. D'Agostino, G. Dacarro, L. Montanaro, D. Campoccia, L. Cucca, M. Vercellino, A. Poggi, P. Pallavicini and L. Visai, *Biomaterials*, 2014, **35**, 1779-1788.

87.   M. Mazur, A. Barras, V. Kuncser, A. Galatanu, V. Zaitzev, K. V. Turcheniuk, P. Woisel, J. Lyskawa, W. Laure and A. Siriwardena, *Nanoscale*, 2013, **5**, 2692-2702.

88.   M. Arslan, T. N. Gevrek, J. Lyskawa, S. Szunerits, R. Boukherroub, R. Sanyal, P. Woisel and A. Sanyal, *Macromolecules*, 2014, **47**, 5124-5134.

89.   L. Wang, G. Li, Y. Lin, Z. Zhang, Z. Chen and S. Wu, *Polym Chem*, 2016, **7**, 4964-4974.

90.   A. S. Goldmann, C. Schödel, A. Walther, J. Yuan, K. Loos and A. H. Müller, *Macromol rapid commun*, 2010, **31**, 1608-1615.

91.   H. O. Ham, Z. Liu, K. Lau, H. Lee and P. B. Messersmith, *Angew Chem Int Ed*, 2011, **50**, 732-736.

92.   H. Lee, J. Rho and P. B. Messersmith, *Adv Mater*, 2009, **21**, 431-434.

93.   A. Rai and C. C. Perry, *J Mater Chem*, 2012, **22**, 4790-4796.

94.   Y. M. Shin, I. Jun, Y. M. Lim, T. Rhim and H. Shin, *Macromol Mater Eng*, 2013, **298**, 555-564.

95.   B.-H. Choi, Y. S. Choi, D. S. Hwang and H. J. Cha, *Tissue Eng Pt C Methods*, 2011, **18**, 71-79.

96.   Y. Cong, T. Xia, M. Zou, Z. Li, B. Peng, D. Guo and Z. Deng, *J Mater Chem B*, 2014, **2**, 3450-3461.

97.   X. Liu, J. Cao, H. Li, J. Li, Q. Jin, K. Ren and J. Ji, *Acs Nano*, 2013, **7**, 9384-9395.

98.   M. Nurunnabi, Z. Khatun, M. Nafiujjaman, D.-g. Lee and Y.-k. Lee, *ACS appl mater interfaces*, 2013, **5**, 8246-8253.

99.   M. D. Hager, P. Greil, C. Leyens, S. van der Zwaag and U. S. Schubert, *Adv Mater*, 2010, **22**, 5424-5430.

100.   B. Blaiszik, S. Kramer, S. Olugebefola, J. S. Moore, N. R. Sottos and S. R. White, *Ann Rev Mater Res*, 2010, **40**, 179-211.

101.   E. Vaccaro and J. H. Waite, *Biomacromolecules*, 2001, **2**, 906-911.

102.   P. S. Yavvari and A. Srivastava, *J Mater Chem B*, 2015, **3**, 899-910.

103. P. Sun, J. Wang, X. Yao, Y. Peng, X. Tu, P. Du, Z. Zheng and X. Wang, *ACS appl mater interfaces*, 2014, **6**, 12495-12504.

104. H. Ceylan, M. Urel, T. S. Erkal, A. B. Tekinay, A. Dana and M. O. Guler, *Adv Funct Mater*, 2013, **23**, 2081-2090.

105. Z. Shafiq, J. Cui, L. Pastor-Pérez, V. San Miguel, R. A. Gropeanu, C. Serrano and A. del Campo, *Angew Chem*, 2012, **124**, 4408-4411.

106. M. Krogsgaard, A. Andersen and H. Birkedal, *Chem Commun*, 2014, **50**, 13278-13281.

107. N. Holten-Andersen, A. Jaishankar, M. J. Harrington, D. E. Fullenkamp, G. DiMarco, L. He, G. H. McKinley, P. B. Messersmith and K. Y. C. Lee, *J Mater Chem B*, 2014, **2**, 2467-2472.

108. M. Krogsgaard, M. R. Hansen and H. Birkedal, *J Mater Chem B*, 2014, **2**, 8292-8297.

109. D. Roy, J. N. Cambre and B. S. Sumerlin, *Chem Commun*, 2009, DOI: 10.1039/B900374F, 2106-2108.

110. J. N. Cambre, D. Roy and B. S. Sumerlin, *J Polym Sci A Polyme Chem*, 2012, **50**, 3373-3382.

111. J. Yan, G. Springsteen, S. Deeter and B. Wang, *Tetrahedron*, 2004, **60**, 11205-11209.

112. L. He, D. E. Fullenkamp, J. G. Rivera and P. B. Messersmith, *Chem Commun*, 2011, **47**, 7497-7499.

113. M. Nakahata, S. Mori, Y. Takashima, A. Hashidzume, H. Yamaguchi and A. Harada, *ACS Macro Lett*, 2014, **3**, 337-340.

114. M. Vatankhah-Varnoosfaderani, A. GhavamiNejad, S. Hashmi and F. J. Stadler, *ChemCommun*, 2013, **49**, 4685-4687.

115. M. Vatankhah-Varnoosfaderani, S. Hashmi, A. GhavamiNejad and F. J. Stadler, *Polym Chem*, 2014, **5**, 512-523.

116. J. Su, F. Chen, V. L. Cryns and P. B. Messersmith, *J Am Chem Soc*, 2011, **133**, 11850-11853.

117. D. Tarus, E. Hachet, L. Messager, B. Catargi, V. Ravaine and R. Auzély-Velty, *Macromol Rapid Commun*, 2014, **35**, 2089-2095.

118. D. Roy and B. S. Sumerlin, *ACS Macro Lett*, 2012, **1**, 529-532.

119. K. T. Kim, J. J. L. M. Cornelissen, R. J. M. Nolte and J. C. M. v. Hest, *J Am Chem Soc*, 2009, **131**, 13908-13909.

120. C. C. Deng, W. L. Brooks, K. A. Abboud and B. S. Sumerlin, *ACS Macro Lett*, 2015, **4**, 220-224.

121. M. Vatankhah-Varnoosfaderani, A. GhavamiNejad, S. Hashmi and F. J. Stadler, *Macromol Rapid Commun*, 2015, 36, 447-452.

122. C. Werner, M. F. Maitz and C. Sperling, *J Mater Chem*, 2007, **17**, 3376-3384.

123. H. Otsuka, Y. Nagasaki and K. Kataoka, *Adv Drug Delivery Rev*, 2003, **55**, 403-419.

124. L. Li, B. Yan, J. Yang, L. Chen and H. Zeng, *Adv Mater*, 2015, **27**, 1294-1299.

125. M. Krishnamoorthy, S. Hakobyan, M. Ramstedt and J. E. Gautrot, *Chem Rev*, 2014, **114**, 10976-11026.

126. S. J. Sofia, V. Premnath and E. W. Merrill, *Macromolecules*, 1998, **31**, 5059-5070.

127. B. Dong, S. Manolache, A. C. Wong and F. S. Denes, *Polym Bull*, 2011, **66**, 517-528.

128. W. Norde and D. Gage, *Langmuir*, 2004, **20**, 4162-4167.

129. L. D. Unsworth, H. Sheardown and J. L. Brash, *Langmuir*, 2008, **24**, 1924-1929.

130. W. Zhao, Q. Ye, H. Hu, X. Wang and F. Zhou, *J Mater Chem B*, 2014, **2**, 5352-5357.

131. S. Maity, S. Nir, T. Zada and M. Reches, *Chem Commun*, 2014, **50**, 11154-11157.

132. J. H. Cho, K. Shanmuganathan and C. J. Ellison, *Acs Appl Mater Interfaces*, 2013, **5**, 3794-3802.

133. X. Ding, C. Yang, T. P. Lim, L. Y. Hsu, A. C. Engler, J. L. Hedrick and Y.-Y. Yang, *Biomaterials*, 2012, **33**, 6593-6603.

134. J. Kuang and P. B. Messersmith, *Langmuir*, 2012, **28**, 7258-7266.

135. M. Kobayashi, Y. Terayama, H. Yamaguchi, M. Terada, D. Murakami, K. Ishihara and A. Takahara, *Langmuir*, 2012, **28**, 7212-7222.

136. B. P. Lee, P. B. Messersmith, J. N. Israelachvili and J. H. Waite, *Ann Rev Mater Res*, 2011, **41**, 99.

137. M. Yu, J. Hwang and T. J. Deming, *J Am Chem Soc*, 1999, **121**, 5825-5826.

138. H. Zeng, D. S. Hwang, J. N. Israelachvili and J. H. Waite, *Proc Natl Acad Sci*, 2010, **107**, 12850-12853.

139.   Q. Lu, D. S. Hwang, Y. Liu and H. Zeng, *Biomaterials*, 2012, **33**, 1903-1911.

140.   Q. Lu, D. X. Oh, Y. Lee, Y. Jho, D. S. Hwang and H. Zeng, *Angew Chem*, 2013, **125**, 4036-4040.

141.   A. Ma, Y. Xie, J. Xu, H. Zeng and H. Xu, *Chem Commun*, 2015, **51**, 1469-1471.

142.   A. R. Statz, R. J. Meagher, A. E. Barron and P. B. Messersmith, *J Am Chem Soc*, 2005, **127**, 7972-7973.

143.   J. L. Dalsin, B.-H. Hu, B. P. Lee and P. B. Messersmith, *J Am Chem Soc*, 2003, **125**, 4253-4258.

144.   O. Pop-Georgievski, D. Verreault, M.-O. Diesner, V. Proks, S. Heissler, F. e. Rypáček and P. Koelsch, *Langmuir*, 2012, **28**, 14273-14283.

145.   G. Li, G. Cheng, H. Xue, S. Chen, F. Zhang and S. Jiang, *Biomaterials*, 2008, **29**, 4592-4597.

146.   D. Hong, K. Bae, S.-P. Hong, J. H. Park, I. S. Choi and W. K. Cho, *Chem Commun*, 2014, **50**, 11649-11652.

147.   L. Li, W. Smitthipong and H. Zeng, *Polym Chem*, 2015, **6**, 353-358.

148.   Z. Haung, H. Ji, J. Mays, M. Dadmun, G. Smith, D. Bedrov and Y. Zhang, *Langmuir*, 2009, **26**, 202-209.

149.   Z. Huang, H. Ji, J. W. Mays and M. D. Dadmun, *Macromolecules*, 2008, **41**, 1009-1018.

150.   Y. He and T. P. Lodge, *Macromolecules*, 2008, **41**, 167-174.

151. J. Nishida, M. Kobayashi and A. Takahara, *ACS Macro Lett*, 2013, **2**, 112-115.

152. P. L. Hansen, J. A. Cohen, R. Podgornik and V. A. Parsegian, *Biophys J*, 2003, **84**, 350-355.

153. I. Teraoka, *Polymer solutions: an introduction to physical properties*, Wiley. com, 2002.

154. P. De Gennes, *Adv Colloid Interface*, 1987, **27**, 189-209.

155. J. N. Israelachvili and G. E. Adams, *J Chem Soc Faraday Trans 1*, 1978, **74**, 975-1001.

156. G. Luengo, F.-J. Schmitt, R. Hill and J. Israelachvili, *Macromolecules*, 1997, **30**, 2482-2494.

157. H. Zeng, Y. Tian, T. H. Anderson, M. Tirrell and J. N. Israelachvili, *Langmuir*, 2007, **24**, 1173-1182.

158. Q. Lu, J. Wang, A. Faghihnejad, H. Zeng and Y. Liu, *Soft Matter*, 2011, **7**, 9366-9379.

159. D. S. Hwang, H. Zeng, A. Srivastava, D. V. Krogstad, M. Tirrell, J. N. Israelachvili and J. H. Waite, *Soft Matter*, 2010, **6**, 3232-3236.

160. J. Israelachvili, Y. Min, M. Akbulut, A. Alig, G. Carver, W. Greene, K. Kristiansen, E. Meyer, N. Pesika and K. Rosenberg, *Rep Prog Phys*, 2010, **73**, 036601.

161. L. Zhang, H. Zeng and Q. Liu, *J Phys Chem C*, 2012, **116**, 17554-17562.

162. L. Dai and C. Toprakcioglu, *Macromolecules*, 1992, **25**, 6000-6006.

163. D. Cao and J. Wu, *Langmuir*, 2006, **22**, 2712-2718.

164.   L. Dai, C. Toprakcioglu and G. Hadziioannou, *Macromolecules*, 1995, **28**, 5512-5517.

165.   E. Eiser, J. Klein, T. A. Witten and L. J. Fetters, *Phys Rev Lett*, 1999, **82**, 5076.

166.   S. R. Bhatia and W. B. Russel, *Macromolecules*, 2000, **33**, 5713-5720.

167.   J. Klein, *J Phys Condens Matter*, 2000, **12**, A19.

168.   S. Sheth and D. Leckband, *Proc Natl Acad Sci*, 1997, **94**, 8399-8404.

169.   L. Yu and J. Ding, *Chem Soc Rev*, 2008, **37**, 1473-1481.

170.   N. A. Peppas, J. Z. Hilt, A. Khademhosseini and R. Langer, *Adv Mater*, 2006, **18**, 1345-1360.

171.   H. Park, J. S. Temenoff, Y. Tabata, A. I. Caplan and A. G. Mikos, *Biomaterials*, 2007, **28**, 3217-3227.

172.   D. Sivakumaran, D. Maitland and T. Hoare, *Biomacromolecules*, 2011, **12**, 4112-4120.

173.   A. Parisi-Amon, W. Mulyasasmita, C. Chung and S. C. Heilshorn, *Adv Healthc Mater*, 2013, **2**, 428-432.

174.   T. Nakai, T. Hirakura, Y. Sakurai, T. Shimoboji, M. Ishigai and K. Akiyoshi, *Macromol Biosci*, 2012, **12**, 475-483.

175.   A. Paul, A. Hasan, H. A. Kindi, A. K. Gaharwar, V. T. Rao, M. Nikkhah, S. R. Shin, D. Krafft, M. R. Dokmeci and D. Shum-Tim, *ACS nano*, 2014, **8**, 8050-8062.

176.   A. L. Lee, V. W. Ng, S. Gao, J. L. Hedrick and Y. Y. Yang, *Adv Funct Mater*, 2014, **24**, 1538-1550.

177. B. F. Lin, K. A. Megley, N. Viswanathan, D. V. Krogstad, L. B. Drews, M. J. Kade, Y. Qian and M. V. Tirrell, *J Mater Chem*, 2012, **22**, 19447-19454.

178. A. López-Noriega, C. L. Hastings, B. Ozbakir, K. E. O'Donnell, F. J. O'Brien, G. Storm, W. E. Hennink, G. P. Duffy and E. Ruiz-Hernández, *Adv healthc mater*, 2014.

179. C. Ding, L. Zhao, F. Liu, J. Cheng, J. Gu, S.-. Dan, C. Liu, X. Qu and Z. Yang, *Biomacromolecules*, 2010, **11**, 1043-1051.

180. J. Yu, H. Fan, J. Huang and J. Chen, *Soft Matter*, 2011, **7**, 7386-7394.

181. Y. Zhang, Y. Sun, X. Yang, J. Hilborn, A. Heerschap and D. A. Ossipov, *Macromol Biosci*, 2014.

182. L. Tan, Y. Liu, W. Ha, L.-S. Ding, S.-L. Peng, S. Zhang and B.-J. Li, *Soft Matter*, 2012, **8**, 5746-5749.

183. X. Jiang, S. Jin, Q. Zhong, M. D. Dadmun and B. Zhao, *Macromolecules*, 2009, **42**, 8468-8476.

184. A. Servant, V. Leon, D. Jasim, L. Methven, P. Limousin, E. V. Fernandez-Pacheco, M. Prato and K. Kostarelos, *Adv healthc mater*, 2014.

185. E. Brynda, N. A. Cepalova and M. Štol, *J Biomed Mater Res*, 1984, **18**, 685-693.

186. B. Wehrle-Haller, *Curr Opin Cell Biol*, 2012, **24**, 569-581.

187. M. Black, A. Trent, Y. Kostenko, J. S. Lee, C. Olive and M. Tirrell, *Adv Mater*, 2012, **24**, 3845-3849.

188. L. Mi and S. Jiang, *Angew Chem Int Ed*, 2014, **53**, 1746-1754.

189. T. Kakuta, Y. Takashima, M. Nakahata, M. Otsubo, H. Yamaguchi and A. Harada, *Adv Mater*, 2013, **25**, 2849-2853.

190. A. Phadke, C. Zhang, B. Arman, C.-C. Hsu, R. A. Mashelkar, A. K. Lele, M. J. Tauber, G. Arya and S. Varghese, *Proc Natl Acad Sci*, 2012, **109**, 4383-4388.

191. Y. Amamoto, J. Kamada, H. Otsuka, A. Takahara and K. Matyjaszewski, *Angew Chem*, 2011, **123**, 1698-1701.

192. Y. Amamoto, H. Otsuka, A. Takahara and K. Matyjaszewski, *Adv Mater*, 2012, **24**, 3975-3980.

193. P. Cordier, F. Tournilhac, C. Soulie-Ziakovic and L. Leibler, *Nature*, 2008, **451**, 977-980.

194. S. Rose, A. Prevoteau, P. Elzière, D. Hourdet, A. Marcellan and L. Leibler, *Nature*, 2013.

195. A. Faghihnejad, K. E. Feldman, J. Yu, M. V. Tirrell, J. N. Israelachvili, C. J. Hawker, E. J. Kramer and H. Zeng, *Adv Funct Mater*, 2014, **24**, 2322-2333.

196. D. Liu, D. Wang, M. Wang, Y. Zheng, K. Koynov, G. K. Auernhammer, H.-J. Butt and T. Ikeda, *Macromolecules*, 2013, **46**, 4617-4625.

197. J. Sedó, J. Saiz-Poseu, F. Busqué and D. Ruiz-Molina, *Adv Mater*, 2013, **25**, 653-701.

198. Y. Zhao, F. Sakai, L. Su, Y. Liu, K. Wei, G. Chen and M. Jiang, *Adv Mater*, 2013, **25**, 5215-5256.

199. Y. Liu, K. Ai and L. Lu, *Chem Rev*, 2014.

200. B. Yang, N. Ayyadurai, H. Yun, Y. S. Choi, B. H. Hwang, J. Huang, Q. Lu, H. Zeng and H. J. Cha, *Angew Chem Int Ed*, 2014.

201. N. Holten-Andersen, M. J. Harrington, H. Birkedal, B. P. Lee, P. B. Messersmith, K. Y. C. Lee and J. H. Waite, *Proc Natl Acad Sci*, 2011, **108**, 2651-2655.

202. M. Krogsgaard, M. A. Behrens, J. S. Pedersen and H. Birkedal, *Biomacromolecules*, 2013, **14**, 297-301.

203. L. He, D. E. Fullenkamp, J. G. Rivera and P. B. Messersmith, *Chem Commun*, 2011, **47**, 7497-7499.

204. M. Vatankhah-Varnoosfaderani, S. Hashmi, A. GhavamiNejad and F. J. Stadler, *Polym Chem*, 2014, **5**, 512-523.

205. B. J. Kim, D. X. Oh, S. Kim, J. H. Seo, D. S. Hwang, A. Masic, D. K. Han and H. J. Cha, *Biomacromolecules*, 2014, **15**, 1579-1585.

206. B. P. Lee, P. B. Messersmith, J. N. Israelachvili and J. H. Waite, *Ann Rev Mater Res*, 2011, **41**, 99.

207. H. Zeng, D. S. Hwang, J. N. Israelachvili and J. H. Waite, *Proc Natl Acad Sci*, 2010, **107**, 12850-12853.

208. Q. Lu, D. S. Hwang, Y. Liu and H. Zeng, *Biomaterials*, 2012, **33**, 1903-1911.

209. Q. Lu, D. X. Oh, Y. Lee, Y. Jho, D. S. Hwang and H. Zeng, *Angew Chem Int Ed*, 2013, **52**, 3944-3948.

210. D. S. Hwang, H. Zeng, A. Masic, M. J. Harrington, J. N. Israelachvili and J. H. Waite, *J Biol Chem*, 2010, **285**, 25850-25858.

211. B. K. Ahn, D. W. Lee, J. N. Israelachvili and J. H. Waite, *Nat mater*, 2014, **13**, 867-872.

212. Y. He and T. P. Lodge, *Macromolecules*, 2008, **41**, 167-174.

213. W. Wei, J. Yu, C. Broomell, J. N. Israelachvili and J. H. Waite, *J Am Chem Soc*, 2012, **135**, 377-383.

214. M. Eberhardt, R. Mruk, R. Zentel and P. Théato, *Eur Polym J*, 2005, **41**, 1569-1575.

215. T. G. O'Lenick, N. Jin, J. W. Woodcock and B. Zhao, *J Phys Chem B*, 2011, **115**, 2870-2881.

216. A. Vagias, P. Košovan, K. Koynov, C. Holm, H.-J. r. Butt and G. Fytas, *Macromolecules*, 2014, **47**, 5303-5312.

217. R. Bodvik, L. Karlson, K. Edwards, J. Eriksson, E. Thormann and P. M. Claesson, *Langmuir*, 2012, **28**, 13562-13569.

218. L. M. Salonen, M. Ellermann and F. Diederich, *Angew Chem Int Ed*, 2011, **50**, 4808-4842.

219. S. Herrwerth, W. Eck, S. Reinhardt and M. Grunze, *J Am Chem Soc*, 2003, **125**, 9359-9366.

220. E. Ostuni, R. G. Chapman, R. E. Holmlin, S. Takayama and G. M. Whitesides, *Langmuir*, 2001, **17**, 5605-5620.

221. S. Lü, C. Gao, X. Xu, X. Bai, H. Duan, N. Gao, C. Feng, Y. Xiong and M. Liu, *ACS Appl Mater Interfaces*, 2015, **7**, 13029-13037.

222. T. T. Reddy and A. Takahara, *Polymer*, 2009, **50**, 3537-3546.

223. Y. Zhang, J. Zhang, M. Chen, H. Gong, S. Thamphiwatana, L. Eckmann, W. Gao and L. Zhang, *ACS Appl Mater Interfaces*, 2016, **8**, 18367-18374.

224. F. Yu, X. Cao, J. Du, G. Wang and X. Chen, *ACS Appl Mater Interfaces*, 2015, **7**, 24023-24031.

225. B. Wehrle-Haller, *Curr Opin Cell Biol*, 2012, **24**, 569-581.

226. M. Black, A. Trent, Y. Kostenko, J. S. Lee, C. Olive and M. Tirrell, *Adv Mater*, 2012, **24**, 3845-3849.

227. G. Cheng, H. Xue, G. Li and S. Jiang, *Langmuir*, 2010, **26**, 10425-10428.

228. B. Cao, Q. Tang, L. Li, J. Humble, H. Wu, L. Liu and G. Cheng, *Adv healthc mater*, 2013, **2**, 1096-1102.

229. L. Mi and S. Jiang, *Biomaterials*, 2012, **33**, 8928-8933.

230. K. Baek, J. Liang, W. T. Lim, H. Zhao, D. H. Kim and H. Kong, *Acs Appl Mater Interfaces*, 2015, **7**, 15359-15367.

231. C. Zhao, X. Li, L. Li, G. Cheng, X. Gong and J. Zheng, *Langmuir*, 2013, **29**, 1517-1524.

232. A. GhavamiNejad, C.-H. Park and C. S. Kim, *Biomacromolecules*, 2016.

233. D. E. Fullenkamp, J. G. Rivera, Y.-k. Gong, K. H. A. Lau, L. He, R. Varshney and P. B. Messersmith, *Biomaterials*, 2012, **33**, 3783-3791.

234. S. Q. Liu, C. Yang, Y. Huang, X. Ding, Y. Li, W. M. Fan, J. L. Hedrick and Y. Y. Yang, *Adv Mater*, 2012, **24**, 6484-6489.

235. Y.-H. La, B. D. McCloskey, R. Sooriyakumaran, A. Vora, B. Freeman, M. Nassar, J. Hedrick, A. Nelson and R. Allen, *J Membrane Sci*, 2011, **372**, 285-291.

236.   L. Yu, G. Y. Chen, H. Xu and X. Liu, *ACS Nano*, 2016, **10**, 1076-1085.

237.   H.-P. Cong, P. Wang and S.-H. Yu, *Chem Mater*, 2013, **25**, 3357-3362.

238.   S. Burattini, B. W. Greenland, D. H. Merino, W. Weng, J. Seppala, H. M. Colquhoun, W. Hayes, M. E. Mackay, I. W. Hamley and S. J. Rowan, *J Am Chem Soc*, 2010, **132**, 12051-12058.

239.   H. Zeng, D. S. Hwang, J. N. Israelachvili and J. H. Waite, *Proc Natl Acad Sci*, 2010, **107**, 12850-12853.

240.   L. Li, W. Smitthipong and H. Zeng, *Polym Chem*, 2015, **6**, 353-358.

241.   B. K. Ahn, D. W. Lee, J. N. Israelachvili and J. H. Waite, *Nat Mater*, 2014, **13**, 867-872.

242.   L. Li, B. Yan, J. Yang, L. Chen and H. Zeng, *Adv Mater*, 2015, **27**, 1294-1299.

243.   J.-F. Lutz, K. Weichenhan, Ö. Akdemir and A. Hoth, *Macromolecules*, 2007, **40**, 2503-2508.

244.   J. E. St. Dennis, Q. Meng, R. Zheng, N. S. Pesika, G. L. McPherson, J. He, H. S. Ashbaugh, V. T. John, M. B. Dowling and S. R. Raghavan, *Soft Matter*, 2011, **7**, 4170-4173.

245.   Y. He, W. He, D. Liu, T. Gu, R. Wei and X. Wang, *Polym Chem*, 2013, **4**, 402-406.

246.   M. Eberhardt, R. Mruk, R. Zentel and P. Théato, *Eur Polym J*, 2005, **41**, 1569-1575.

247.   A. Strassburg, F. Kracke, J. Wenners, A. Jemeljanova, J. Kuepper, H. Petersen and J. C. Tiller, *Macromol Biosci*, 2015, **15**, 1710-1723.

248. D. Campoccia, L. Montanaro and C. R. Arciola, *Biomaterials*, 2013, **34**, 8533-8554.

249. L. Li, B. Yan, L. Zhang, Y. Tian and H. Zeng, *Chem Commun*, 2015, **51**, 15780-15783.

250. T. Ekblad, G. Bergström, T. Ederth, S. L. Conlan, R. Mutton, A. S. Clare, S. Wang, Y. Liu, Q. Zhao, F. D'Souza, G. T. Donnelly, P. R. Willemsen, M. E. Pettitt, M. E. Callow, J. A. Callow and B. Liedberg, *Biomacromolecules*, 2008, **9**, 2775-2783.

251. M. Guvendiren, H. D. Lu and J. A. Burdick, *Soft Matter*, 2012, **8**, 260-272.

Appendix
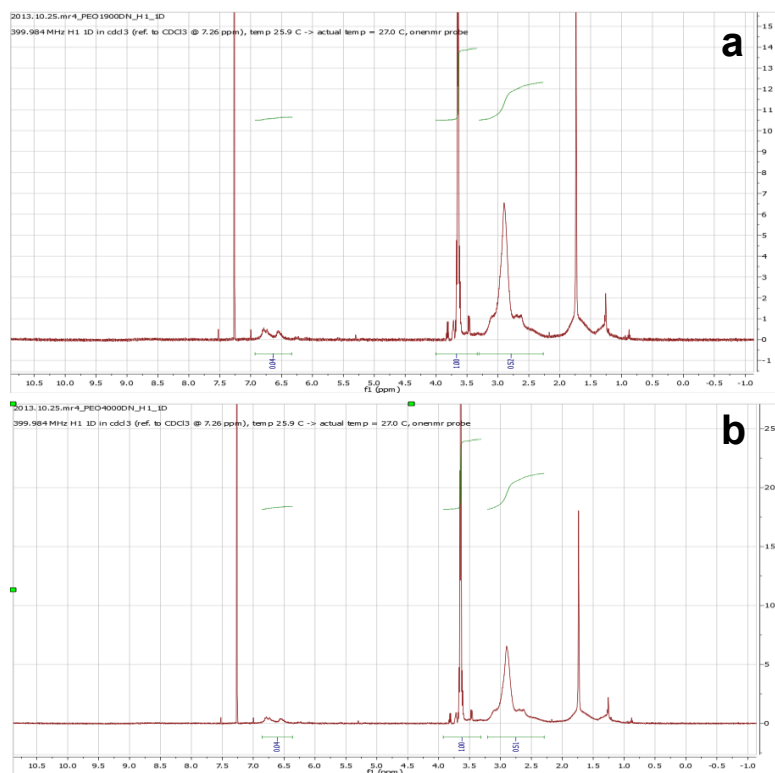
Figure S2.1 Raw NMR data for PDN-PEG-PDN(a) and PDN-PEG (b).
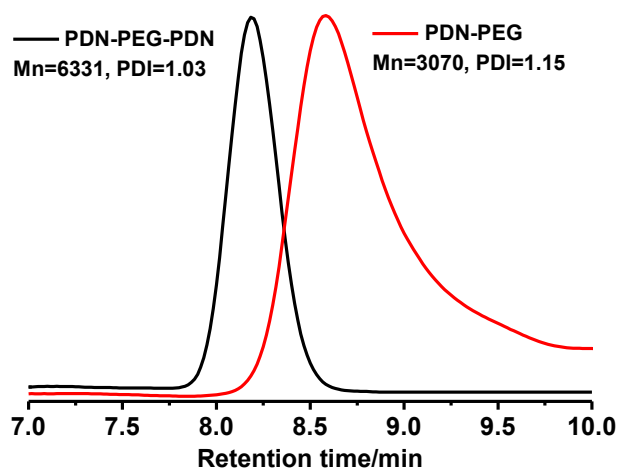
Figure S2.2 GPC trace of PDN-PEG-PDN and PDN-PEG.
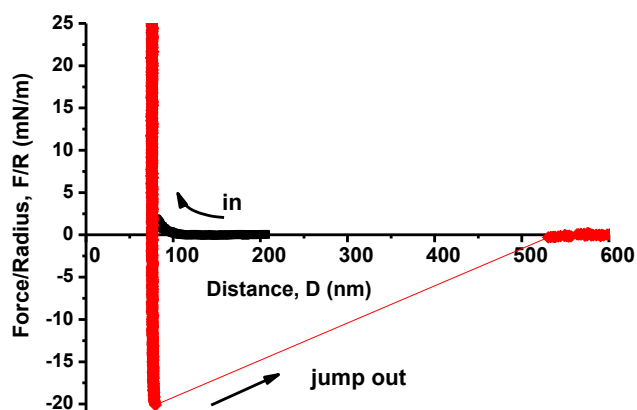
Figure S2.3 Force-distance profiles between two thick PDN-PEG-PDN films prepared by spin-coating using relatively high concentration of polymer solution (2.5mg/ml in toluene and DCM).
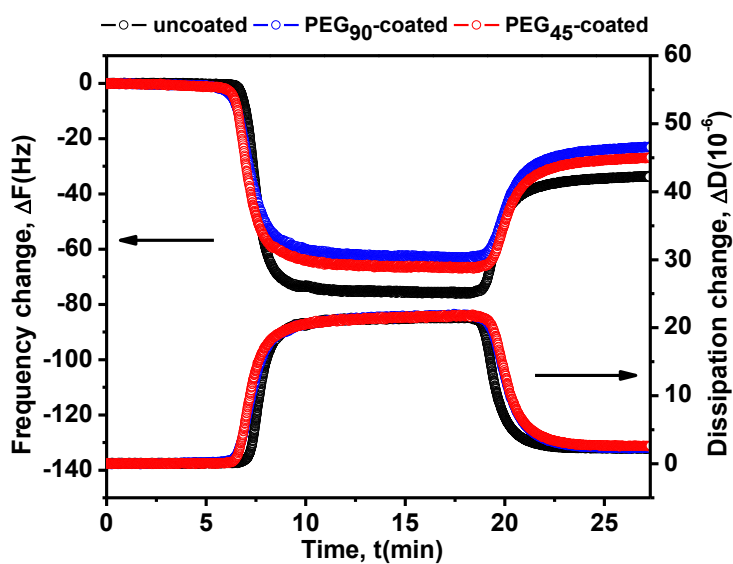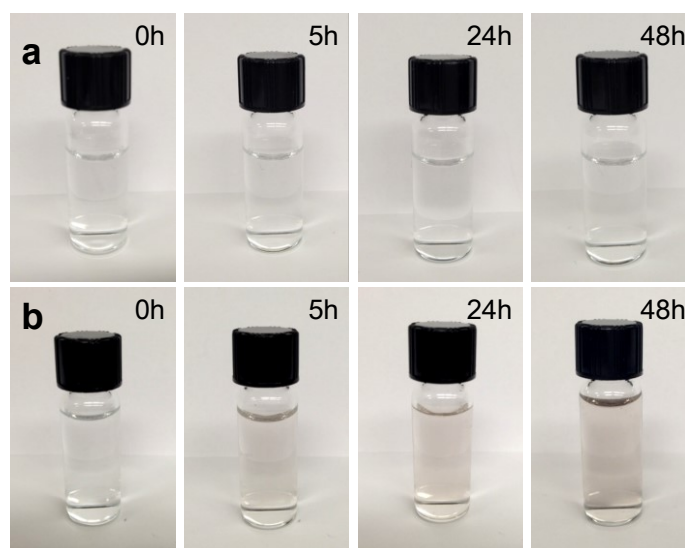

Figure S2.4 Changes in frequency and dissipation during the adsorption of BSA protein on silica sensors coated with different polymers using a QCM-D.
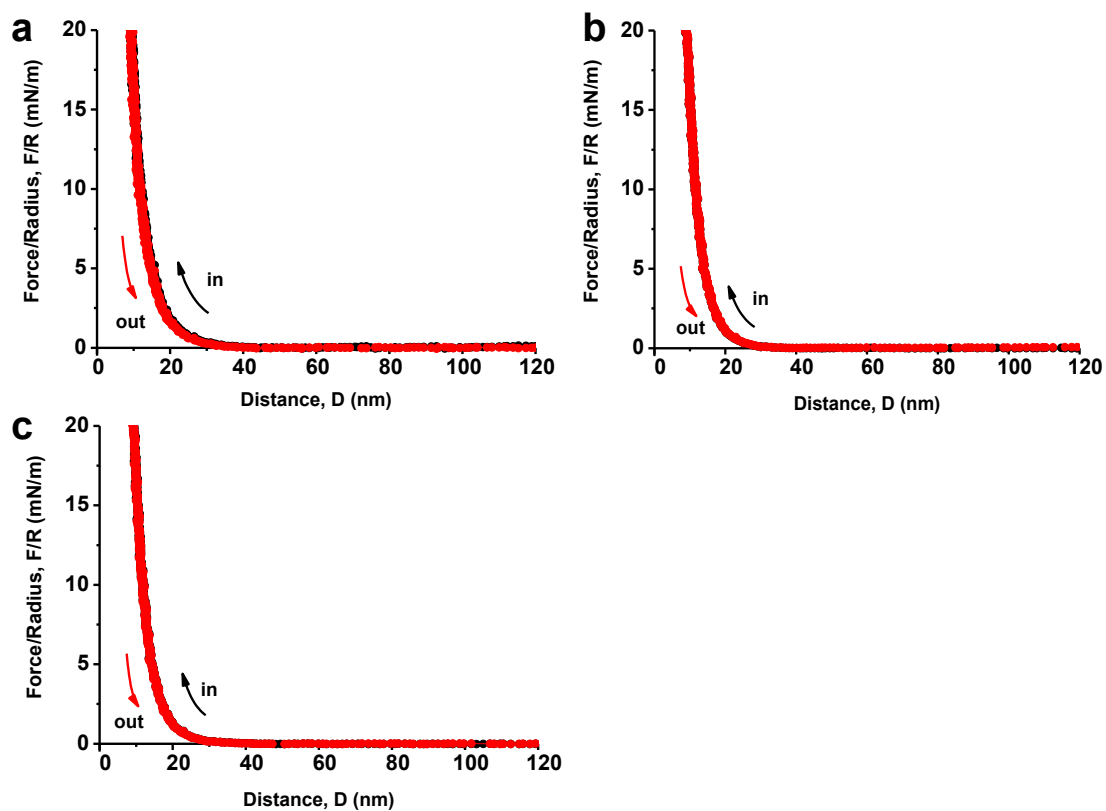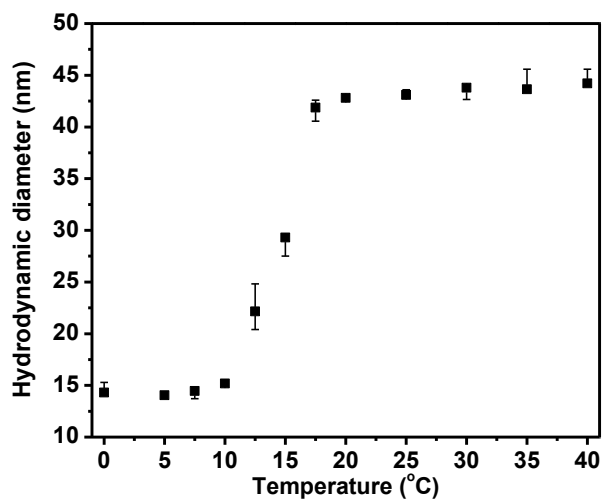
Figure S2.5 Force-distance profiles between two PDN-PEG-PDN films in (a) 0.001M, (b) 0.01M and (c) 0.1M NaCl solutions.
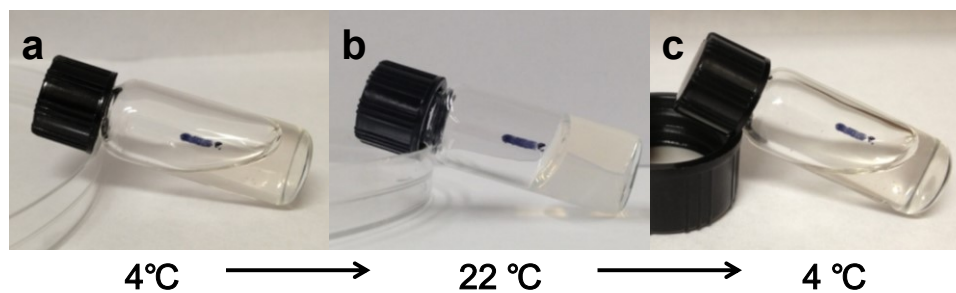
Figure S3.1 Thermo-induced sol-gel-sol phase change of a10 wt% DNODN hydrogel.

Figure S3.2 DNODN solution (1 mg/ml in DI water, a) and dopamine hydrochloride solution (0.23 mg/ml in DI water, b) monitored within 48 h at room temperature.

Figure S3.3 DLS results showing the changes of hydrodynamic diameters with increased temperature. The LCST was determined as 15 °C where a sudden increase in particle size occurred.
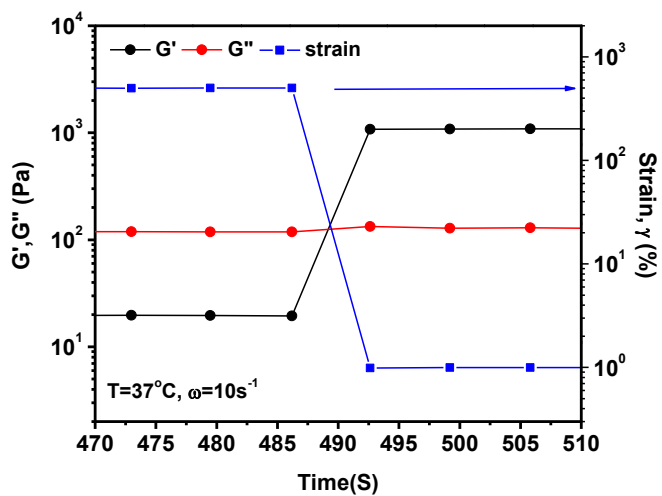

Figure S3.4 Dynamic strain amplitude cyclic test (γ =1% or 500%) of 10 wt% DNODN hydrogel at 37°C showing self-healing behaviour, zooming in the first strain recovery region in Figure 3.3b. Note the data points were obtained every 6

seconds during the rheological measurements, indicating the recovery could be completed within <6 seconds.
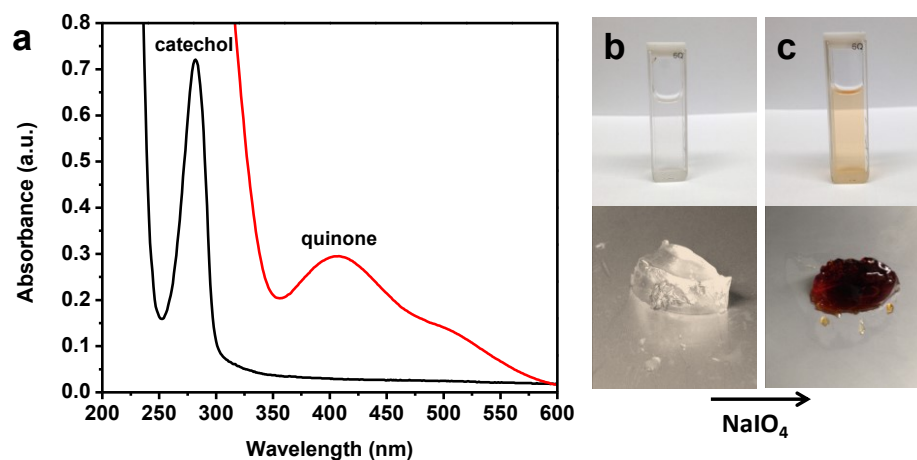
Figure S3.5 (a) UV/Vis spectrum of DNODN solution with a concentration of 0.3 mg/ml, untreated (black) and NaIO4-oxidized (red). (b) Image of cell (upper) containing 1 mg/ml DNODN solution and its corresponding 10 wt% hydrogel (lower). (c) Image of cell containing 1 mg/ml DNODN solution oxidized by NaIO4 (upper) and its corresponding 10 wt% hydrogel (lower).
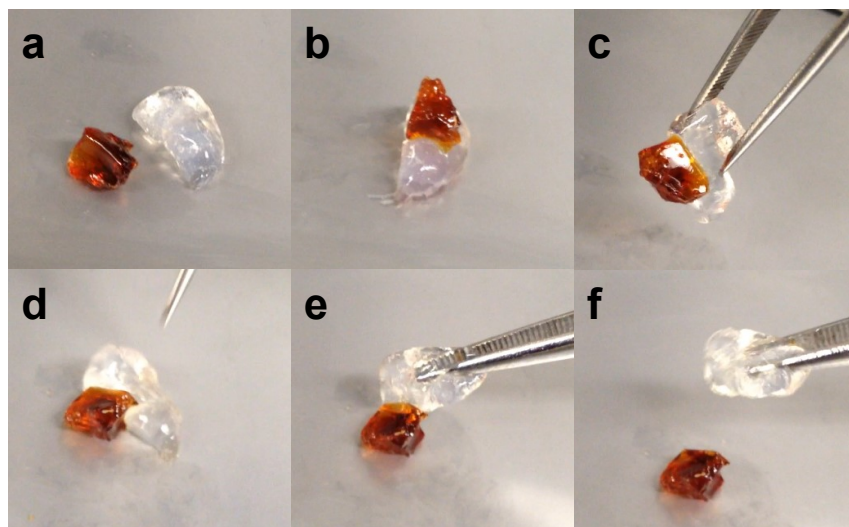
Figure S3.6 Characterization of the healing behavior between a fully oxidized (NaIO4 treated, excess periodate removed, dark red) and a freshly-prepared (colorless) DNODN hydrogel. (a-b) The two pieces were brought together for a healing process. (c) 10 seconds after contact, the two pieces adhered to each other. (d-f) The adhered hydrogel pieces could be relatively easily separated to two pieces right from the contact interface.
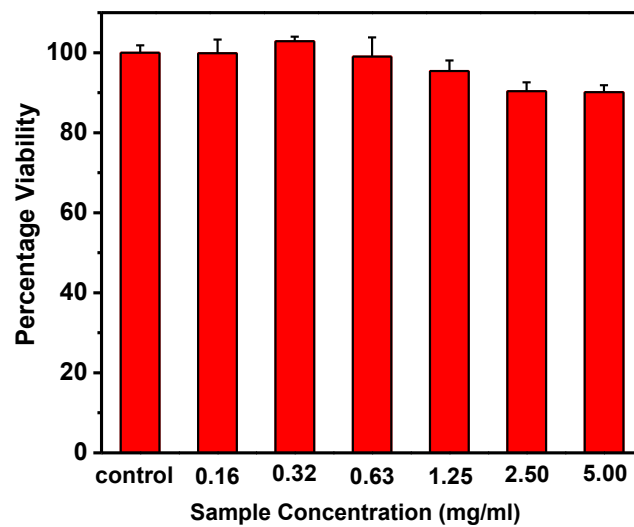
Figure S3.7 Cell viability measurements of DNODN polymer with different concentrations by MTT assay after 24 h of incubation. Data were presented as means ± standard deviations (n=5).